5. THE THEORY OF NONLINEAR OPTICS IN WAVEGUIDES

It is apparent from the previous two chapters that a good understanding has been gained of the processes of unguided Stimulated Raman and Brillouin scattering and that an adequate theory exists that can make useful predictions of threshold pump powers. Unfortunately, these threshold powers are generally rather high for gases such as hydrogen and methane when using conventional single-pass, tightly focussed configurations - or even unguided resonator configurations. This problem gets worse, as we have seen, at the longer wavelengths, precisely where it would be hoped that Raman generation could provide wide tunability into the infrared. Much thought has been given, therefore, to the development of techniques to lower these threshold powers. The answer is provided by the fact that, in general, the Stokes waves grow as $\exp\{gI_pl\}$. Assuming the gain g is fixed, a lower value of I_p, and hence pump power, is required if the interaction length l can be increased. We have seen how the unguided resonator effectively increases this length by reflecting the Stokes wave backwards and forwards through the gain medium whilst the pump radiation is present. Similar to this is the multiple-pass cell described by Herriot et al (1964) and Trutna and Byer (1980). In this approach both Stokes and pump are reflected backwards and forwards many times between totally reflecting and refocussing mirrors. This would not be possible with the ordinary linear resonator since there would be no way of coupling the pump in. The multiple-pass cell achieves this by having the pump injected in off-axis and at an angle to it. The many transits pass through different parts of the gain medium and can be arranged such that the pump and resultant Stokes beam do not arrive back at the injection point until the number of transits has reached a (generally large) predetermined number.

In this way the interaction length is greatly increased, the Stokes is always growing in the presence of the maximum pump power (for forward Raman scattering) and consequently impressive threshold reductions can be achieved. Trutna and Byer (1980) report an SRS threshold reduction of about a factor of 20 over the single-pass, tight focussing value for a 1.064μm in hydrogen. This is a considerable reduction, but to achieve it they use a 4m long, 8" diameter high pressure hydrogen cell containing sophisticated mirrors and requiring highly critical beam matching. The last two points give us a clue to a more efficient solution of the problem. After each pass of the multiple-pass cell, or indeed the ordinary resonator, it is necessary to refocus the pump to retain the high intensities desired i.e. the diffraction process prevents the large intensities obtained by focussing from persisting over more than just a short length. Hence, the only really effective regions in the multiple-pass cell or the ordinary resonator are those short regions in the centre, about the foci of the pump beams. The rest of the gain medium is virtually wasted. A much better approach would be to somehow overcome this diffraction effect and thereby maintain the high intensities over much longer lengths. Such an effect is possible by confining the pump radiation within a waveguide. We shall see in the following sections that if the entrance to a cylindrical waveguide of an appropriate bore radius is made to coincide with the high intensity focus of a pump beam, then that beam can be transmitted with low loss through a long length of the guide, keeping approximately the same high intensity and the same small spotsize all the way through. If, then, this guide is filled with a nonlinear medium such as hydrogen or methane, it is clear that very low threshold powers are going to be possible. It is to the theory of these guided nonlinear interactions that this chapter is devoted.

We begin by taking a brief look at the allowed modes of a hollow dielectric waveguide. Some of these prove to have low losses and one of them is very similar in profile to a linearly polarised Gaussian typical of many laser outputs, particularly that from the telescopic resonator. It will be shown that this mode, the EH_{11} mode, can be efficiently excited by the Gaussian beam, and can give low loss guided transmission over large distances. Filling the hollow guide with hydrogen or methane does not alter its guidance properties. Consequently, nonlinear threshold measurements can be performed, and expressions for the threshold powers will be derived in the cases of SRS and SBS. These expressions will be used to make threshold predictions for various pump wavelengths, and for various waveguide bores and lengths. As in the case of unguided nonlinear processes, thresholds can be further reduced by resonating the Stokes radiation. Consequently, the theory will be extended to cover the case of a waveguide resonator and threshold predictions will be made. A further extension of these techniques employs picosecond pulses. Provided the nonlinear process still displays an approximately steady-state response such an approach greatly reduces the energy thresholds required in a pulse. In addition, those processes such as SBS which are highly transient will be suppressed. If, as in the case of 'mode-locked' lasers, the energy is distributed in a train of these short pulses, further energy threshold reductions can be obtained by using them to synchronously pump a waveguide resonator. The theory of this, and the possibly transient single-pass case, will be presented and again threshold predictions made. Finally, it will be shown that a waveguide oscillator/amplifier system can produce large amounts of 1st Stokes energy in cases where, if we were to use just an oscillator with a large pump input, efficient operation would be prevented by competing nonlinear processes.

5.1 Radiation in a Hollow, Cylindrical, Dielectric Waveguide

The allowed modes of a hollow cylindrical waveguide with an infinitely thick dielectric cladding are found by solving the wave equation derived from Maxwell's equations. This problem has been treated by many authors including Marcatili and Schmeltzer (1964) and M J Adams (1981). The basic result is as follows: we look for some guided running waves of the form;

$$E(z, r, \theta) = E_z(r,\theta) \exp\{ i(\gamma z - wt)\} \qquad 5.1$$

where; $$\gamma = n_1 k - \beta \qquad 5.2$$

with a similar expression for $H(z,r,\theta)$; and if we also make the approximation that typical bore diameters are very much larger than the wavelength, then the analysis predicts low-loss, guided modes in the core in the form of Bessel functions. The relevant subset of these, for there are three basic types, can be written in cylindrical polar co-ordinates as;

$$E_z(r)_{nm} \approx J_{n-1}\left(\frac{U_{nm} r}{a}\right) \text{Sin } n\theta \exp\{ i\ (\gamma z - wt)\} \qquad 5.3$$

$$E_z(\theta)_{nm} \approx J_{n-1}\left(\frac{U_{nm} r}{a}\right) \text{Cos } n\theta \exp\{ i\ (\gamma z - wt)\} \qquad 5.4$$

where the complex propagation coefficient is given by;

$$\gamma = k\left[n_1 - \frac{1}{2}\left(\frac{U_{nm}\lambda}{2\pi a}\right)^2 \left(1 - \frac{U_n \lambda}{\pi a}\right)\right] \qquad 5.5$$

Here, a is the bore radius of the guide, n_1 the refractive index of any medium in the hollow core, U_{nm} is given by;

$$J_{n-1} \quad (U_{nm}) = 0 \qquad 5.6$$

l is the length of the guide, k is the free-space wave vector and ν_n is a function of the cladding material which also depends on the class of waveguide mode and may be complex. The electric fields of equations 5.3 and 5.4 (and similar ones for the magnetic fields) constitute a set of hybrid modes normally known as the EH_{nm} modes. These have the advantage over the other possible guided modes (TE and TM) in that they are approximately transverse i.e. there is only a very small component of the electric and magnetic fields in the z-direction. Clearly, this is going to be important for efficient coupling to the transverse TEM_{oo} free space mode from a laser. Of particular importance, however, is the EH_{11} mode. The reason for this becomes apparent when we resolve equations 5.3 and 5.4 into the x and y directions;

$$E_{y_{1,1}} = E(r)_{1,1} \sin\theta + E(\theta)_{1,1} \cos\theta$$

$$= \left[J_o(U_{11} r/a) \sin^2\theta + J_o (U_{11} r/a) \cos^2\theta\right] \exp\left\{ i(\gamma z - wt)\right\}$$

$$= J_o(U_{11} r/a) \exp\left\{ i (\gamma z - wt)\right\} \qquad 5.7$$

$$E_{x_{1,1}} = E(r)_{1,1} \cos\theta - E(\theta)_{1,1} \sin\theta$$

$$= \left[J_o(U_{11}r/a)\sin\theta\cos\theta - J_o(U_{11}r/a)\cos\theta\sin\theta\right]\exp\left\{i(\gamma z - wt)\right\}$$

$$= 0 \qquad 5.8$$

Thus, the EH_{11} mode is linearly polarised. Not only this, the zeroth order Bessel function is very similar to a Gaussian function. Figure 5.1 shows a comparison between the $J(U_{11}r/a)$ function and the TEM_{oo} mode $\exp\left\{-r^2/W^2\right\}$ where $W = 2a/3$ (this choice will be explained later). As can be seen, there is very little difference. Again, this bodes well for coupling between the two modes.

Finally, it can be shown that for a dielectric cladding with refractive index $n_2<2.02$, the EH_{11} mode is the one with the smallest attenuation coefficient and therefore the lowest transmission loss. Equation 5.5 gives the attenuation coefficient, where for EH_{nm} modes ν_n is given by;

$$\nu_n = \frac{\nu^2 + 1}{2(\nu^2-1)^{\frac{1}{2}}} \qquad 5.9$$

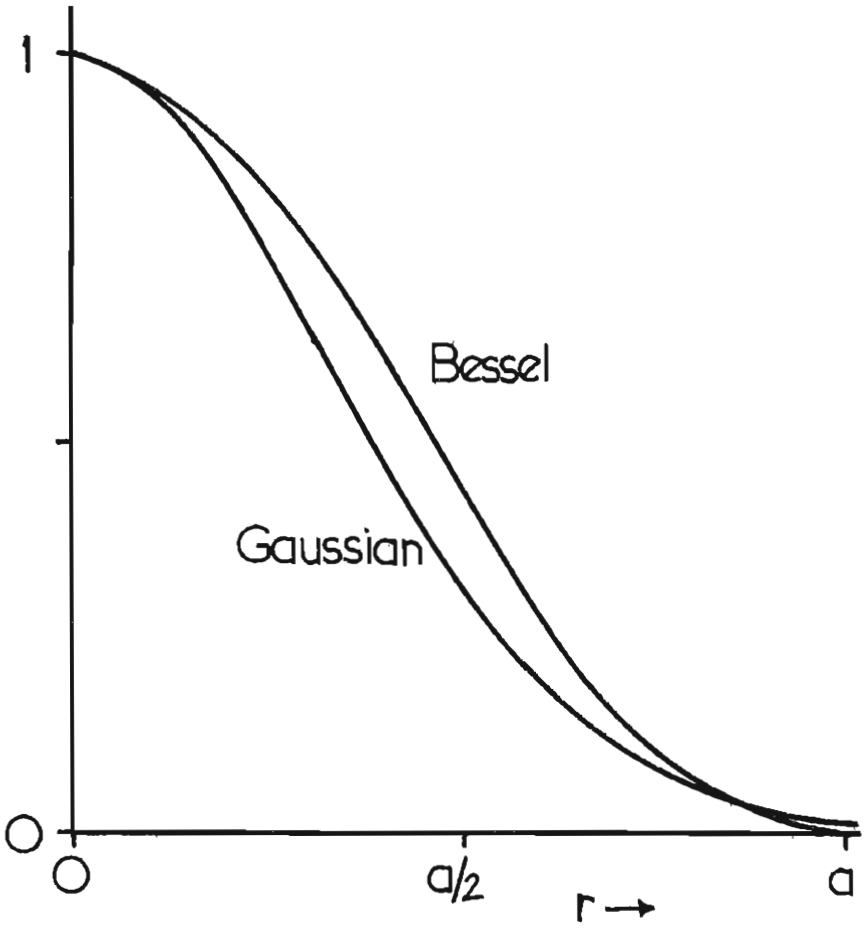

Figure 5.1: Comparison between the zeroth order Bessel function $J_o(u_{1,1}r/a)$ and the TEM_{00} mode $\exp(-r^2/W^2)$ where $W=2a/3$.

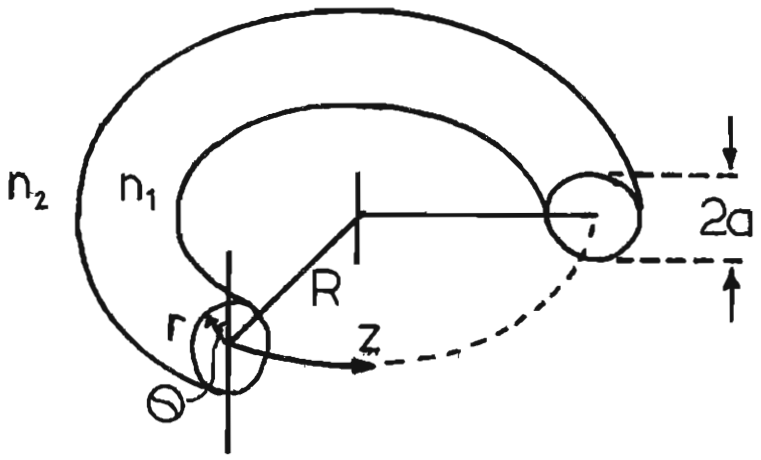

Figure 5.2: Toroidal guide used by Marcatili and Schmeltzer to evaluate an expression for the bending losses.

For a non-absorbing dielectric cladding (such as quartz in the visible and near infrared) ν is entirely real and equal to the refractive index. Thus, if we resolve equation 5.5 into a phase constant (the real part) and an attenuation coefficient (the imaginary part), the latter can be written as;

$$\alpha_{nm} = \left(\frac{U_{nm}}{2\pi}\right)^2 \cdot \frac{\lambda^2}{a^3} \cdot \frac{n_2^2 + 1}{2(n_2^2-1)^{\frac{1}{2}}} \qquad 5.10$$

The smallest value of U_{nm} occurs for U_{11} and so the EH_{11} mode has the lowest loss (above $n_2 = 2.02$ the TE_{01} mode has the lowest loss. However, this mode in no way resembles a TEM_{oo} mode and would not be efficiently excited by one).

Equations 5.7, 5.8 and 5.10 are the basic results of this section. They show that a straight waveguide will transmit with a low loss a linearly polarised transverse mode which is very similar to the TEM_{oo} mode.

Before we go on to consider just how well the free-space TEM_{oo} mode will couple to the EH_{11} waveguide mode it is necessary to consider the additional losses caused by waveguides that are not perfectly straight, since this is going to be the case in practice. This problem is dealt with by Marcatili and Schmeltzer (1964). They consider the case of a toroidal guide, as shown in fig. 5.2 i.e. they assume a constant bend with radius of curvature R.

Their technique is again to solve Maxwells equations, but now with a toroidal co-ordinate system. However, as $R \to \infty$ the problem degenerates into the straight guide case. Thus, if R is kept large, a solution can be found as a perturbation on the straight guide solution. Employing such a perturbation technique, Marcatili and Schmeltzer show that the electric and magnetic fields within the core of the curved guide are related to those of the straight guide by equations of the form;

$$E,H_{\theta,r}(\text{curved}) = (1 + \sigma r/a\sin\theta)\ E,H_{\theta,r}(\text{straight})$$

Where; $$\sigma \approx 2\left(\frac{2\pi a}{U_{nm}\lambda}\right)^2 \cdot \frac{a}{R} \qquad 5.11$$

and where R is so large that $\sigma << 1$. The E_z and H_z are also slightly modified, but are still small. We still have, therefore, a largely transverse mode which, in the case of the EH_{11} mode, is still very similar to the linearly polarised TEM_{oo} mode of free-space. Of great importance, however, is the change a bend causes in the attenuation coefficient. From the same analysis, Marcatili and Schmeltzer show that for the EH_{nm} modes this can now be written as;

$$\alpha_{nm}(R) = \alpha_{nm}(\infty) + \frac{a^3}{\lambda^2 R^2} \cdot R_e V_{nm}(\nu) \qquad 5.12$$

Where;

$$V_{nm}(\nu) = \frac{4}{3}\left[\frac{\nu^2+1}{2(\nu^2-1)^{\frac{1}{2}}}\right]\left(\frac{2\pi}{U_{nm}}\right)^2\left\{1 - \frac{n_1(n_1-2)}{U_{nm}} + \frac{3}{4}\delta(\pm 1)\left(\frac{\nu^2-1}{\nu^2+1}\right)\cos(2\theta_o)\right\}$$

where all the symbols are the same as before and θ_o is the angle between the axis that θ is measured from and the plane of the guide curvature. For the EH_{11} mode equation 5.12 becomes;

$$\alpha_{11}(R) = \alpha_{11}(\infty) + \frac{a^3}{\lambda^2 R^2} \cdot 15.5\ (1 + 0.246\ \text{Cos}\ 2\theta_o) \qquad 5.13$$

Where we have assumed $n_2 \simeq 1.5$ for quartz waveguides. θ_o is now the angle between the linearly polarised electric field and the plane of curvature. It can be seen that, as expected, the losses are highest when the electric field lies in the plane of curvature ($\theta_o = 0$), agreeing with simple Fresnel coefficient considerations.

It is instructive at this point to evaluate some typical waveguide transmissions considering only losses due to the attenuation coefficients of equations 5.10 and 5.13. The percentage power transmissions of a guide of length L is given by;

$$T = 100 \exp(-2\alpha L) \qquad 5.14$$

Fig. 5.3 shows the variation with wavelength of guides with various bore radii a, but all of length L = 1m (the maximum convenient length to use in practice). The transmissions are shown both for a straight guide (α given by equation 5.10) and for a curved guide with R = 100m (α given by equation 5.13). It is clear from the curves that bending losses become more important for large bores and short wavelengths.

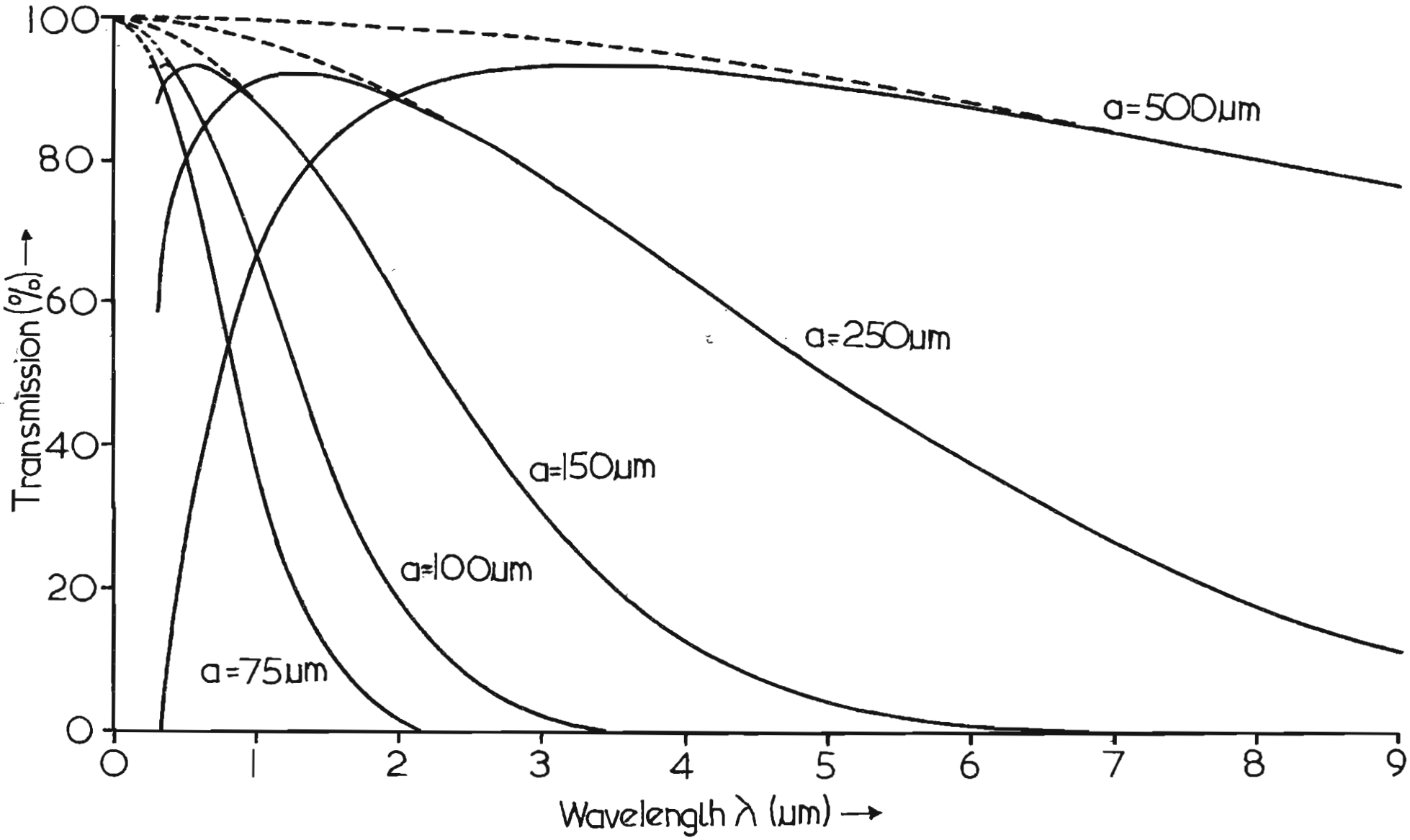

Figure 5.3: Graph of transmissions of 1m long straight (broken line) and bent (R=100m, full line) waveguides.

Fortunately these are not the cases in which we are primarily interested but some experiments will still be performed to test the theory in this region. Of much more interest are the examples of smaller bores and longer wavelengths ($\lambda \gtrsim 1\mu m$). Here we are only limited by the ordinary straight guide attenuation. We have seen in previous chapters that Raman scattering of 1.064μm radiation in hydrogen and methane takes us to $\lambda_s = 1{\cdot}907\mu m$ and 1.544μm respectively. From the graph it is clear that we are going to be primarily interested in the 100 μm and 150 μm bore radii capillaries since smaller bores would give unacceptably large Stokes losses.

So we now know that even a moderately curved guide can transmit a mode very similar to a linearly polarised TEM_{oo} mode, and do so with a reasonably low and quantitatively predictable loss. This mode is generally known as the EH_{11} mode. We now investigate how well this mode is excited by an injected TEM_{oo} free-space mode, an analysis which will then allow us to make overall waveguide transmission calculations for a TEM_{oo} mode input.

5.1 Coupling between Free-Space Modes and the EH_{11} Mode of a Cylindrical Waveguide

We need to know how much of an injected free-space TEM_{oo} mode is converted into the EH_{11} mode of the guide (possibly, also, how much is converted into other modes of the guide) and then how much of the EH_{11} mode is coupled back into the various free-space modes at the other end of the guide. The second of these two questions is treated by Abrams (1972) and Degnan (1973). Abrams shows that the EH_{11} mode can be written as an expansion of the Gaussian normal modes,

$$\psi_p = \sqrt{\frac{2}{\pi}} \cdot \frac{1}{W_o} \cdot Lp\left(\frac{2r^2}{W_o^2}\right) \exp\left\{-\frac{r^2}{W_o^2}\right\} \qquad 5.15$$

of which the TEM_{oo} mode is the lowest order. L_p is the Laguerre polynomial of order p and W_o is the 1/e radius of the mode amplitude. He calculates the expansion coefficients A_p (the relative amount of each normal mode required in the expansion) and finds that for $W_o/a = 0.644$, A_o is a maximum, corresponding to 98% of the EH_{11} mode energy entering a TEM_{oo} mode with this spot-size. No energy enters the TEM_{01} mode, the remaining 2% being dispersed amongst even higher modes.

Because Abram's work was directed at waveguide lasers which themselves generate the EH_{11} mode that is then launched into free-space, he does not consider the opposite case where a TEM_{oo} mode is injected into a waveguide. This would require a similar treatment to the one just outlined where the TEM_{oo} mode would be expanded as a series of Bessel functions. We would then look for the TEM_{oo} mode spotsize that maximises the energy conversion into the EH_{11} mode. Without actually performing this calculation, Hall, Gorton and Jenkins (1976) argue that the same spotsize of $W_o = 0.644a$ would be the optimum and would convert 98% of the TEM_{oo} mode energy into the EH_{11} mode of the guide. This is not an unreasonable assumption in view of the fact that Abrams does show, as we shall see later, that an EH_{11} mode can be coupled out of, and back into, a guide, and still result in $\sim$98% of the energy being in the EH_{11} mode.

Thus, if we are to make a simple transmission measurement of a length of waveguide using a TEM_{oo} mode beam, we will obtain a maximum when we focus to $W_o = 0.644a$ and, if we collect all the energy from the output end, the final transmission result should be 0.98 times the transmission predicted by equations 5.14, 5.10 and 5.13 of the previous section. We are assuming, therefore, that the guide is long enough to act as an EH_{11} filter, all other modes being attenuated away.

The analysis so far is appropriate for predicting the waveguiding properties of a guide when it is used in a one-way, single-pass configuration. It was mentioned in the introduction to the chapter that a waveguide can also be used in a resonator configuration. This will involve coupling generated Stokes radiation out of, and then back into, the waveguide. We need to know, therefore, how much energy re-enters the EH_{11} mode after it has left the guide, been resolved into free space modes, travelled to a mirror, been reflected, and finally travelled back to the guide entrance. Abrams performs this calculation, the results of which are reproduced in the graph of fig. 5.4. The coupling loss as plotted is that percentage of the original energy in the EH_{11} mode that does not get reinjected into the guide and so is assumed to be lost. The broken line gives the coupling losses resulting from mirrors which at all positions z have a curvature equal to the beam curvature. This is clearly the optimum curvature at all positions, and yet three regions are still markedly better than the rest i.e. $Z/b \lesssim 0.1$, $Z/b \approx 1$ and $Z/b \gtrsim 10$. Once a guide bore has been chosen it is best to try and use a correctly chosen mirror curvature in one of these regions where coupling losses are typically around 2% or less.

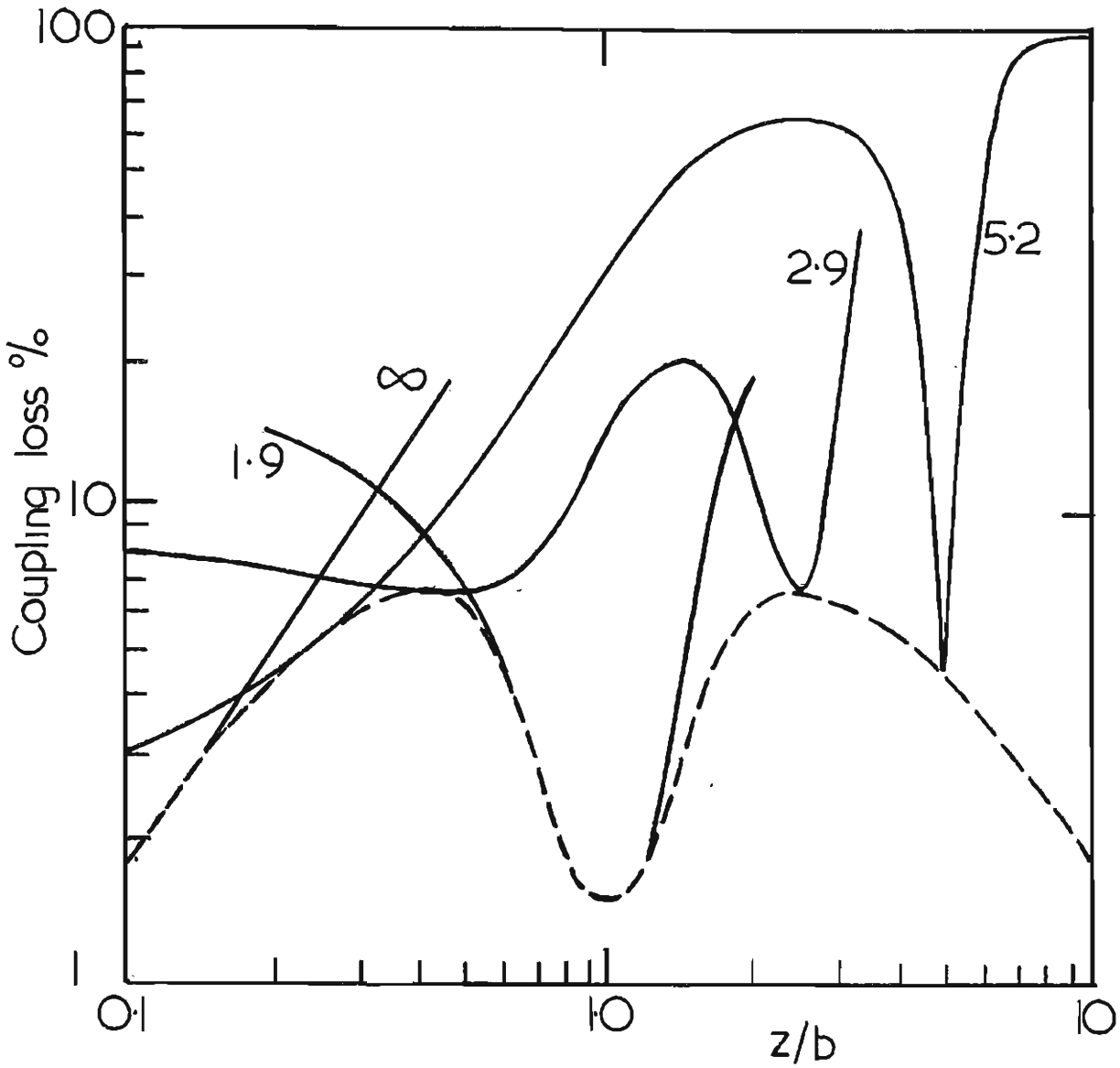

Figure 5.4: Coupling loss versus mirror position z for mirrors of fixed curvature R. Each curve is labeled with the value of R/b, where b is the confocal parameter of the TEM_{oo} mode.

If this cannot be done for some experimental reason the maximum coupling loss for a correctly positioned mirror is still only 7%. But the mirror must be correctly positioned once its curvature has been chosen. The full lines of fig. 5.4 show the coupling losses that result if it is not. Of particular interest to us would be a line for $R/b = \infty$ (a flat mirror) and $R/b \approx 10$. The former clearly needs to be placed right up to the end of the waveguide and we therefore anticipate possible damage problems with coated mirrors when using very small waveguide bores. The condition $R/b \approx 10$ implies that the beam is allowed to grow substantially before it reaches the mirror, and, experimentally, it allows greater ease of construction of gas filled waveguide cells (see next chapter).

This completes the analysis of the waveguide properties relevant to the theory of nonlinear interactions in waveguides that will be outlined in the following sections.

5.3 Single-Pass SRS and SBS in a Waveguide

We have seen in the previous sections that once a TEM_{oo} mode beam has been injected into a cylindrical waveguide it can be propagated over large distances with a very small spotsize i.e. the effects of diffraction are considerably reduced. We have, therefore, ideal conditions for performing non-linear interactions since the hollow core of the waveguide can be filled with a nonlinear medium such as hydrogen or methane without altering its properties.

Long interaction lengths are therefore achievable, resulting in lower pump intensity requirements. This in turn results in considerably lower pump power requirements since very small waveguide bores can be used.

An additional advantage resulting from the use of waveguides is the fact that the generated Stokes beam is also guided. Equations 5.7 and 5.8 of section 5.1 show us that the size and polarisation of the EH_{11} mode are wavelength independent. This implies complete overlap of pump and Stokes over the entire length of the guide, a fact which is clearly going to help reduce the pump thresholds further. We have seen, however, that the attenuation constants of equations 5.10 and 5.13 are strongly wavelength dependent. For SRS, therefore, the Stokes transmission losses are always higher than the pump losses. We have seen, however, that bore radii can be chosen which allow reasonable transmission of both pump and Stokes whilst still providing tight confinement of both beams.

This last point of Stokes guidance seems to suggest that the theory of Boyd and Johnson (1969) would be the best to employ in a development of expressions for SRS gain in waveguides. This is because their treatment assumes that the modes of the pump and Stokes are both prescribed and remain unaltered by the nonlinear process itself. In the present case the waveguide constrains both pump and Stokes to be in EH_{11} modes. Boyd and Johnson do point out, however, that their analysis is strictly true only in the limit of low gain per transit, appropriate, as we have seen in section 3.6 of chapter 3, to the Raman or Brillouin resonator.

In the high gain conditions required to reach threshold in a single pass it is no longer clear whether the Stokes mode is determined by the waveguide or whether gain focussing and the associated diffraction effects result in a significantly modified Stokes profile. The problem has been looked at in great detail by M C Ibison (1982 and 1983). He obtains threshold expressions very similar to those that are obtained if the Boyd and Johnson approach is followed, the predicted thresholds being typically around 10% higher in Ibison's case. It is not inappropriate, therefore, to outline the simpler theory using Boyd and Johnson's approach.

5.3.1 The Theory of Single-Pass Nonlinear Interactions in Waveguides

We recall that the increment in Stokes power per transit in a particular mode TEM_{mn} of a resonator is given by equation 3.62 and rewritten here as;

$$\Delta P_{s(m,n)} = -Im\left\{ \frac{w_s}{2} \int E^*_{s(m,n)}\, P_s \, dxdydz \right\} \qquad 5.16$$

Where again P_s is the nonlinear polarisation given by equation 3.11 and rewritten as;

$$P_s = -i\chi_R''\epsilon_o E_p E_p^* E_s \qquad 5.17$$

where χ_R'' is the imaginary part of the nonlinear susceptibility.

Note that we are going to assume that the EH_{11} mode of the guide can be approximated by a TEM_{oo} mode with a spotsize $W_o = 0.644a$ as discussed earlier. Ibison uses the correct Bessel functions in his analysis. Our TEM_{oo} mode spotsize is fixed, however, resulting in very simple expressions for the pump and Stokes fields i.e.;

$$E_{p,s}(r) = E_{Po,So} \exp(-r^2/W_o^2) \qquad 5.18$$

Substituting these fields into equations 5.16 via equation 5.17, and including waveguide losses of the form $\exp(-\gamma z)$ where γ is given by equations 5.10 and 5.13, we obtain;

$$\Delta P_s = \frac{W_s}{2} \int_0^L \int_0^\infty \left[\chi_R'' \epsilon_o E_{PO}^2 E_{SO}^2 \exp\left\{ -4r^2/W_o^2 - 2\gamma_p z \right\} - P_s 2\gamma_s z \right] r dr . 2\pi . dz \qquad 5.19$$

where we have converted to cylindrical polar co-ordinates. For a TEM_{oo} mode beam the relationship between electric field and instantaneous power is given by;

$$E_{po}^2 = \frac{4P_p}{\pi W_o^2} \sqrt{\frac{\mu_o}{\epsilon_o}} \qquad 5.20$$

If this expression is substituted into equation 5.19 for both pump and Stokes it can be rewritten as;

$$\int_{P_N}^{P_L} \frac{dP_s}{P_s} = \frac{W_s}{2} \int_0^L \int_0^\infty \left[\chi_R'' \mu_o \frac{16 P_p}{\pi^2 W_o^4} \exp\left\{ \frac{-4r^2}{W_o^2} - 2\gamma_p z \right\} - 2\gamma_s z \right] r dr . 2\pi . dz \qquad 5.21$$

Performing the integrals and rearranging for P_p gives us the final result;

$$P_p = (\pi W_o^2) \frac{[\ln(Ps(L)/Pn) + 2\gamma_s L]}{g L_{eff}} \qquad 5.22$$

$$\text{Where, } L_{eff} = \frac{1}{2\gamma_p} \left[1 - \exp(-2\gamma_p L) \right] \qquad 5.23$$

and g is the planewave gain coefficient defined in previous chapters. Note that again we have assumed no depletion of the pump except for the unavoidable wageguide transmission losses embodied in a decreased effective interaction length L_{eff}. This treatment is valid, therefore, only up to the point at which detector threshold is reached, where, as always, we approximate $\ln (P_s (L)/P_n)$ to 30.

If the EH_{11} mode profile is used (Ibison 1982) a better threshold prediction is given by the expression,

$$P_p = 0.885\pi W_o^2 \frac{[30 + 2\gamma_s L]}{g L_{eff}} \qquad 5.24$$

where again $W_o = 0.644a$ and L_{eff} is given by equation 5.23. In the more detailed theory by Ibison (1983) it is shown explicitly that the Stokes is generated predominantly into the EH_{11} mode. We assume here that all of it is and therefore, using Abrams (1972), suggest that 98% of the capillary output energy is coupled into the TEM_{oo} making it an essentially diffraction limited output.

With the theoretical expressions of this section and the gain coefficients of chapter 3 we are now in a position to make predictions of the pump powers necessary for reaching Raman or Brillouin threshold in waveguides. We anticipate that the thresholds will be substantially lower than those that can be obtained by single-pass, tight focussing, or even the unguided Raman or Brillouin oscillator.

5.3.2 Numerical Predictions for SRS in Hydrogen

For a direct comparison of the predicted waveguide threshold with the tight-focussing thresholds we will evaluate the former at the same wavelengths of 1.65μm, 1.064μm, 532nm, 355nm and 266nm. We will also use again the experimentally typical pressure of 400psi (27.6Atm). We will see later that it is always better to use a longer waveguide provided that the bore is chosen appropriately. Predictions will be made, therefore, for the longest waveguide which can be conveniently used (or perhaps marketed) which is about 100 cm.

A number of different bore radii will be investigated, but for each we will evaluate the thresholds assuming two different characteristic losses. The first will be the theoretical losses predicted by Marcatili and Schmeltzer (1966) for a straight guide which are given by equation 5.10. The second will be the losses calculated from assumed waveguide transmissions which will be substantially less than those predicted by Marcatili and Schmeltzner. These losses could be caused by core curvature, core wander, impurities in the material of the waveguide or impurities adhering to the walls. We assume that these losses can be written as an effective attenuation coefficient γ_{eff} which is given by;

$$\gamma_{eff} = \frac{-\ln(T)}{2L} \qquad 5.25$$

Where T is the measured energy transmission of the guide and L is its length. γ_{eff} now replaces γ_p wherever it appears (γ_s will, however, be assumed to be that predicted by Marcatili and Schmeltzer). The reason for introducing γ_{eff} is our experimental observation of transmissions that are smaller than those theoretically predicted by sections 5.1 and 5.2.

The theoretical results are all those predicted by equations 5.24 for P_p, 5.23 for L_{eff}, 5.10 and 5.25 for $\gamma_{s,p}$ and γ_{eff} and finally table 3.1 for g_R in hydrogen at 400 psi. They are all presented in table 5.1 along with the tight focussing results of table 3.1 for comparison. Note that in nearly all cases the use of a 1m long waveguide reduces the threshold powers below the tight focussing values. The only exceptions to this are the short wavelengths ($<1.06\mu m$) when using large bore radii ($>330\mu m$) under which condition the guidance will be slight.

We can also see that at long wavelengths and very small bores the use of a 1m long waveguide will be ineffective for lowering the threshold because the transmission losses will then be very high. We can see this effect beginning to set in for the 1.65μm results, where the 75μm bore radius threshold is greater than the 100μm bore radius value. Between these two limits, however, substantial threshold reductions can be obtained, especially at the longer wavelengths. A factor of 20 reduction should be possible at 1.064μm when using a 75μm bore radius capillary. The same capillary gives only a reduction of a factor of about 10 at 0.266μm, but at this wavelength the bore radius could be reduced still further before transmission losses started to increase rapidly.

So for hydrogen at least on the basis of these calculations the use of waveguides looks highly promising as a means for lowering the Raman threshold. Note that a factor of 20 reduction at 1.064 is just what Trutna and Byer (1980) obtained using their very large and complex multiple-pass cell.

5.3.3 Numerical Predictions for SRS in Methane

Again we anticipate the fact that steady-state Raman thresholds in CH_4 will not be reached at all except the shortest wavelengths when using SLM pump pulses and typical pressures. Again the reason is that Brillouin scattering should reach threshold first. We have seen, however, that Brillouin scattering can be suppressed by using short pulses. For SLM pulse lengths that are short enough to force the Brillouin scattering process into the transient regime whilst at the same time still being long enough to produce the steady-state Raman response, the expected threshold powers at 400 psi (27.6Atm) in 1m long waveguides of various bores are given in table 5.2.

WAVELENGTH (μm) ⟶ BORE RADII (μm) ↓	1.65	1.064	0.532	0.355	0.266
Tight focussing	12778	1370	175	50	22
500	6360 (7062 for T=0.8)	1282 (1429 for T=0.8)	309 (355 for T=0.85)	154 (167 for T=0.85)	89 (97 for T=0.85)
165	847 (1035 for T=0.5)	149 (180 for T=0.6)	34 (40.1 for T=0.7)	16.9 (15.75 for T=0.8)	9.8 (10.5 for T=0.85)
100	593 (706 for T = 0.2)	68 (82 for T=0.4)	13.2 (20.1 for T=0.28, P=320psi, L=110cm)	6.35 (8.4 for T=0.43, P=320psi, L=110cm)	3.63 (4.57 for T=0.6
75	803 (917 for T=0.04)	54 (66.3 for T=0.15, L=110)	8.1 (10.8 for T=0.4)	3.7 (4.45 for T=0.6)	2.1 (2.4 for T=0.7)

Table 5.1 Predicted pump threshold powers (kW) for Raman scattering in hydrogen using 1m long waveguides with various bore radii.

They are calculated in the same way as for hydrogen, althogh here only the theoretical Marcatilli and Schmeltzer losses are presented. All thresholds are in kW.

Table 5.2: Predicted threshold powers for guided SRS in CH_4

WAVELENGTH (μm) ⟶ μm BORE RADIUS ↓	1.65	1.064	0.532	0.355	0.266
Tight focussing	22310	4958	781	303	162
500	13107	4783	1594	945	669
165	1661	552	176	104	73
100	1006	249	68	39	27.2
75	1151	194	42	22.8	15.6

Again we have the same limiting behaviour as for hydrogen at short wavelengths and large bores and also at long wavelengths and very small bores. We shall see in chapter 6 that a value of around 250kW when using a 1.064μm pump in a 1m long, 100 μm bore radius waveguide can indeed be achieved without Brillouin scattering by using a 470 ps pump pulse. It would appear, therefore, that for methane as well as hydrogen the use of waveguide techniques again looks highly promising as a means for reducing Raman Scattering thresholds below those of the tight focussing limit.

5.3.4 Numerical Predictions for SBS in Methane

A straight application of equation 5.24 to Brillouin scattering would again reveal that thresholds can be substantially reduced by using waveguides instead of tight focussing. Since the main interest of this thesis is towards the generation of longer wavelengths via SRS, however, our only interest here in Brillouin scattering is to determine under what conditions it can be avoided. We consider, therefore, specific examples of configurations that have relevance elsewhere in this thesis.

The first example is Brillouin scattering at 1.064μm in a 32cm long, 100μm bore radius waveguide at a number of different, but still fairly low, methane pressures. As in the case of the single-pass tight focussing experiments, a 30ns long pump pulse is used, which means that again we are not in the steady-state regime. This requires a modification of equation 5.24. To a good approximation one can replace $\ln(Ps(L)/Pso)$ by $T/4t\left[(\ln(Ps(L)/Pso)+ t/T\right]^2$, where t is the pump pulse length and T is the response time of the medium (again given by equation 3.35). Equation 5.24 becomes;

$$P_p = 0.885\pi W_o^2 \left[\frac{T/4t(30 + t/T)^2 + 2\gamma_s L}{g_B L_{eff}}\right] \qquad 5.26$$

Where again $W_o = 0.644a$ and g_B is now given by equation 3.57. Using this equation we obtain the predicted thresholds presented in table 5.3 for the various low pressures of interest. Also shown are the predicted Raman thresholds using the same method as described in the previous section;

Table 5.3: Predicted threshold powers for guided SRS and SBS using 1.064μm pumping in a methane filled waveguide of length 32cm and bore radius of 100μm

Pressure (Atm)	g_B (cm/GW)	P_{th} (Brillouin) (kW)	g_R (cm/GW)	P_{th} (Raman) (kW)
4.83	0.212	680	0.055	2554
5.87	0.313	485	0.064	2170
6.90	0.433	370	0.073	1905
10.35	0.974	197	0.100	1400
11.73	1.251	164	0.109	1282

Comparing with table 3.4 for tight focussing Brillouin thresholds in methane it is clear that at these low pressures even a 32cm long, 100μm bore radius capillary can reduce thresholds by an order of magnitude. Compare the values at ~10 Atm. The tight focussing threshold using the transient Boyd and Johnson theory (last column) predicts $P_{th} = 1.77$ MW. In the waveguide the threshold predicted is ~197kW i.e. a reduction of ~9. Also apparent from these results, however, is that even at these low pressures, where Brillouin scattering is discriminated against by the P^2 dependence of the gain, the predicted Brillouin thresholds are still very much lower than the Raman threshold powers for 1.544μm generation.

The second example to be considered is Brillouin scattering using a 1.064μm pump in an 82 cm long, 100μm bore radius waveguide filled with methane to various pressures. This time, however, a pump pulse length of 470ps is assumed.

Brillouin scattering is clearly goint to be in the transient regime and again the thresholds are calculated using equation 5.26. Gain coefficients and now response times are obtained from table 3.4 since we use the same pressures as were used there. The results are presented in table 5.4 along with the expected Raman thresholds, calculated as before. Note that Raman scattering is still in the steady-state regime.

Table 5.4: Predicted threshold powers for guided SRS and SBS using short pulse 1.064μm pumping in a methane filled guide of length 82cm and bore radius 100μm

Pressure (Atm)	g_B(cm/GW)	P_{th}(Brillouin)(kW)	g_R(cm/GW)	P_{th}(Raman)(kW)
10	0.909	3560	0.097	681
20	3.636	1780	0.153	433
25	5.681	1410	0.172	384
30	8.181	1180	0.188	350

We now have the opposite case to the previous example. Despite the fact that the steady-state Brillouin gain coefficients are much larger than the corresponding Raman ones, the Brillouin threshold powers are still much higher than the Raman threshold powers because of the extremely transient nature of the Brillouin scattering process. In this regime, therefore, we expect to be able to generate radiation at 1.544μm untroubled by Brillouin scattering and yet still with a low threshold. Compare, for instance, the threshold for Raman scattering at 30Atm from table 5.4 with the tight focussing values of 4.96MW from table 3.2. Again, we see a reduction of over an order of magnitude by using a waveguide.

The results of this and the previous two sections, therefore, show that under certain conditions and with suitable choices of parameters substantial threshold reductions can be achieved by the use of waveguides. In the next section a general expression will be derived to describe just how worthwhile the use of a particular waveguide actually is, and also the general competition between Raman and Brillouin threshold will be looked at with particular reference again to the use of guides.

5.3.5 General Points concerning Single-Pass SRS and SBS

The criterion for the worthwhile use of a waveguide as compared to tight focussing can be obtained simply by equating the thresholds for each, but also including a required threshold reduction factor R. Thus, from equations 5.24 for the waveguide and 3.25 for tight-focussing (i.e. assuming the analysis of Cotter et al) we obtain the expression;

$$R \times \frac{0.885\pi W_o^2\left[30 + 2\gamma_s L\right]}{gL_{eff}} \leqslant \frac{\lambda s}{4} \cdot \frac{\left[1 + \left\{1 + (19.11\lambda_p/\lambda_s)\right\}^{\frac{1}{2}}\right]^2}{9}$$

Rearranging gives us;

$$\left\{\left[\left(\frac{R \times 4.612a^2\left[30 + 2\gamma_s L\right]}{\lambda_s L_{eff}}\right)^{\frac{1}{2}} - 1\right]^2 - 1\right\} \frac{\lambda s}{\lambda p} \leqslant 19.11 \qquad 5.27$$

Where we have used $W_o = 0.644a$ and taken the tight focussing case of $\ln(^{Ps(L)}/_{P_N})/\arctan(^{L}/_{b_p}) = {}^{30}/_{1.57} = 19.11$. Equation 5.27 should apply well for Raman scattering where we have seen that the analysis of Cotter et al gives good threshold predictions.

Perhaps for Brillouin scattering it would be better to use the Boyd and Johnson predicted tight focussing expression given by equation 3.58. Then, for the steady-state, equation 5.27 must be replaced by;

$$\frac{1}{2} \cdot \frac{R \times 4.612a^2[30 + 2\gamma_s L]}{\lambda_s L_{eff}} \leqslant 19.11 \qquad 5.28$$

If the Brillouin scattering is also in the transient regime we need the further modification to;

$$\frac{R \times 4.612a^2}{(\lambda_s L_{eff}/15)} \frac{[T/4t(30 + t/T)^2 + 2\gamma_s L]}{[T/4t(30 + t/T)^2]} \leqslant 19.11 \qquad 5.29$$

Where, as usual, $\ln(P_s(L)/p_N) = 30$ has everywhere been replaced by $T/4t\ (30 + t/T)^2$, t being the pulse length and T the response time of the medium.

Thus, if we want to know when it just becomes worthwhile to use a waveguide we put R = 1 and use the equalities in equations 5.27 to 5.29. Taking the example of Raman scattering in hydrogen using pump radiation of various frequencies, equation 5.27 was used to plot the graph of fig. 5.5 for various lengths of waveguide up to 1m assuming Mariatilli and Schmeltzer losses. Clearly, for a specified length there are two bore radii between which the use of a waveguide gives a threshold reduction. More interestingly, fig. 5.6 shows a graph of the lengths and bore radii needed to give threshold reductions by specified amounts R for a 1.064μm pump when Raman scattering in hydrogen. Again equation 5.27 was used with theoretical straight guide losses. We can see clearly the expected trend of greater reductions being obtained by smaller bores at a fixed length - but only to a certain limit.

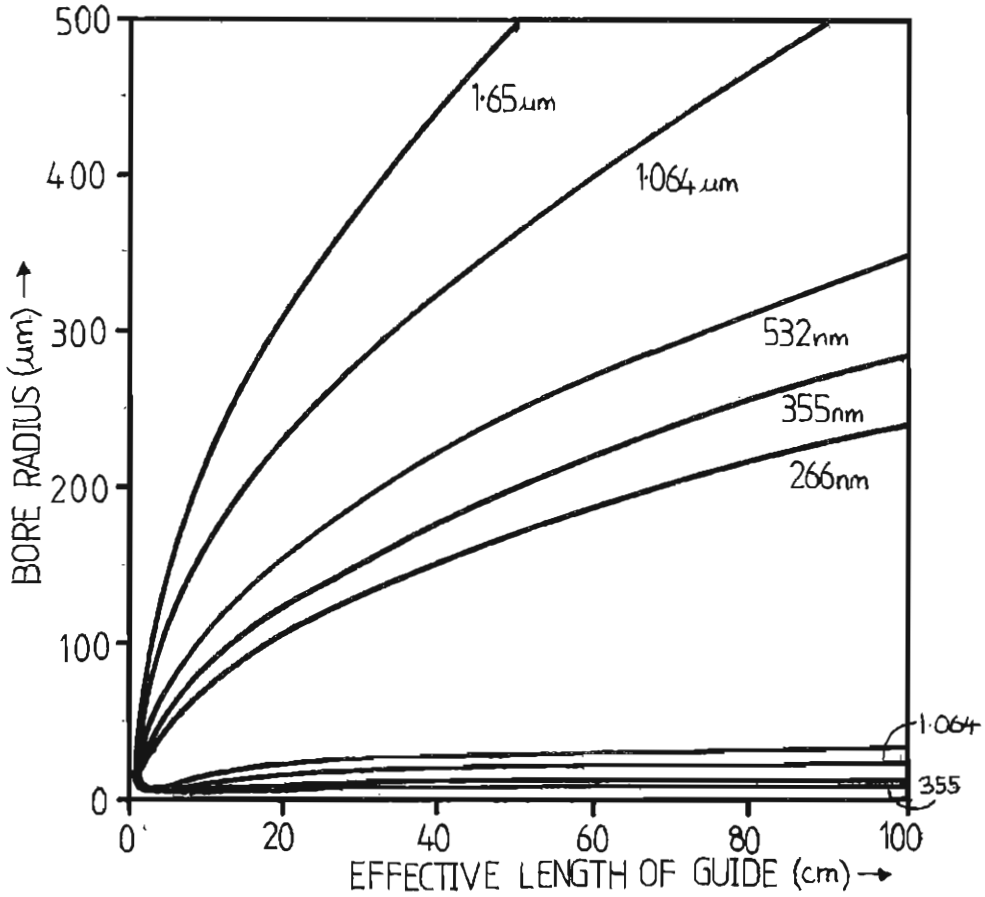

Figure 5.5: Graphs of waveguide lengths versus bore radius for R=1 (see text) and various pump wavelengths.

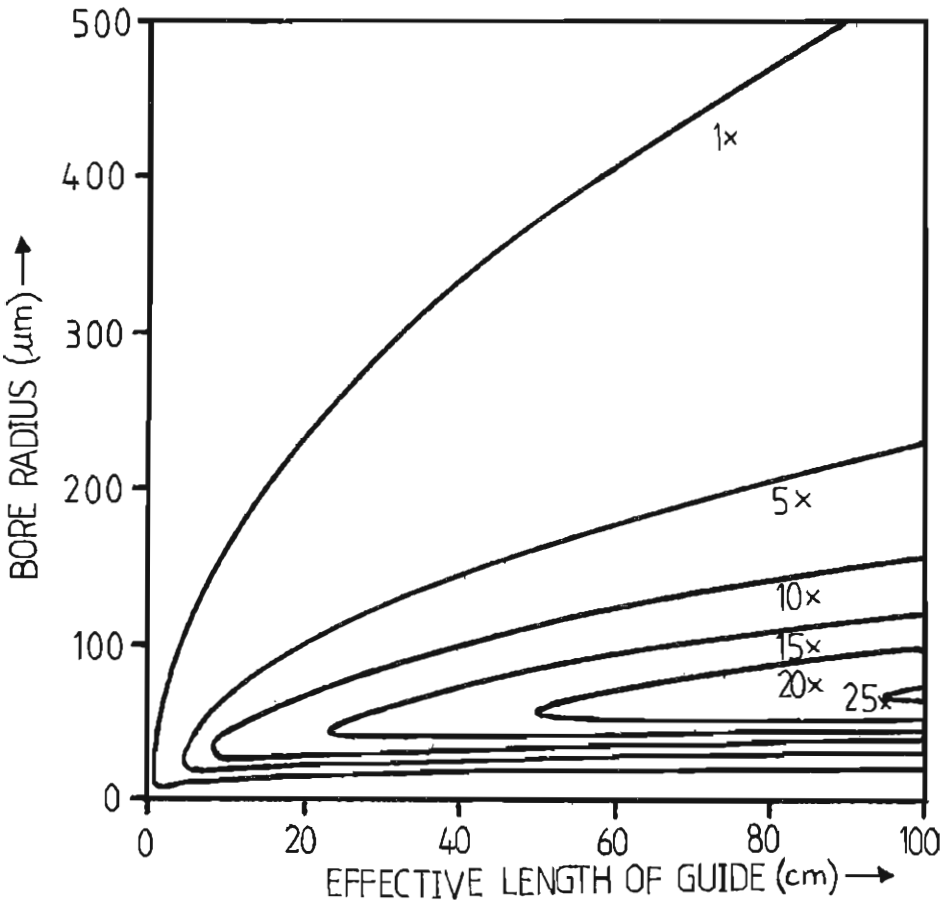

Figure 5.6: Graphs of waveguide lengths versus bore radius for various R and a 1.064μm pump.

For a chosen length it is possible that the increased transmission losses due to a reduced bore radius can start to have an effect before the threshold has been reduced by a specified amount. For example, when using a 50cm long capillary the maximum reduction obtainable is about 20, corresponding to the use of a bore radius of ~55μm. Reducing the bore radius further starts to decrease the reduction factor. But perhaps the most important point to be obtained from this graph is that the longer the length of the waveguide, then the greater the reduction factor that can be obtained if the optimum bore radius is chosen. Notice that a factor of 25 is to be expected for waveguides longer than about 95cm. But waveguides longer than this, however, are going to be inconvenient to use. It is clear, therefore, that these arguments suggest the use of waveguide resonators where the effective interaction length can be greatly increased and where further substantial threshold reductions should be obtainable as a result. This will be the subject of the next section.

Before moving on, however, we will investigate in more detail the competition between the Raman and Brillouin processes and how the use of waveguides allows us to discriminate against Brillouin scattering in cases where its steady-state, plane-wave gain coefficient is larger than that for Raman scattering.

If we just had steady-state, plane-wave scattering configurations all that would be required to reach threshold for either Raman or Brillouin scattering would be to ensure that the required steady-state, plane-wave gain coefficient was bigger than that for the competing process. In gases this can sometimes be achieved by altering the pressure. We have seen in chapter 3 that for methane the Raman gain coefficient g_R is proportioned to $P/\Delta\nu_R(P)$ and that the Brillouin gain coefficient is proportioned to P^2. Thus, for the pressure at which the gain coefficients are equal;

$$g_B(P_1) \cdot \frac{P^2}{P_1^2} = g_R(\lambda, P_2) \frac{P}{P_2} \cdot \frac{\Delta\nu_R(P_2)}{\Delta\nu_R(P)} \qquad 5.30$$

Using the values from chapter 3 it can be shown that for a 1.064μm pump in methane, equation 5.30 predicts that the gain coefficients will be equal at a pressure of P = 1.42 Atm (and not P=8.5 Atm as predicted by Murray et al, 1979). However, below this pressure one would require very high plane-wave pump powers to reach Raman threshold. Tight focussing helps, as we have seen, but the powers required are still too high. But using a waveguide reduces thresholds by more than an order of magnitude such that even at low pressures, where the gain coefficients are low, threshold can still be reached with reasonable pump powers. We saw an example of this in the last section. With these new configurations, however, equation 5.30 needs modifying to take into account effects such as wavelength dependent diffraction in the tight focussing case, and wavelength dependent losses in the case of waveguides. Also of importance, as we have seen, is the possibly transient nature of the nonlinear process where the steady-state gain coefficient is no longer the relevant one. If we restrict ourselves to the question "When will Raman threshold be reached before Brillouin threshold?" the answer can be written as the equation;

$$\frac{g_R}{g_B} > K \qquad 5.31$$

For the plane-wave, steady-state case the constant K = 1 but for the other cases just mentioned K is given by the expressions found in table 5.5. In each case the expression is derived by relating the relevant Raman and Brillouin thresholds and then rearranging to obtain an expression for g_R/g_B. In all cases the subscript S refers to the Stokes wavelength of the Raman process.

	WAVEGUIDES	TIGHT FOCUSSING (Cotter et al for both Raman and Brillouin)	TIGHT FOCUSSING (Cotter et al for Raman, Boyd and Johnson for Brillouin)
STEADY-STATE RAMAN AND BRILLOUIN	$\frac{30 + 2\gamma_S L}{30 + 2\gamma_P L}$	$\frac{\lambda_S}{\lambda_P} \frac{\left[1+\left\{1+(19.11\lambda_P/\lambda_S\right\}^{\frac{1}{2}}\right]^2}{30.065}$	$\frac{\lambda_S}{\lambda_P} \frac{\left[1+\left\{1+(19.11\lambda_P/\lambda_S\right\}^{\frac{1}{2}}\right]^2}{38.22}$
STEADY-STATE RAMAN TRANSIENT BRILLOUIN	$\frac{30 + 2\gamma_S L}{\left[T/4t(30+t/T)^2+2\gamma_P L\right]}$	$\frac{\lambda_S}{\lambda_P} \frac{\left[1+\left\{1+19.11\lambda_P/\lambda_S\right\}^{\frac{1}{2}}\right]^2}{\left[1+\left\{1+\frac{T}{4x1.57xt}(30+t/T)^2\right\}^{\frac{1}{2}}\right]^2}$	$\frac{\lambda_S}{\lambda_P} \frac{\left[1+\left\{1+(19.11\lambda_P/\lambda_S)\right\}^{\frac{1}{2}}\right]^2}{\frac{2T}{4x1.57 \times t}(30+t/T)^2}$

Table 5.5 Values of the constant K for tight focussing and waveguided configurations where the Raman process is steady-state and the Brillouin process is either steady-state or transient.

The subscript p refers to the pump as usual, but also to the Stokes wavelength of the Brillouin process which we assume is approximately equal to the pump wavelength. For the steady-state cases the constant K is generally of order unity, but for the transient Brillouin cases K can get very small implying that Raman scattering can still occur even though $g_R \ll g_B$.

This completes the analysis of single-pass SRS and SBS in waveguides. Substantial threshold reductions should be achievable and experimental verification of this will be described in the next chapter. The analysis in this last subsection, however, suggests that even further threshold reductions might be obtainable by constructing waveguide resonators, and it is this possibility that will now be investigated.

5.4 SRS and SBS in Waveguide Resonators

The simplified theory used in section 5.3 to develop expressions for single-pass nonlinear thresholds in waveguides was, as mentioned, strictly true only when there is only a low gain per waveguide transit. Clearly this is not true if one requires to reach threshold from noise in a single transit. Consequently a more rigorous analysis was required and was supplied by Ibison (1983). But in the waveguide resonator, as in the unguided resonator, threshold is reached over many Stokes transits, requiring, therefore, a relatively small gain per transit. Thus, the analysis outlined at the beginning of section 5.3 (derived from Boyd and Johnson) should, when extended further, be the appropriate one for describing adequately the operation of a waveguide resonator.

Thus, from equation 5.21, we find that the Stokes power after a single transit of length L through a waveguide of that length is given by;

$$P_s(L) = P_s(0)\ \exp\left\{\frac{gP_pL_{eff}}{0.855\pi(0.644a)^2} - 2\gamma_sL\right\} \qquad 5.32$$

This can be written as

$$P_s(L) = P_s(0)\ \exp\{gCP - 2\gamma_sL\} \qquad 5.33$$

Where; $$C = \frac{L_{eff}}{1.153a^2} \qquad 5.34$$

Equation 5.33 is now in the form of equation A1 in appendix III, where the general resonator threshold expression has been derived for a temporally varying pump power $P_p(t)$. If,therefore, a pump pulse with a Gaussian temporal profile is transmitted through the waveguide the peak pulse power necessary for threshold to be reached during this pulse is given by equation A7 and is reproduced here as;

$$P_{PO} = \frac{30 - (n-1/2)\ln(R_1R_2) - \ln(1-R_2) + 2n\gamma_sL}{g_FCS} \qquad 5.35$$

Where

$$S = 1 + 2b\ \exp\left\{\frac{-at^2}{T^2}\right\} + 2\exp\left\{\frac{-a(2t_T)^2}{T^2}\right\} + \ldots\ldots +2\ \exp\left\{\frac{-a\left[\left(\frac{n-1}{2}\right)\ t_T\right]^2}{T^2}\right\} \qquad 5.36$$

g_F is the plane wave gain coefficient for a Stokes wave travelling in the same direction as the pump. For Raman scattering this the normal situation but for Brillouin scattering $g_F \simeq 0$. Thus, only those terms in the summation are left which are multiplied by the factor $b = g_{Ba}/g_F$ where g_{Ba} is the coefficient for Stokes travelling in the opposite direction to the pump.

Note that because for Raman scattering $g_{Ba} \approx g_F$, the use of a resonator discriminates against Brillouin scattering. This is because there are twice as many terms in the summation for Raman scattering as there are for Brillouin scattering for the same number of transits. Note, however, that in general the summation is much greater than unity (the case for a single pass) and so, despite the increased value of the numerator due to various mirror losses R_1 and R_2 (and here we include the coupling losses from section 5.2) and transmission losses $2n\gamma_s L$, we expect to be able to obtain further significant threshold reductions over the steady state case. Indeed, equation 5.35 can be rewritten as follows:

$$P_{PO} = \frac{\left[30 - \left(\frac{n-1}{2}\right)\ln R_1 R_2 - \ln(1-R_2) + 2n\gamma_s L\right]}{gSL_{eff}/1.153a^2} \cdot \frac{\left[30+2\gamma_s L\right]}{\left[30+2\gamma_s L\right]}$$

$$P_{PO} = \frac{1.153Ka^2\left[30+2\gamma_s L\right]}{gL_{eff}} \qquad 5.37$$

Where; $$K = \frac{\left[30-\left(\frac{n-1}{2}\right)\ln R_1 R_2 - \ln(1-R_2) + 2n\gamma_s L\right]}{\left[30+2\gamma_s L\right] \times S} \qquad 5.38$$

We now have a direct comparison with the single pass threshold for a waveguide with the same length as the waveguide resonator length.

If we now demand a threshold reduction R' over the tight focussing case (Cotter's theory) equation 5.27 of subsection 5.3.5 becomes,

$$\left\{\left[\left(\frac{R'K \times 4.612a^2\left[30+2\gamma_s L\right]}{\lambda_s L_{eff}}\right)^{\frac{1}{2}} -1\right]^2 -1\right\}\frac{\lambda_s}{\lambda_p} \leqslant 19.11 \qquad 5.39$$

This equation is used in just the same way as equation 5.27. Indeed, the only difference is that R has been replaced by R'K. Thus, for the case of Raman scattering in hydrogen in waveguides of various lengths and bore radii, the same graph - fig. 5.6 - shows the expected threshold reductions where now the plotted curves are curves at constant $R = R'K$. Thus, the actual threshold reduction is given by $R' = R/K$, and since K is generally less than 1, the threshold reductions obtained from resonators are generally larger than those from a single pass waveguide of the same length. Clearly, this is because of an increased effective interaction length due to the many transits of the waveguide that the Stokes radiation makes whilst the pump is present. This becomes obvious if equation 5.35 is rewritten in the form;

$$P_{PO} = \frac{1.53a^2\left[30 + 2\gamma_s L\right]}{gL'_{eff}} \qquad 5.40$$

$$\text{Where } L'_{eff} = L_{eff}\cdot \frac{\left[30 + 2\gamma_s L\right]\times S}{\left[30-\left(\frac{n-1}{2}\right)\ln R_1 R_2 - \ln(1-R_2)+2\gamma_s nL\right]} \qquad 5.41$$

Going back to equations 5.35 and 5.36, however, the determination of the actual threshold reduction obtainable is now not only a question of choosing an optimum length and waveguide bore radius, but also a question of choosing mirror reflectivities R_1 and R_2.

Then there is the more important problem of determining how many terms should be included in the summation of equation 5.36 i.e. how many cavity transits are involved. It is clear that the terms in the summation of equation 5.36 get smaller and smaller as the number of waveguide transits n is increased i.e. each subsequent transit makes less and less of a contribution. On the other hand, the loss terms $-(\frac{n-1}{2})\ln R_1 R_2$ and $2n\gamma_s L$ get larger and larger as n is increased. Some point is going to be reached, therefore, at which the increased losses will cancel out the effect of a slightly increased interaction length. Up to this point the predicted threshold powers required will have been gradually reducing. This point, therefore, corresponds to the minimum threshold and the one which will be realised experimentally. In practice this minimum threshold condition can only be found by evaluating equation 5.35 on a computer for increasing values of n. At some value of n there will be a minimum. Obviously, choosing R_1 and R_2 as big as possible reduces the threshold, but the variation with R_1 and R_2 is not large. The difference in threshold between $R_1 = R_2 = 0.8$ and $R_1 = R_2 = 0.04$, i.e. a factor of 400 reduction in the product R_1R_2, is only about 30% (though it must be remembered that for the high reflectivity case the resonator is longer, contains more dead space and therefore allows fewer cavity round trips during the pump pulse time). We will make use of this fact in the next chapter where the construction of a very simple waveguide resonator will be described in which the end mirrors are formed by glass flats placed right up to the ends of the waveguide. As mentioned in section 5.2 this is the optimum position for a plane reflector as regards minimising coupling losses. Unfortunately, the small bore radii still implies pump intensities that would damage coated flats and so only uncoated flats can be used, and these provide the 4% reflectivities just mentioned in the example.

As we have just seen, however, it is not a problem as regards threshold reduction, but it does mean the resonator will have two outputs travelling in opposite directions. In general, however, it is always possible to allow a sufficient distance between waveguide and mirror with correctly chosen curvature such that the converging pump beam being injected is still large enough to pass through any coatings without damaging them. The space between mirror and waveguide end is also useful in that it means the mirrors used can be external to the high pressure waveguide cell itself, easing the problems of construction considerably. However, as we saw in section 5.2, certain spacings are better than others. With the small bore radii that tend to be used in practice, we are generally forced to use the $z/b \gtrsim 10$ criterion where z is the spacing a mirror of the correct radius of curvature needs to be placed from the end of a waveguide producing a TEM_{oo} Stokes beam of confocal parameter b. Under such condition coupling losses of less than 2% can be obtained, which make negligible differences to the predicted thresholds when combined into the R_1 and R_2 values.

But having an ample space between mirror and waveguide end has one further major advantage. It allows the inclusion of a dispersive element in the resonator - in the simplest case this could be a prism. The use of such a configuration becomes clear when we consider cases where the single pass waveguide thresholds of two competing processes are similar. The use of a dispersive element then ensures that the further threshold reduction obtainable by resonating the Stokes beam is only available to one of the nonlinear processes. An illustration of this effect can be derived from the first example of subsection 5.3.4. There the single pass SRS and SBS thresholds in a 32cm long, 100μm bore radius waveguide filled with methane to various pressures are predicted.

At 6.9Atm the predicted Raman threshold for an SLM, 30ns long 1.064μm pump pulse is 1905kW, whereas the Brillouin threshold is only 375kW (table 5.3). If, however, the dispersive resonator gives a further threshold reduction of more than 5.08 for Raman scattering, by resonating the Stokes wave at 1.544μm, and no further reduction for the Brillouin effect, then Raman threshold will be reached first. We shall see in the next chapter that this is indeed possible, the results agreeing well with theoretical predictions employing the experimental parameters.

Unfortunately, it is not a simple task to choose the optimum waveguide length, bore radius, reflectivities and pump pulse length that will give the minimum achievable thresholds. In practice it was more a case of trying resonators that could be conveniently built and then modelling them on a computer using equation 5.35. It is clear, however, that substantial further threshold reductions should be obtainable from waveguide resonators. This will be verified in the next chapter, where we shall also find that there is excellent agreement between experiment and the theory presented above.

5.5. SRS in Waveguides using Picosecond Pulses

We have seen in subsection 5.3.4 that the use of short pulses discriminates against the nonlinear processes with the longer response times because they become transient and experience a reduced effective gain. An example was given of how this effect could be used to prevent Brillouin scattering and allow Raman scattering in the case of 1.064μm pumping of low pressure methane. This example will be further analysed here to give predictions of the SRS behaviour.

5.5.1 Single-Pass Thresholds

If the Raman scattering process was still well into the steady-state regime and the pulses were bandwidth-limited, then the theoretical analysis and predictions presented in subsection 5.3.4 would still apply. The Raman linewidths ofmethane, given by equation 3.33 of chapter 3, correspond to the following reponse times T_2 at various pressures (Using $T_2\Delta\nu = 1/\pi$);

Table 5.6: Raman Linewidths and Response Times in CH_4

Pressure (Atm)	Linewidth (cm^{-1}) $\Delta\nu$,FWHM	Response Time (ps)
10	0.44	24
20	0.56	19
30	0.68	15.6

The strictly steady-state condition is $t \gtrsim 30T$, where t is the pulse length and T is the response time. Thus, a pulse length of 470ps is just about steady-state at the three pressures given. On the other hand, however, if the 470ps pulse is not bandwidth limited and contains structure that is slow compared with the medium response time, then a reduced threshold would be expected. This is the same type of behaviour as found in H_2 using a Q-switched laser and reported in Berry and Hanna(1983) (reproduced as appendix II).

Note, however, that the case of short pulses does not, in general, result in any lowering of the pump powers required to reach threshold. It does, on the other hand, greatly reduce the energies required in a single pulse.

This suggests that if a particular laser is capable of providing only a low, fixed energy output then Raman thresholds can still be reached if this energy can be supplied in a single, or at least a train, of short, high power pulses, as, for example, by mode-locking the laser. However, a pulsed, mode-locked laser still has an output of the general form shown in fig. 5.7. As can be seen, the energy is distributed in a train of pulses. If threshold is just reached by the largest pulse the energy in the other pulses is wasted. A more efficient way of using all the pulses to reach threshold, and hence reducing the overall energy required, is to extend the resonator idea to the form relevant to short pulses, that of a synchronously pumped resonator.

5.5.2 Synchronously Pumped Oscillator Threshold

The synchronous pumping of an unguided Raman resonator has been reported by Colles (1971).

Very simply, an arbitrary pulse in the mode-locked pulse train arrives at the input of the resonator just as the Stokes pulse generated by the preceeding pump pulse arrives back there, having been reflected by a mirror at the output end of the resonator. There is also a Stokes mirror at the input end, usually of 100% reflectivity, and so the Stokes pulse ends up travelling along in the forwards direction with the new pump pulse, being further amplified. This is shown in fig. 5.8. In order that this synchronous pumping can occur, the length of the Raman cell between the two Stokes mirrors must be chosen such that the Stokes pulse round trip time is equal to the time t_c between the individual mode-locked pump pulses.

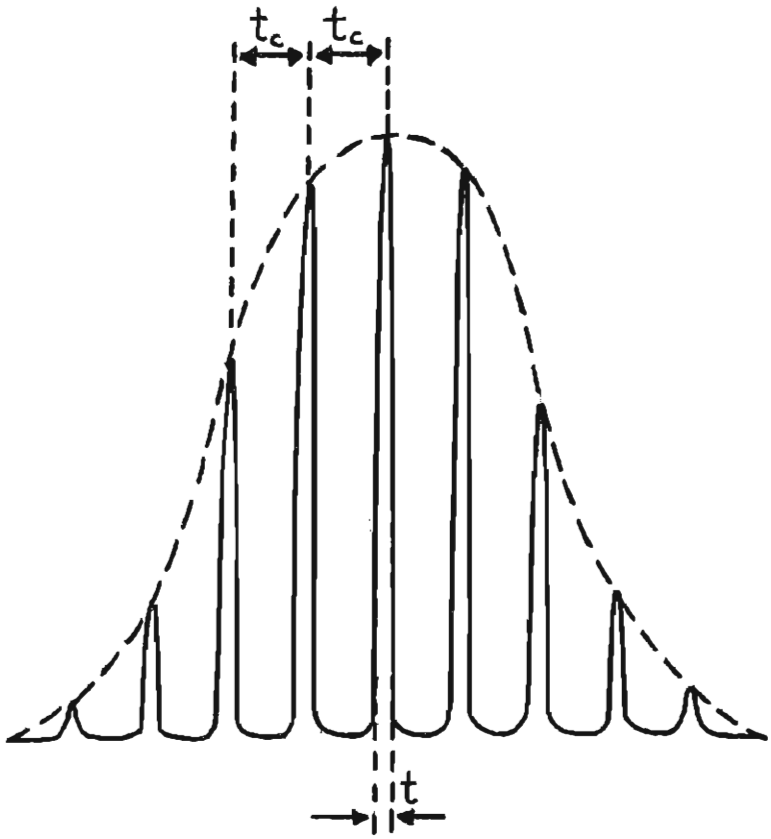

Figure 5.7: Typical output from pulsed mode-locked lasers. t_c is the laser cavity round-trip time, t is the FWHM of the individual pulses.

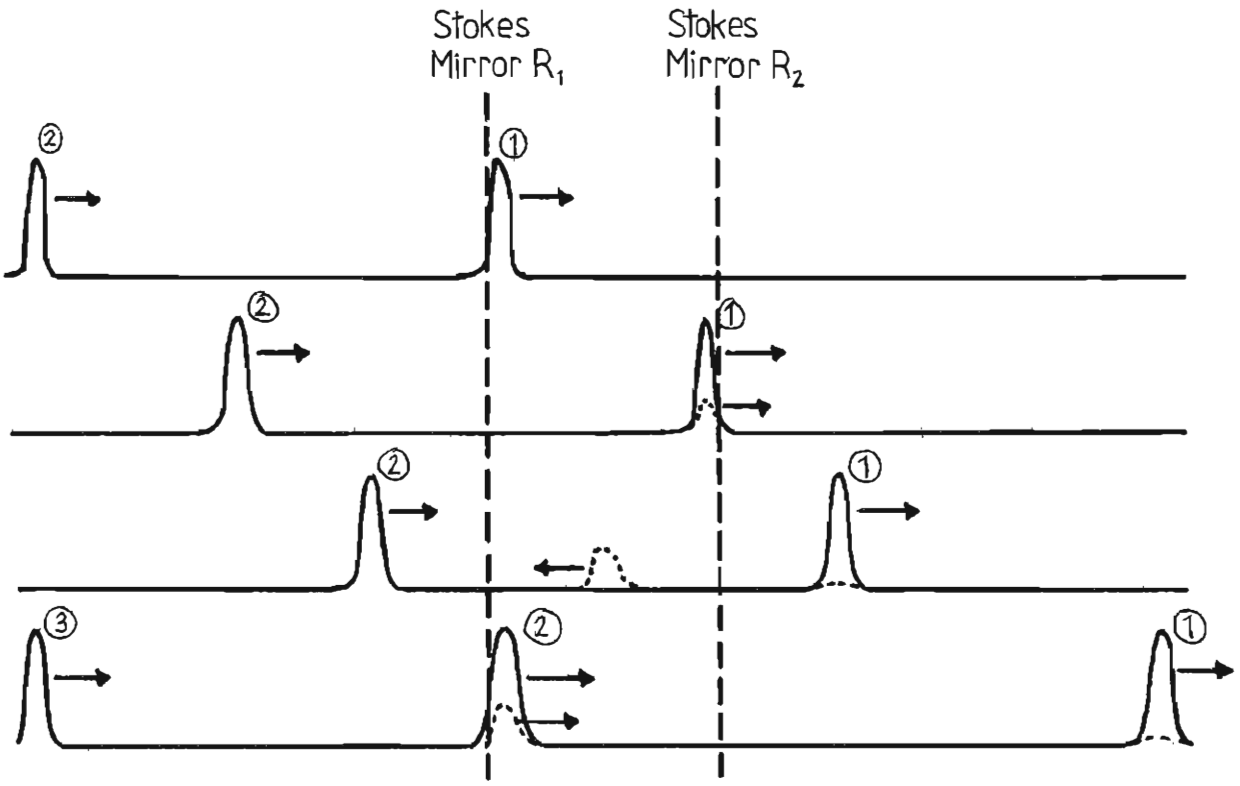

Figure 5.8: Schematic of the operation of a synchronously pumped Raman resonator. Pump pulses (full lines), Stokes pulses (broken lines).

In general, this means that the Raman resonator and the mode-locked laser cavity have approximately the same length. It is clear, however, that this arrangement makes good use of all the energy in a mode-locked pulse train and it suggests that the overall energy might be reduced whilst still reaching threshold.

A theoretical expression for the threshold power in the central maximum pulse of the mode-locked pulse train can be derived using the theory of appendix III. The only real difference between this situation and that analysed in appendix III is that we now have essentially no gain for the backward journey of the Stokes pulse. Equation A4 for the Stokes power leaving the resonator through output mirror R_2 is still;

$$P_{S,out_n} = P_{S0} \cdot (R_1R_2)^{\frac{n-1}{2}} (1-R_2) \exp\{-2n\gamma_s L\} \qquad 5.42$$

$$\times \exp\left\{ g_F C P_{P0} \left[f(t=0) + bf(t=t_T) + f(t=2t_T) + \ldots . \right.\right.$$

$$\left.\left. \ldots . f(t=(n-1)t_T) \right] \right\}$$

Where n is the number of Stokes resonator transits made. If P_{P0} is now defined as the power of the central maximum pulse in the pulse train and we set the f(t) with odd coefficients of t_T to zero (i.e. the backwards transits where there is no pump present) we can then rewrite equation 5.42 in terms of the number of pulses N in the pulse train;

$$P_{S,out,N} = P_{S0} \cdot (R_1R_2)^{N-1} (1-R_2) \exp\{-(2N-1)2\gamma_s L\} \qquad 5.43$$

$$\times \exp\left\{ g_F \, C P_{P0} \left[\frac{P_{P1}}{P_{P0}} + \frac{P_{P2}}{P_{P0}} \ldots . +1+ \ldots + \frac{P_{PN}}{P_{P0}} \right] \right\}$$

All the remaining f(t) have been replaced by the ratio of the power in the Nth pulse to the power in the highest power pulse, P_{P0}. These ratios can either be derived theoretically from theories of mode-locked laser outputs, or worked out experimentally from a photograph of the laser's output. The rest of the analysis proceeds in the normal way to give the threshold power of the central maximum pump pulse;

$$P_{th} = \frac{0.855nW_p^2\left[30-(N-1)\ln R_1R_2-\ln(1-R_2) + (2n-1)2\gamma_s L\right]}{g_F L_{eff} S} \qquad 5.44$$

Where;

$$S = \left[\frac{P_{P_1}}{P_{P0}} + \frac{P_{P_2}}{P_{P0}} + \ldots\ldots + 1 + \ldots\ldots + \frac{P_{pm}}{P_{P0}}\right] \qquad 5.45$$

This is the final result for the power in the largest, central pulse which will be necessary for the energy in the entire pulse train to treach threshold. Clearly, this energy can be derived from a knowledge of P_{po}, the pulse lengths of each pulse and the value of the summation of equation 5.45. As before we expect the value of the summation S to have a largereffect than the loss-induced increase of the numerator in equation 5.44, and so result in threshold power and total energy reductions. Experiments will be described in the next chapter where this theory is verified. Before ending this section, however,it is worth pointing out, as Colles did in his paper, that the synchronously pumped resonator has a further attractive feature when really short pump pulses are being used. Because of the normal dispersion of typical nonlinear media, a Stokes and a pump pulse will travel through it at slightly different speeds.

If the pulses are spatially very short this would result in them getting completely separated over a certain distance. The advantage of using a synchronously pumped resonator over a much longer one used in a single-pass configuration and pumped by a much higher power pulse is that this getting-out-of-step can be corrected for on every round trip simply by having the resonator just the right length. Our preliminary results will, however, be taken using 470ps pulses, a length at which dispersive effects are negligible.

5.6 Raman Oscillator-Amplifier Systems using Waveguides - A Discussion

In recent years interest has been growing in Raman oscillator-amplifier systems (e.g. H Komine et al, 1982). The main reasons for this are twofold. Firstly, they can result in higher conversion efficiencies to the higher order Stokes components than a single Raman oscillator can provide. Secondly, they allow energy scaling and better beam quality control. This second advantage is a result of the fact that if large energies are used to pump a typical Raman oscillator with a small beam waist in the centre, then either medium saturation, or even breakdown, are limiting processes. If, to avoid these problems, one uses a large mode-volume pumping geometry, unacceptable beam divergences tend to be the result. Thus, if a good quality, but low energy, Stokes beam can be obtained from an oscillator using only a small fraction of the pump,this can be injected into a large volume, high pump energy amplifier to produce a high energy, good quality Stokes output beam. A possible use for a waveguide in a system like this would be to ensure a low energy requirement for the Raman oscillator.

In this case even lower energies could be used to generate the good Stokes beam to be injected into the amplifier, leaving more energy for the amplification process itself. This is a technique currently being investigated for the new KrF fusion driver laser at the Rutherford Lab (C B Edwards, private communication).

Another interesting application of the oscillator - amplifier technique, one which we have investigated experimentally and is detailed in the next chapter, is as a means of discriminating against competing nonlinear processes whilst at the same time obtaining large amounts of energy at the required Raman Stokes wavelength. The medium used as an example of this is methane. The problem addressed was that of obtaining large amounts of 1st Stokes energy at 1.544μm using 50mJ, 1.064μm pump pulses which are SLM, TEM_{oo} mode and 30ns long. Bruns et al (1982) obtained about 25mJ of 1.544μ radiation from ~70mJ of the pump using just tight focussing in a simple Raman oscillator. They used, however, multi-longitudinal and multi-transverse mode pump pulses and consequently obtained an output beam with a broad linewidth and large divergence. The use of such a pump, however, did allow them to overcome the Brillouin scattering problem, which, as we have seen, would prevent Raman scattering if an SLM laser were used. We have also seen, however, that the use of a dispersive waveguide Raman resonator should allow the generation of small amounts of radiation at 1.544μm using a very low energy 1.064μm pulse which was non-the-less SLM, TEM_{oo} and 30ns long (subsection 5.3.5). Thus, if a small fraction of a 50mJ pulse is separated off and used to generate some 1.544μm radiation in a dispersive waveguide resonator, the rest of the pump radiation can be used to amplify this to a large energy in a large volume amplifier cell.

Such an amplifier, hopefully, can be operated at a pump intensity which, although sufficient to reach saturation for the Raman amplification process and hence result in high Stokes energies, is still below the Brillouin threshold intensity. This is feasible because the Brillouin wave must build up from noise whereas the Raman wave builds up from an injected signal of comparatively high power. The amplifier itself can just be an unguided, single pass methane cell where the high energy pump and Stokes to be amplified are arranged to be coaxial along its length, possibly with some mild focussing. Alternatively, a second, large bore waveguide can be used as the amplifier cell. If both pump and Stokes are matched into it optimally, as described in previous sections, we are again assured of complete overlap between pump and Stokes and therefore more efficient operation. Care must be taken, however, to ensure that the bore is not so small that the pump radiation reaches the Brillouin threshold.

The amplifier cell can be pumped in either the forwards direction (same direction as Stokes input) or the backwards direction (opposite direction to the Stokes input). The latter case is currently of particular interest because the resulting Stokes output pulses are considerably shortened temporally and can consequently reach powers much higher than the pump pulse (J M Murray et al, 1979 and references therein). Furthermore, backwards pumping prevents many competing processes, such as anti-Stokes generation, from occurring. Both forwards and backwards pumping, however, are limited by the fact that at a certain Stokes intensity level it will start to act as a pump source for 2nd Stokes generation. This again suggests that large volume amplifier cells should be used.

A further limitation when operating into the saturated gain regime is caused by the removal of molecules from the ground state by the Raman process. If the rate of excitation exceeds the rate of relaxation back there will be a reductior in the gain. Since in most gasses the relaxation time is longer than the pulse length t this condition is embodied in the equation (Glass 1967);

$$\frac{g I_p I_s}{\hbar w_s} \sim \frac{N}{t} \qquad 5.46$$

Where g is the plane-wave Raman gain coefficient, N is the number of molecules per unit volume, and I_p and I_s are pump and Stokes intensities. We require the LHS of equation 5.46 to be much less than the RHS if the gain is not to be reduced by this depletion effect.

Even if all those limitations are avoided, however, there is still the fundamental limitation that the number of photons in the Stokes pulse cannot exceed the number that was in the pump pulse. To get anywhere near this limit in practice one must use high intensity pump beams with "top hat" spatial and temporal profiles as described in, for example, Von der Linde et al (1969).

Thus, at best one can only achieve a factor of w_s/w_p of the energy of the pump ending up in the Stokes beam. The rest remains as material excitation. For pump and Stokes beams which are both approximately Gaussians in space and time, we must expect energy conversion efficiencies substantially less than this. Despite, this, however, we expect to be able to achieve quite respectable photon conversion efficiencies to the first Stokes in Methane, and consequently to obtain substantial amounts of energy at 1.544μm in a narrow linewidth, diffraction limited beam.

6, EXPERIMENTAL INVESTIGATIONS OF NONLINEAR OPTICS IN WAVEGUIDES

The experimental investigations which will be described here provide a test of the theoretical calculations and predictions presented in the previous four chapters.

The chapter will begin with an experimental check of the basic waveguiding properties of hollow, fused-quartz capillaries. The results of particular importance will be the transmission and the output beam characteristics. Details of the construction of practical high pressure waveguide cells are then presented. This is followed by a description of the first guided SRS and SBS experiments. To begin with, simple, single-pass experiments are performed in hydrogen and methane using various waveguides and pump wavelengths. It will be shown that substantial threshold reductions are obtainable and the results will be compared favourably with the theoretical predictions. Following this the experiments performed in waveguide resonaors will be described. Of particular importance will be the demonstration that even lower thresholds can be obtained than in the case of single-pass experiments, but also the resonator allows useful discriminations to be made between competing nonlinear processes. The results of these experiments will also be compared favourably with the theoretical predictions of the last chapter. We have seen that it ought to be possible to discriminate against the nonlinear process with the longest response time by using shorter pump pulses. Thus, the next set of experiments will be concerned with Raman scattering in a methane filled waveguide using picosecond pulses. Two basic configurations will be looked at, the straightforward single-pass arrangement, and the sychronously pumped Raman resonator. In each case the measured threshold powers and energies will be compared with theory. We shall find that, as predicted, very low energy thresholds can be obtained.

Finally, the experiments performed on Raman oscillator-amplifier systems will be described. These will show that, as expected, quite large amounts of 1st Stokes energy at 1.544μm can be obtained from two methane filled waveguide cells; one a dispersive waveguide resonator, the other a forwards or backwards pumped single-pass waveguide amplifier; when pumped with the SLM, TEM_{oo} mode, 1.064μm output of the telescopic resonator.

6.1 Experimental Investigations of the Waveguiding Properties of Fused-Quartz Capillaries

From the theory of the previous chapter we expect hollow cylindrical waveguides to be capable of transmitting a high quality beam over large distances with a low loss. We shall investigate in this section whether all these expectations are borne out in practice.

6.1.1 The Choice of Waveguide

Given beams with cylindrical symmetry, it was an obvious choice to use hollow cylindrical waveguides, and this much was assumed in the development of the theory of the previous chapter. The choice of material is a different matter, however. The requirements are simply that the waveguide chosen will give as high a transmission as possible for a TEM_{oo} mode input beam, whilst at the same time not damaging when quite high powers are used. Marcatili and Schmeltzer (1964) show that a cylindrical metallic waveguide can provide much better transmissions than a glass guide of the same dimensions. There are drawbacks, however, to metallic guides. They have much lower power handling capabilities and, in any case, the low loss modes are the TE modes and not the TM and EH modes which now have very high losses.

Thus, there is no linearly polarised, nearly transverse EH_{11} mode with which a TEM_{oo} mode can couple efficiently.

So metallic guides are not suitable for our intended use. The next general choice is for non-conducting dielectric waveguides. Marcatili and Schmeltzer show that the EH_{11} mode is the mode with the lowest loss only if n_1, the refractive index of the cladding material, is less than 2.02. The optimum value is actually 1.73. All this is suggesting the use of a cylindrical glass waveguide with a refractive index around 1.5. This is an ideal choice since the waveguides are easy to construct and are readily available in the form of capillaries. The theory presented in the last chapter assumed that the refractive index of the cladding was, in fact, entirely real, i.e. absolutely no absorbtion of the guided radiation was assumed. At visible and near infrared frequencies fused-quartz best fits this prescription and so fused-quartz capillaries were chosen as the waveguides for use in all our experiments. Most of the fused-quartz capillaries used were obtained from "Heraeus Silica and Metals, Ltd". Since waveguide straightness is expected to be important the capillaries should ideally be of the "precision bore" variety, though at the time of writing this was unavailable in fused-quartz. The rest of the wave-guides used in our experiments were, in fact, very thin fused-quartz capillaries made by the Fibre Optics group of Southampton University. The most common type had dimensions of 200μm i.d. and 320μm o.d. These had tolerances better than the ±10μm quoted for precision bore pyrex capillaries, but because of their very small size were difficult to hold straight anyway. In use, however, they were held in the core of a larger capillary with a 330μm bore diameter whose straightness, therefore, determined that of the smaller capillary.

Ideally, the larger capillary should have a precision bore, and since it is not acting as the waveguide, it need not be fused-quartz (for example, pyrex would be suitable). It must be noted at this point, however, that precision bore does not mean that the bore does not wander about sideways within the bulk of the capillary, only that the diameter is a fixed value within certain tolerances. Thus, it is still possible to have bends within the waveguide. In practice, therefore, one must resort to testing each capillary experimentally to establish its quality.

The theory of the previous chapter also assumed that the cladding material extended to infinity. Clearly, this is not the case with a capillary, and in particular not the case with the very thin ones where the walls are only 60μm thick. Marcatili and Schmeltzer recommend frosting the outside of any glass waveguide so that there are no reflections to interfere with the waves within the core and cladding. Interference from such a source could easily increase the loss coefficients.

Finally, the theory assumed that the waveguides had abrupt ends, their faces normal to the direction of propagation. Great care must be taken, therefore, when cutting a capillary to length. Each end is generally checked with a microscope objective to ensure an unbroken inner edge. A clean break when cutting the capillary generally ensures this, and such a break is normally obtained by putting a small scratch on one side of the capillary with a carborundum blade and then bending the capillary the other way until it snaps.

Having prepared the waveguide the first property of interest is generally its transmission since this quantity gives a good indication of the waveguide quality.

6.1.2 Preliminary Transmission Measurements

Transmission measurements involve the accurate matching of a TEM_{oo} mode beam into a waveguide. To achieve this either the beam axis and direction must be adjustable or the waveguide must be moveable. The latter proved to be the easiest approach to take. Figure 6.1 shows the basic experimental arrangement and also the adjustments that must be provided for the waveguide to allow optimum alignment. The laser can be any laser that provides a clean TEM_{oo} mode output. Clearly, therefore, the telescopic resonator is one choice but also a Helium-Neon laser was used with the further advantage that it is conveniently visible. The harmonics of the 1.064μm output from the telescopic resonator could also be used, but the resulting beam qualities are generally not as good as that of the fundamental as a result of the transmission through the many optical elements that generally have to be used, in particular the harmonic generating crystals themselves. In general, the beam from the laser requires a matching lens or lenses to produce the appropriate waist size exactly at the entrance of the capillary. Again, the fewer the number of lenses the better, and one is usually sufficient. It has been found that the transmissions obtained when using longer focal length lenses as the final matching lens are slightly better than those obtained when using a shorter focal length. The reason for this is possibly related to aberations introduced by the lens.

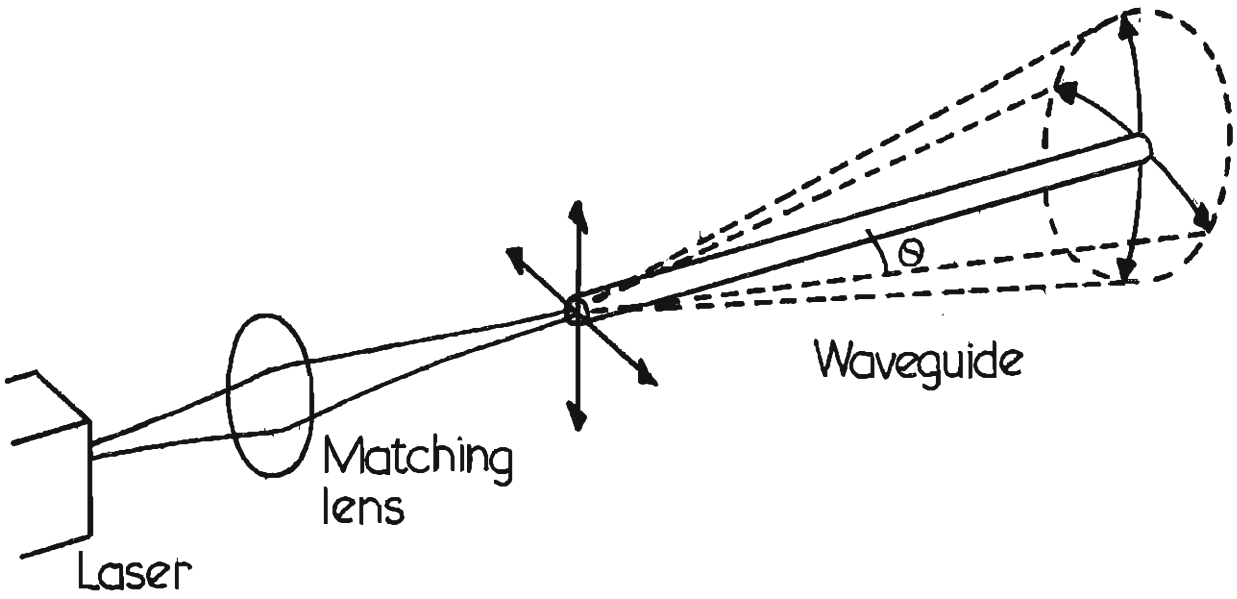

Figure 6.1: General experimental arrangement for transmission measurements showing the waveguide movements necessary for alignment.

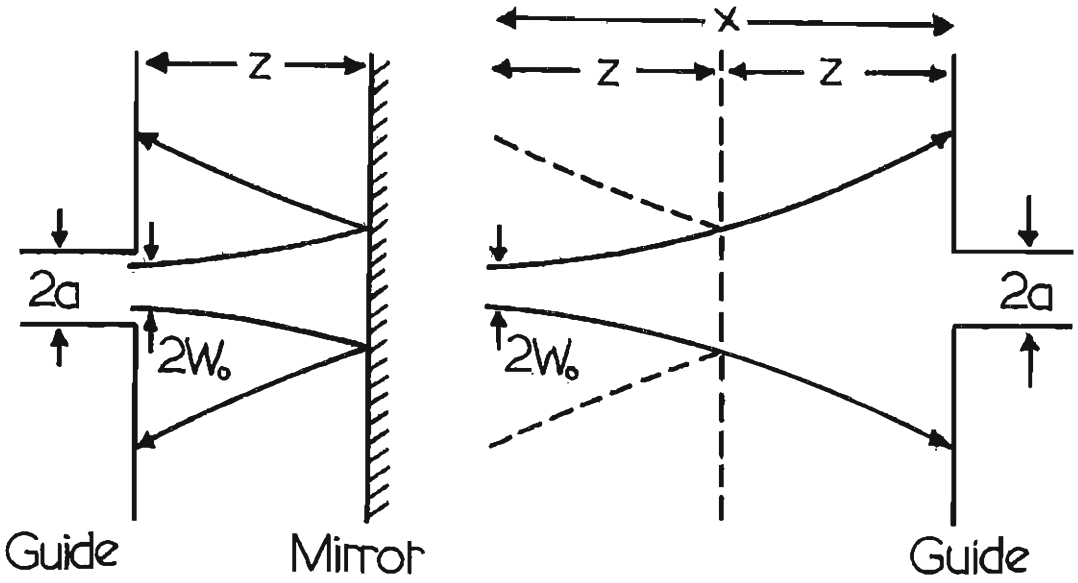

Figure 6.2: Comparison between matching an EH_{11} mode back into a guide using a plane mirror and the problem of the non-incidence of pump waist and waveguide entrance.

The waist size the lenses are chosen to produce at the entrance to the guide is the one given by Abram's criterion; $W_o = 0.644a$, where a is the waveguide bore radius.

Thus, having set up the laser and the matching optics the waveguide entrance is placed at the beam waist. The longitudinal accuracy with which this must be done can also be deduced from the work of Abrams (1972). He considers, amongst other things, the overall coupling losses for an EH_{11} mode leaving a waveguide, travelling to a plane mirror, being reflected, and then re-entering the guide as an EH_{11} mode. This is very similar to the case of a TEM_{oo} mode waist size located at a finite distance from the guide. The similarity is made clearer by fig. 6.2. Abrams' results, reproduced as fig. 5.4 of this thesis, show that the coupling losses can be kept below 2% for $z/b_p < 0.1$, b_p being the confocal parameter. In our case this clearly modifies to $X/b_p < 0.2$ where X is the distance between waist and capillary entrance. For the smallest waveguides used b_p is of order 1cm and so the tolerance is down to $\approx$ 2mm.*

The transverse tolerance is, of course, much less than this since typical bore radii are themselves only a few hundred microns. In practice misadjustments of around 1/10th of the diameter start to reduce the transmission, so this can put tolerances as low as $\pm$ 20μm for the smaller capillaries.

Once the input end of the capillary has been positioned using vertical and horizontal translation stages the output end must be adjusted to ensure that the capillary is optimally aligned axially. These adjustments must not alter the position of the input end and so need to be about axes lying in the input plane, as shown in fig.6.1.

* This agrees well with the results of Hall et al (1977) (their fig.2) where b_p = 1.4m and they can vary d/f by $\pm$ 30%. For f = 1m this means d can vary by 25cm. Thus, our $x/b_p = 0.25/1.4 \approx 0.2$.

Thus, the arrows showing the necessary movements for the input end also denote the axes around which the capillary must pivot, and so the supports must be designed accordingly. This overall axial adjustment can, of course, be provided by vertical and horizontal translation stages somewhere near the other end of the capillary, the exact position and means of support not being critical. An estimate of the upper limit on the angle θ between guide axis and ideal beam axis can be obtained by considering the half divergence angle of the beam at the input. This is given by $\theta_D = \lambda/\pi W_o$. The required angular tolerance θ is expected to be less than this, the equality being shown in fig. 6.3. Taking the example of a 200μm bore diameter capillary with a 1.064μm pump one obtains $\theta_D = 5$mRad. Thus, even if we have a metre long capillary the vertical and horizontal adjustments on the far end must be accurate to less than 5mm, and in fact be more like 1 or 2mm. Correct positioning can be ensured by monitoring the mode structure of the output beam, as we shall see later.

Perhaps the most important experimental consideration is the method by which the waveguide is supported and kept straight. We have seen that bends in capillaries can substantially reduce the transmissions, particularly for the larger bores and shorter wavelengths. A capillary supported at its ends as described above would sag in the middle under its own weight. The solution is to mount it in a straight holder which has negligible sag. Initially, the capillaries were clamped into a piece of extended aluminium angle which acted as a V-groove. The final solution used, however, involved clamping them to a specially made precision V-groove, as shown in fig. 6.4. The vertical and horizontal adjustments at either end of the capillary must now be fixed to this V-groove whilst still allowing the various movements just described.

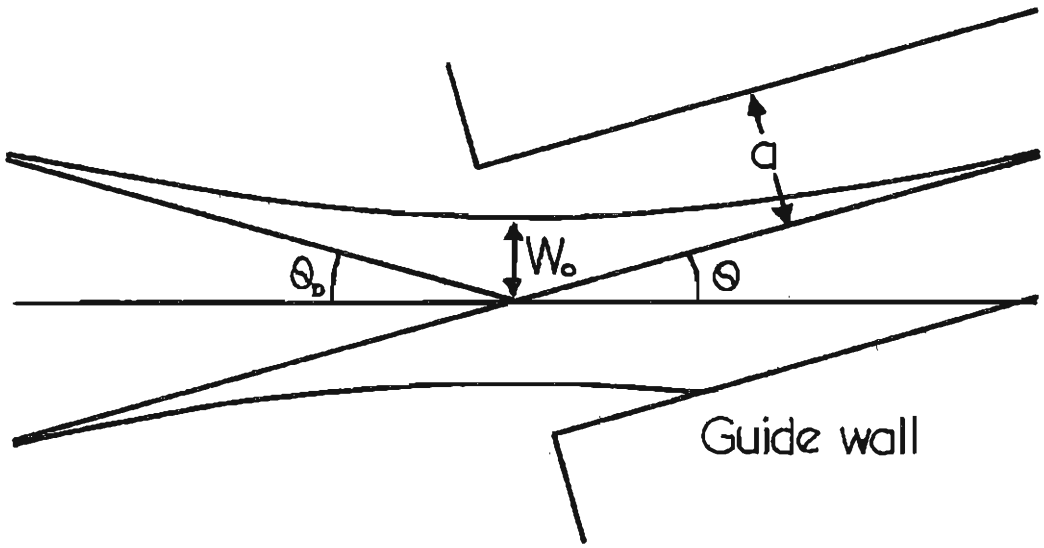

Figure 6.3: Injecting a beam into a misaligned waveguide. The example shown is where $\theta = \theta_b$.

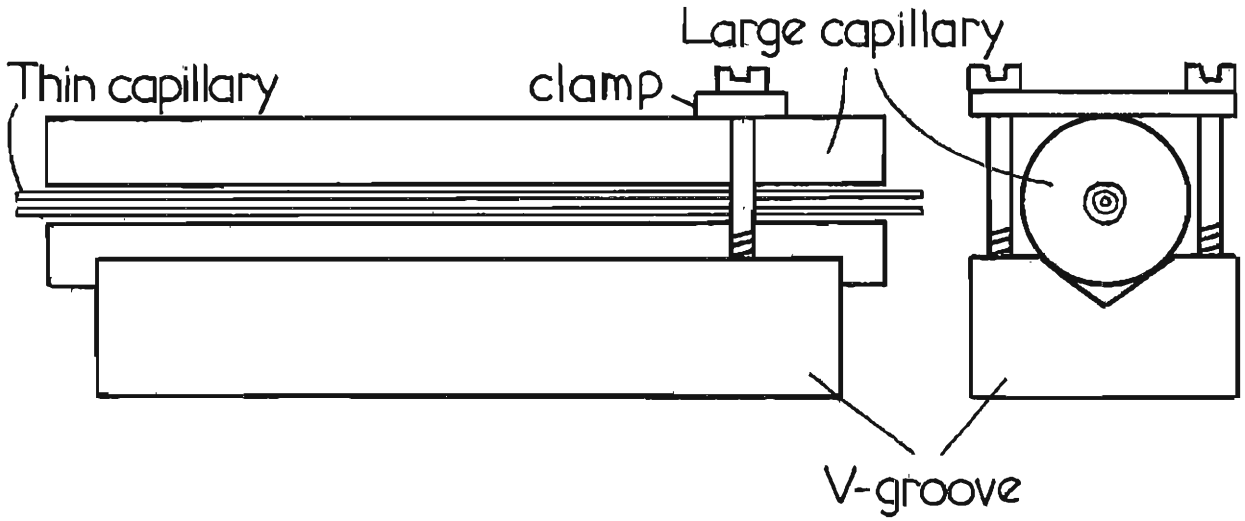

Figure 6.4: Diagram of capillary and V-groove arrangement. The thin capillary in the bore of the larger capillary may or may not be present. Note that there are many clamps along the whole length of the capillary.

Finally, the waveguides must be as clean as possible. Any dirt inside the bore can either be blown out with compressed air or washed out with a suitable solvent such as acetone. We are now in a position to align the capillaries and measure the transmissions. A capillary is considered to be optimally aligned when the transmitted energy or power is a maximum and emerges from the capillary in a TEM_{oo} mode output or as near as one can get to one. When using a Helium-Neon laser the output mode structure can be seen on a piece of white card. When using an Nd:YAG laser burns on photographic paper give an adequate indication of the mode structure. In the case of the HeNe laser, input and output powers were measured with a large area photodiode and voltmeter. For the YAG laser an energy meter was used to measure the input and output energies. Table 6.1 shows some typical results, and also lists the theoretical predictions of chapter 5, section 5.1, where 2% has been subtracted from each value to account for coupling-in losses (section 5.2). The results for guides 1 and 2 show good agreement between experiment and theory and imply that these were good capillaries. The three results for capillary number 3 show the importance of using a precision V-groove - although not quite as high as the values theoretically predicted, the use of the precision V-groove gives a marked increase in the measured transmission. The result for capillary 4, which is a thin walled, 200μm i.d. capillary, shows reasonable agreement with theory. The results for capillaries 5 and 6 which should be approximately the same, show how important it is to check the capillary transmission first before use. One gives a near theoretical transmission whilst the other gives a transmission substantially lower. The discrepancy can be due to bends in the capillary, bends in the supporting capillary, faults in the capillary - including dirt, or degradation of the input beam due to poor quality optical elements.

Capillary No.	Bore Radius (μm)	Length (cm)	Support	Wavelength (nm)	Exp. Trans.	Theoretical Trans
1	315	100	Precision V-Groove	1064	93%	95%
2	165	100	Precision V-Groove	633	92%	94%
3	165	100	Aluminium Angle	1064	60%	84%
3	165	100	Precision V-Groove	1064	75%	84%
3	165	100	Precision V-Groove	633	82%	94%
4	100	100	Precision V-Groove	633	67%	82%
5	100	25	Inside a 165μm Capillary Held at its ends	1064	90%	92%
6	100	32	Inside a 165μm Capillary Held at its ends	1064	65%	92%
7	100	30	Inside a 165μm Capillary Held at its ends	633	90%	95%

Table 6.1 Measured capillary transmissions and theoretically predicted transmissions for a straight guide.

As with Hall et al (1977) we feel that these results are consistent with the general λ^2/a^3 dependence of the loss coefficients given by equation 5.10 of the previous chapter. As can be seen, however, each capillary must be checked before use and its transmission measured. In most of the experiments that follow in the rest of this chapter the actual value of the transmission need not be the theoretical one as long as the actual value is known. The measured transmission can always be accounted for as a new effective length for the interaction, as previously described in section 5.3 (equation 5.25).

6.1.3 Characteristics of the Output Beam from a Waveguide

The output beam from a waveguide, when it is properly aligned, is expected to be a TEM_{oo} mode with the same polarisation as the input beam. We also expect the transmission to drop and the spatial profile to become multimode as the angle θ in fig. 6.1 is increased.

The TEM_{oo} mode behaviour was checked using a diode array at a known distance from the end of the capillary. The spatial profiles were the same as those of fig. 2.8 in chapter 1, with widths at the $1/e^2$ points corresponding to those expected for a TEM_{oo} mode ($\pm$ 10%). This was the case for both 633nm and 1.064μm pumping. When using 1.064μm pumping the output beam could burn photographic paper, the results being similar to those shown in fig. 2.7 of chapter 2. Hall et al (1977) also found the output beam in the far-field to be a good TEM_{oo} mode.

The polarisation of the output beam was checked using a 1.064μm pump of a known polarisation, either linear or circular. The transmission was found to be the same for both polarisations and further, the use of another polariser in the output beam from the capillary revealed that the plane of polarisation was also unaltered by transmission through the guide.

(the fact that the transmission for circularly polarised light is the same as that for linearly polarised light can be understood by considering the circularly polarised light to be resolved into two orthogonal linearly polarised light waves)

The effect of misaligning the capillary has been looked at by Hall et al (1971) but was also examined in this work. In all cases transmissions began to drop and multimode output behaviour began to manifest itself when the misalignment θ was increased to something approaching the half-divergence angle θ_D, this being the behaviour expected from subsection 6.1.2.

6.1.4 Power Handling Capability of Waveguides

When using very small bore waveguides the intensities can be very high despite the fact that the powers may be quite modest. Because the waveguides are hollow, however, we expect to be able to transmit peak intensities that are much higher than the intensities that would damage a sample of the surrounding material, in this case, fused quartz. Not unexpectedly, damage has always manifested itself first at the entrance to the capillary where the inner edge of the capillary is exposed to the wings of the Gaussain distribution. It is possible that damage is aggravated by the presence of a sharp edge.

Despite this, however, we still expect to be able to transmit peak intensities much greater than the damage intensities for quartz, which for pulse lengths of order 25ns are generally considered to be around 4-8GW/cm^2. The reason is simply that at a distance $a = (1/0.644)W_o$ from the axis the intensity is given by;

$$I(a) = I_o \exp\left\{\frac{-2 \times (1/0.644)^2 W_o^2}{W_o^2}\right\} = 0.008 I_o$$

Where I_o is the peak intensity on axis. Thus, the intensity is two orders of magnitude down at the inner walls of the guide. Even allowing for a very large edge sensitivity this should allow peak intensities higher than $\sim 6 GW/cm^2$. This was confirmed by passing 50mJ, 25ns, 1.064μm pulses through a 1m long, 165μm bore radius capillary. Peak intensity $I_o = 2P/\pi W_o^2 = 11.3\ GW/cm^2$. A 100μm bore radius capillary did, however, damage when the peak intensity was increased to $9 GW/cm^2$ (600kW pulses). It is doubtful, however, that much higher intensities could be used anyway since they would probably exceed the breakdown values for the gases of interest for nonlinear interactions.

In both of the cases mentioned above (just below 600kW for the second example) misaligning the input end of the capillary resulted in its total destruction. Similarly, when the waveguide entrance was replaced by a quartz flat, this too was damaged.

6.1.5 High Pressure Waveguide Cell Construction

This chapter has so far dealt with the properties of free standing waveguides with both ends open to the atmosphere. Our interest however, is in waveguides filled to a high pressure with a gaseous nonlinear medium. It is necessary, therefore, to construct high pressure waveguide cells whilst preserving the favourable waveguide properties investigated so far.

Ideally, a high pressure cell should be built which includes Brewster input and output windows and into which could be fitted the entire assembly of waveguide and precision V-groove support.

This would have to incorporate the necessary adjustments discussed in subsection 6.1.2, in particular it must pivot around a point corresponding to the exact centre of the waveguide input plane. Such a cell would be rather large, rather expensive and probably somewhat inflexible in use if capillaries of different lengths and bores are to be investigated. In practice, two basic arrangements were used, both of which had slight drawbacks but were much more flexible and convenient to use. The first arrangement was suitable for short capillaries where straightness could be adequately obtained just by choosing a good piece of capillary and supporting it near either end. Consequently, the same high pressure cells as were used in chapter 4 could be used with the capillary resting on two O-rings in the stainless steel tubing, as shown in fig. 6.5, design 1. This arrangement enables Brewster windows to be used and so experiments can be performed in the knowledge that there is no window induced feedback. Obviously the distance between capillary end and Brewster window can be made large enough to avoid damage to the window by a high power pump beam. Care must be taken, however, to determine exactly where the end of the capillary actually is. This is important for good beam launching, where account must also be taken of the optical thickness of the windows, but also for mounting the cell on translation stages, where we require that, as near as possible, the cell pivots about this end. Cells of this design are suitable mainly for waveguide oscillators that require a short cavity and external mirrors. Because of their short lengths they do not, in general, provide as great a threshold reduction as one would like from single-pass configurations.

More suitable for this type of experiment is design 2 of fig. 6.5. Here the capillary itself is used as the high pressure gas cell. The capillaries are easily strong enough to withstand the high pressures used, having, in fact, the optimum geometrical shape for such a task.

Design 1

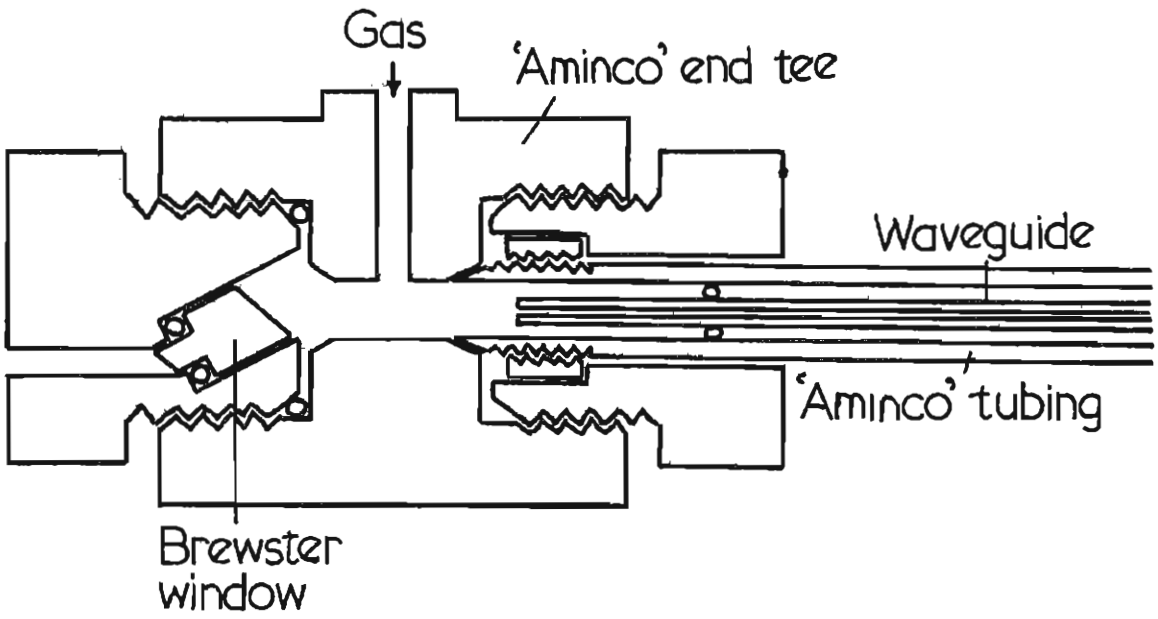

Design 2

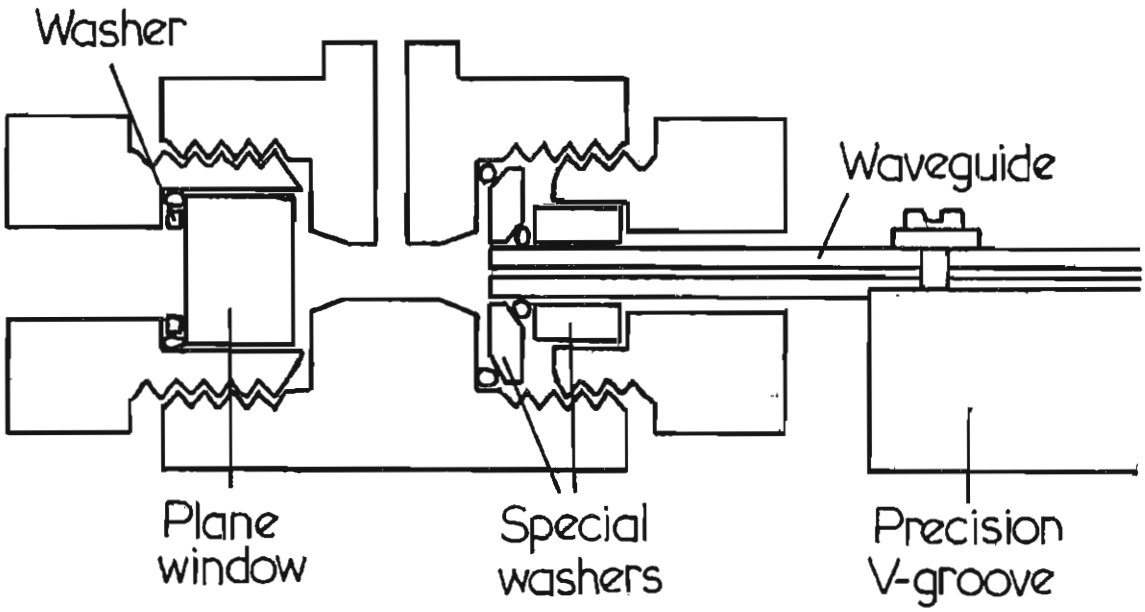

Figure 6.5: The two basic high pressure cell designs.

The advantage of this arrangement is that now the capillary can remain clamped into a precision V-groove. Consequently, much longer waveguide lengths can be used than in design 1, and we have typically used a length of around 100cm. The disadvantage, however, is that now some sort of end window arrangement must be securely fastened to the end of the capillary itself. As can be seen the high pressure seal is provided by compressing two O-rings as the bolt is tightened up, one between the capillary and a washer, the other between the inside of an "Aminco" end tee and the same washer. The end tee must be supported in some way so that its weight does not bend the capillary. Also, it must be prevented from moving longitudinally otherwise the high pressure in the cell would push it off the end of the capillary. Consequently, the end tee and the V-groove must be held rigidly together in such a way that the capillary is not bent, and does not bend when gas at high pressure is admitted. This requires careful adjustment and is the main drawback to this arrangement. Connected with it is the fact that in our experiments this was only achievable with small 'Aminco' end tees, into which Brewster windows could not be fitted. Plane windows were used, therefore, and consequently small arbitrary amounts of feedback are possible.

Table 6.2 shows some transmission measurements for typical cases and compares them to the free-standing and theoretical values. As can be seen, the transmissions (which are corrected for passage through the cell windows) remain essentially unchanged for cells of design 2, and indeed can still be very close to the theoretical ones. For the cell of design 1, however, the transmissions are not quite so good, though it must be pointed out that this design tended only to be used with the very thin bore capillaries held with a capillary of a larger bore.

Capillary No.	Bore Radius(μm)	Length (cm)	Support	Wavelength (nm)	Exp. Trans.	Theoretical Trans.
1	315	100	Free-standing on Precision V-groove	1064	93%	95%
1	315	100	Design 2, Fig. 6.5 on Precision V-groove	1064	90%	95%
3	165	100	Free-standing on Precision V-groove	1064	75%	86%
3	165	100	Design 2, Fig. 6.5 on Precision V-groove	1064	75%	86%
5	100	25	Inside a 165μm Capillary held at its end	1064	90%	92%
	100	25	As above but in a cell Design 1	1064	75%	92%

Table 6.2 Comparison between the transmission of capillaries when free-standing and when incorporated into high pressure gas cells filled to around 25-30 Atm.

One possible explanation for this is that astigmatism resulting from the passage of the beam through a Brewster window could decrease the coupling efficiency to the EH_{11} mode of the guide.

All the other properties of TEM_{oo} mode output, polarisation, temporal profile, and sensitivity to mis-alignment remained unchanged. On the whole, therefore, we can conclude that high pressure cells can be built which include waveguides that perform largely as they should, as determined from the theory of the previous chapter.

6.2 Single-Pass Raman and Brillouin Scattering Experiments

The experimental investigation of single pass Raman and Brillouin thresholds in waveguides will now be described. The results obtained will be compared with the values predicted in section 5.3 of the previous chapter. Typical output energies and conversion efficiencies for the 1st Stokes components will be quoted, and the spatial quality of the Stokes output beam will be investigated. It is worth mentioning again here that the use of a waveguide in single-pass operation has been reported elsewhere by Rabinowitz et al (1976) and Hartig and Schmidt (1979). They concentrate, however, on the increased conversion efficiencies that the use of waveguides allows and make no specific reference to the threshold reducing capability. Similarly, 'Lambda Physik' have just begun to market a Raman shifter that incorporates a hydrogen filled waveguide. They use it to shift an Excimer pumped dye laser further towards the infra-red and claim the use of the waveguide increases the conversion efficiencies and improves the spatial quality of the output beam.

In the present work, however, most of the experimental effort is concentrated on investigations of the threshold behaviour because it is this which determines whether the Raman process is within the reach of low power or low energy lasers.

6.2.1 The General Experimental Arrangement

The general experimental arrangement is the same as that shown in fig. 4.1 of chapter 4 where now the simple unguided cell shown there is replaced by one of the two waveguide cells shown in fig. 6.5. The telescopic resonator, harmonic generator, beam attenuator and matching optics have all been discussed, although there are a few extra experimental points that must be mentioned.

Most of the extra considerations derive from the fact that the use of waveguides involves critical matching and alignment tolerances, as previously discussed. Firstly, the very fact that some of the capillaries to be used have bore radii as small as 75μm requires that the beam does not wander transversely from shot to shot. Fortunately, the telescopic resonator provides such a beam, this being another of its many advantages. Beam steering problems could occur, however, in experiments employing an eximer pumped dye laser as the pump source. The beam from an excimer moves around somewhat from shot to shot and results in corresponding movements in the output of the dye laser.

Similarly, the two-plate beam attenuator must be very accurately aligned to ensure that when the angles are set the beam is not deviated. This is rather difficult to achieve in practice and usually required a subsequent slight realignment of the waveguide to be made.

Perhaps a better method of beam attenuation in this case would be the use of a half-wave Pockells cell followed by a polariser. Increasing the voltage on the Pockells cell decreases the power passing through the polariser without in any way deviating the beam. In practice, however, the two-plate attenuator was just about adequate, though in some cases additional fixed glass plate attenuations were needed to get the powers low enough - a clear indication that thresholds are being reduced by the use of waveguides.

Where possible a single, high quality lens was used to match the waist at the output of the telescopic resonator to a waist at the input of the waveguide. The TEM_{oo} mode output of the telescopic resonator allowed the use of the simple Gaussian beam theory of Kogelnic and Li (1966) for the matching calculations In all cases occasional checks of spot sizes (using a travelling slit) and focus positions (using a rule) agreed well with this theory. When setting the distance between matching lens and capillary entrance, allowance must be made for the additional path in the cell window. The end of the capillary must be moved back a distance $d = t\ (1 - 1/n)$ where t and n are the thickness and refractive index of the window. The windows were either spectrosil B or BK7, although it should be noted that BK7 windows are unsuitable for use with a 355nm pump, a wavelength at which the absorption has become appreciable resulting in a low damage threshold.

The gas handling system for the waveguide cells was the same as for the cells in the unguided experiments. The cells themselves could be either free-standing or permanently connected. In the latter case care must be taken to ensure that the flexible stainless steel tubing leading to the waveguide cell does not exert any appreciable strain on it that would cause gradual misalignment.

In all cases the waveguide cells were aligned to give maximum transmitted pump energy in a good TEM_{oo} mode when being pumped well below threshold power. This involved different diagnostic equipment in the various cases examined and so they will be treated separately when we come to them. Similarly, the method of threshold detection varied from case to case and this too will be dealt with in the same way.

6.2.2 Stimulated Raman Scattering in Hydrogen

Our first investigations of Raman scattering in single pass waveguide cells utilised high pressure hydrogen as the nonlinear medium. To begin with the pump wavelength was restricted to the fundamental of the Nd:YAG laser at 1.064μm, and the results were published in Berry et al (1982) (and presented here as appendix IV). Later the harmonics of Nd:YAG at 532 and 355nm were used as the pump radiation. All pulse lengths were of order 10-40ns and when SLM were therefore in the steady state regime.

Various capillary bore radii were tested, most of them around 1m in length. Consequently, all the waveguide cells were built as in design 2 of fig. 6.5. Thus, all the capillaries were clamped to a precision V-groove, but also had to be used with plane windows. When using 1·064μm as the pump the capillaries were aligned by monitoring the transmitted power with a JK Lasers power meter which utilised an integrating silicon photodiode. The telescopic resonator could be run fixed-Q so that no damage would be done by capillary misalignment. The output beam quality was monitored by burns on photographic paper or just a phosphor card held in the beam.

When optimally aligned an energy transmission measurement was made using a calorimeter. When using 532nm as the pump the output beam quality was monitored by viewing it on a white screen and the capillary was adjusted for optimum energy transmission by monitoring it with a pyroelectric energy meter that responds to a single shot. To obtain sufficient green the telescopic resonator had to be partially Q-switched, but care was taken to ensure the power was still below the Raman or damage thresholds. For the 355nm pump the spatial quality could be deduced from the fluoresence off white card, the pyroelectric energy meter was again used to monitor the transmitted energy and again the telescopic resonator was partially Q-switched. For both 532 and 355nm pumping the transmissions were measured using either a disc or a cone callorimeter.

Threshold was generally detected by monitoring the transmitted pump power with a vacuum photo-diode and transient digitiser. As in the case of the tight focussing experiments, threshold is marked by a tiny dip near the top of the otherwise smooth Gaussian temporal profile, the monitoring equipment and experimental arrangement being the same as that described in chapter 4.

For all threshold measurements it is necessary to know the pulse length (FWHM) and this is measured by monitoring the input beam with the photodiode and digitiser but now with the path to the waveguide cell blocked off. Threshold energies are measured in the same way as the transmission energies, but as near to the input of the waveguide cell as possible. Threshold powers, defined as the peak power of a Gaussian pulse with a full width at half maximum intensity of T, are given by;

$$P_{th} = \frac{0.94E_{th}}{T} \qquad 6.1$$

Where E_{th} is the energy per pulse that actually arrives at the entrance to the waveguide at threshold and is therefore corrected for any relevant window or lens losses.

The experimental results are presented in table 6.3 along with the measured pump transmissions. Also listed are two sets of theoretically predicted thresholds given by equation 5.24. This equation is presented again here in the slightly modified form;

$$P_{p,th} = \frac{1.153a^2\left[30 + 2\gamma_s L\right]}{g L_{eff}} \qquad 6.2$$

When L_{eff} includes the measured transmission losses in terms of a modified loss coefficient along the lines of equation 5.25, equation 6.2 predicts threshold powers that can be compared directly with the experimental results. When L_{eff} includes a pump loss coefficient given by the theory of Marcatili and Schmeltzer equation 6.2 then predicts the theoretical best threshold powers.

As can be seen from table 6.3, all the experimental results except one are a little lower than the theoretically predicted results when the measured transmissions are taken into account (penultimate column). This discrepancy, though not a very large one, is attributed to the arbitrary amounts of feedback provided by the plane windows of the waveguide cell. The theory of appendix III reveals that even small amounts of feedback can lower thresholds appreciably and could easily account for this effect. As a test of this supposition, however, one measurement was made of the single-pass Raman threshold in a hydrogen filled waveguide cell incorporating Brewster windows.

Bore Radius (μm)	Pump (nm)	Length (cm)	Pressure (psi)	Transmission	Expl. Threshold (kW)	Theory Threshold (kW)	Theoretical Best (kW)
315	1064	100	400	90%	470	525	-
165	1064	100	400	60%	130	180	149
165	532	110	400	70%	30	40	34
100	532	110	320	28%	15	20.1	13.2
100	355	110	320	43%	7	8.4	6.34
75	1064	110	400	15%	70.5	66.3	54

Table 6.3 Threshold results and theoretical predictions from table 5.1 for single-pass Raman scattering in waveguides.

The cell was necessarily of design 1 in fig. 6.5 and therefore contained a short capillary supported on two O-rings, one at each end. In fact, a thin 100μm bore radius was held within a thick, 165μm bore radius capillary supported at its ends. The length of the thin capillary was 28cm, its transmission was 63% for 1.064μm pumping and the cell was filled to 350psi. The experimentally measured threshold power was 265kW. The theoretical prediction, incorporating the 63% transmission measurement, was slightly lower at 240kW. Clearly, feedback has been eliminated and the agreement between theory and experiment is better in this case. The theoretical best thresholds show that the imperfect waveguide transmissions do not have too important an effect on the final expected threshold powers. Typically, there is only about a 15% difference.

The most important result, however, is that the threshold powers are, indeed, substantially reduced below the corresponding single-pass, tight focussing results. This was expected from subsection 5.3.2 of the last chapter, the numbers being shown in table 5.2. In particlar, the 70kW result obtained for 1.064μm pumping in a 75μm bore radius capillary represents a 20-fold reduction over the tight-focussing limit. As a demonstration of the usefulness of diagrams like fig. 5.6 in subsection 5.3.5, take the case of the result for the short 100μm bore radius capillary in the cell with Brewster windows. The effective length works out at 22cm (equation 5.23) which for a 100μm bore radius predicts a threshold reduction of almost exactly a factor of 5. The tight focussing threshold for 1.064μm is 1370kW. The experimental result of 265kW therefore represents a reduction of a factor of 5.17, demonstrating again the excellent agreement.

Typical first Stokes output energies and photon conversion efficiencies for 1.064μm pumping are shown in table 6.4 below. Unless otherwise stated the pump pulse was SLM. All the results were taken in hydrogen at around 400psi. The first Stokes energy at 1.907μm was measured using a pyroelectric energy meter behind a mirror with a high reflectivity at 1.064μm and a germanium filter (Transmission ≈30% at 1.907μm).

Table 6.4 Guided SRS performance above threshold in H_2 using a 1.064μm pump

Capillary Description	Pump Energy (mJ)	Stokes Energy (mJ)	XThreshold	Photon Conv. Efficiency
L = 100cm, a = 315μm	17.5	1.0	1.33	10%
L = 28 cm, a = 165μm	11.1	1.1	1.10	18%
L=100 cm, a = 165μm	11.9	1.0	2.82	14.5%
As above, fast Q-switching	14.4	1.59	3.20	20%
Tight Focussing	49	3.59	1.40	13.1%

The photon conversion efficiencies for these small bore waveguides seem to be similar to those for tight focussing and so consequently the energies of the first Stokes outputs bear the same relation to the input pump energies.

Of great interest, however, is the beam divergence of the 1st Stokes output beams. This is expected to be diffraction limited to within about 10-15%. The optical arrangement used for checking this is shown in fig. 6.6.

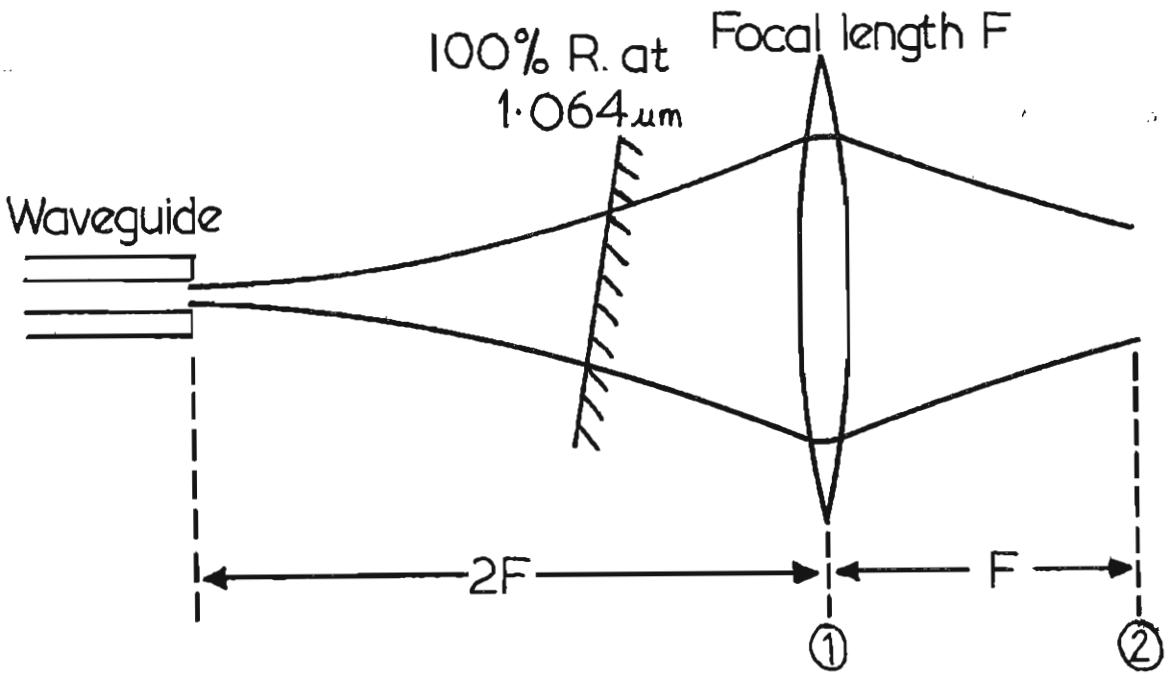

Figure 6.6: Optical arrangement for measuring the divergence of the Stokes output beam.

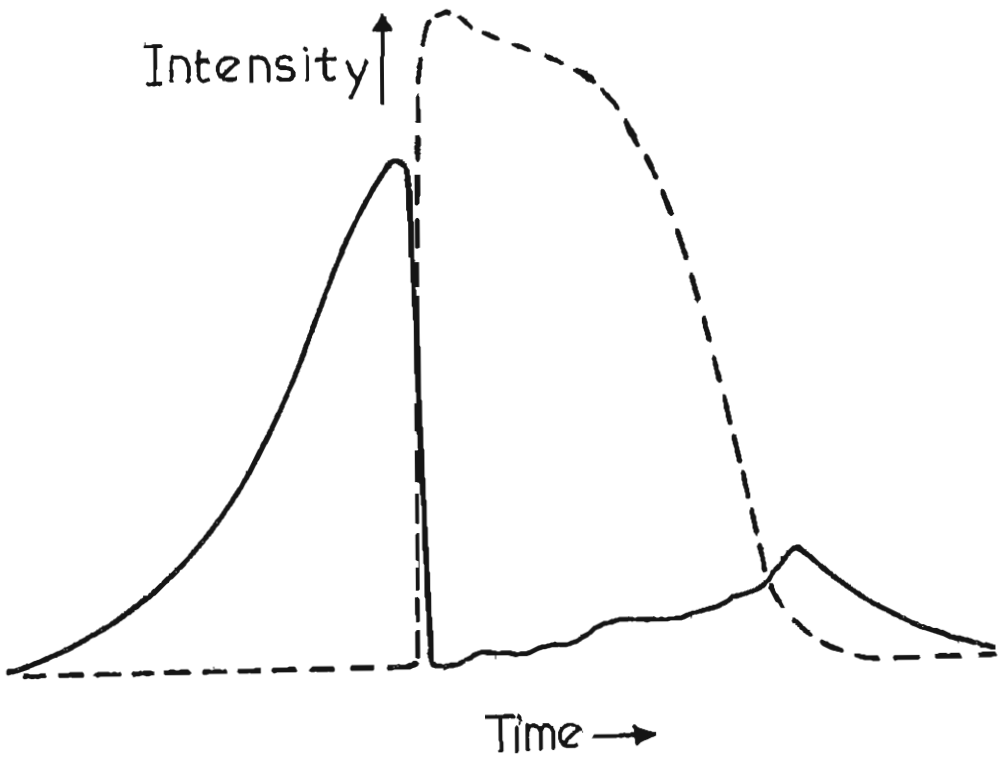

Figure 6.7: Typical temporal profiles of Stokes (broken line) and transmitted pump pulse (full line).(not the same scale in the vertical direction)

A travelling slit with the pyroelectric energy meter attached to it was used to measure the spotsizes at positions (1) and (2). The spotsize was taken as half the distance between the two points at which the measured energy was $1/e^2$ times the maximum energy in the centre. The test was performed on the 28cm long, 100μm bore radius capillary in a cell with Brewster windows. A 15cm focal length lens was placed 30cm from the output. At the lens position the Stokes spotsize was measured to be 3.25 mm when operating the cell at 1.1 x threshold. Assuming a TEM_{oo} mode this implies a waist size of $W_o = 60\mu m$ at the capillary exit, not very different from the 64μm expected. This in turn implies that if the output is indeed a TEM_{oo} mode the spotsize in the focal plane of the lens should be given by;

$$W = F \cdot \frac{\lambda}{\pi W_o} \qquad 6.3$$

which in our case is 1.66mm. The experimentally measured value is 1.8 ± 0.2mm suggesting that our output beams are diffraction limited to within about 10%.

Figure 6.7 shows typical temporal profiles of the generated 1st Stokes pulse and the transmitted pump pulse. The traces are not to the same scale in the vertical direction that measures power, but the temporal behaviour is on the same scale. As can be seen, a sudden Stokes growth coincides with a sudden pump depletion, and the Stokes carries on for the same length of time as the pump shows this depletion. Threshold, as expected, occurs somewhere before the peak of the pump pulse.

This completes the description of our experimental investigations into the behaviour of the steady state single-pass Raman scattering process in hydrogen filled waveguides.

The use of waveguides substantially reduces the threshold powers below those for the unguided, tightly-focussed limit, and the reduction is in accordance with theory. The Stokes output is diffraction limited and although there was not much of an improvement in the conversion efficiencies obtained at pump power levels comparable to the threshold power with the small bores used, the Stokes energies produced were still at a respectable and useful level.

6.2.3 Stimulated Raman and Brillouin Scattering in Methane

The theoretical calculations of subsections 5.3.3 and 5.3.4 of the previous chapter predicted that for the longer wavelengths (1μm and above) and for SLM pulse lengths of order 10's of nanoseconds FWHM, the single-pass Brillouin scattering threshold would always be lower than the Raman scattering threshold for any size of capillary filled with methane gas at any pressure above about 1.5 Atm. Consequently, the required shifting of the pump to longer wavelengths by SRS is not possible.

Various experimental results confirmed this prediction, one of which will be given here and will also serve to demonstrate that we have a good enough understanding of SBS to be able to avoid it whenever necessary.

The experiment to be described involved pumping a waveguide cell of design 1, in fig. 6.5, which contained a 30cm long, 100μm bore radius thin capillary held inside a 29cm long, 165μm bore capillary supported at both ends with an O-ring. The pump radiation was at 1.064μm and the pulses were SLM with a 30ns pulse length.

The cell was filled with methane to various pressures between 4 and 12 Atm.

The experimental arrangement was again as shown in fig. 4.1 of chapter 4, but this time included an angled glass flat in the input which would allow the monitoring of any backwards travelling radiation at 1.064μm from the SBS process. The experimental procedure was the same as for the hydrogen experiments, threshold being detected either by pump depletion or (for Brillouin thresholds) the detection of a backwards travelling wave at 1.064μm using either a silicon PIN photodiode, an S1 vacuum photodiode or even a phosphor card.

As expected Brillouin threshold was reached first at all methane pressures. The experimental results are listed in table 6.5 along with the predicted thresholds given by equation 5.26 and already presented once in table 5.3. Note that though the Brillouin process is in the transient regime the thresholds are still found to be somewhat lower than the steady state Raman thresholds. The theoretical values incorporate the measured transmission of the capillary, which in this case was a rather poor 60%.

Table 6.5: Experimental and theoretical thresholds for guided SBS in CH_4 using a 1.064 μm pump

Pressure (Atm)	Brill.Thresh(Expl) (kW) (± 30%)	Brill.Thresh(Theory) (kW)	Raman Thresh(Theory) (kW)
4.83	573	680	2554
5.87	465	485	2170
6.90	300	370	1905
10.35	200	197	1400

An estimated experimental error of 30% is associated with the experimental results mainly because of the inaccuracy of the particular gas pressure meter used. Since Brillouin thresholds vary as P^2, inaccuracies in the pressure can have quite a large effect. Despite this, however, it is clear that good agreement still exists between experiment and theory.

The main result, however, is the fact that the use of a waveguide has substantially reduced the Brillouin threshold powers below the tight-focussing, unguided limit. At 10 Atm, for example, this is 1.77MW (Table 3.4). This is to be compared with the value of 200kW from table 6.5 above. There is a factor of 8.5 reduction, just the value expected from the theory. The beam quality of the backwards scattered Brillouin Stokes wave was looked at briefly using a phosphor card and photographic paper. The beam profile was perfectly circular and appeared to be the same size as the input beam at the same distance from the waveguide cell.

Raman threshold can, of course, be reached in methane using picosecond pulses and this is the subject of another section. An alternative method that still employs SLM pulses in the 10-30ns range, however, is the use of a dispersive waveguide resonator. This and other waveguide resonators will be described in the next section.

6.3 Capillary Waveguide Resonator Experiments

As suggested in sections 5.3 and 5.4 of the previous chapter, the nonlinear threshold powers should be reduced even further by allowing the generated Stokes radiation to resonate between suitable mirrors placed at the two ends of the waveguides.

Some of the results of the operation of waveguide resonators have already been published in Berry and Hanna (1983), a paper which is included here as Appendix V. In what follows, the design and construction of different types of waveguide resonators will be described, and their operation when filled with hydrogen or methane and pumped with pulses of various wavelengths will be compared with the operation expected from the theory of section 5.4 in the last chapter.

6.3.1 The General Experimental Arrangement

Again the experimental arrangement is the same as that shown in fig. 4.1 of chapter 4. This time, however, an angled glass flat in the input beam to the waveguide resonator is used to monitor possible Raman Stokes components travelling in the backwards direction as well as any Brillouin scattered radiation that may occur. The waveguide resonators themselves were of two basic types, both of which are shown schematically in fig. 6.8. Type 1 incorporates the basic single-pass waveguide cell given as design 1 in fig. 6.5. This stands on its own complete with its own horizontal and vertical adjustments at either end. Completely separate to this, at either end, are the Stokes resonator mirrors. In practice, these usually consist of a lens and plane mirror arrangement, the two elements being as close together as possible. In accordance with the requirements outlined in section 5.2 of the previous chapter the effective radii of curvature of these lens/plane mirror combinations are chosen such that they allow a convenient, although quite short, spacing between lens and capillary end whilst satisfying the two condtions of;

Radius of curvature of mirror = radius of curvature of Stokes wavefront

and;

$$z/b \geq 10$$

Where b is the confocal parameter of the Stokes wave leaving the capillary and z is the distance between capillary end and the lens/plane mirror combination. In practice, if the waveguide has a 100μm bore radius, a 15cm focal length lens placed at $z = 14.9$ cm satisfies these conditions. The confocal parameter $b = 1.35$ cm and so $z/b = 11$. For optimum coupling it is advisable to ensure that the lens and mirror combination can be moved axially as one unit. In addition to this it must be possible to make the normal angle adjustments to the plane mirrors. Ideally the reflectivity of the input mirror should be zero for the pump and 100% for the Stokes being resonated. Both lenses should be A.R. coated for both wavelengths. The output mirror should also have zero reflectivity for the pump, the reflectivity for the Stokes wave being a matter of choice. One of the advantages a waveguide resonator of type 1 offers is that it allows the inclusion of a dispersive element such as a prism. This is shown in fig. 6.8, where the prism is inserted in the output end. The prism could be at either end, but putting it in the output end has the advantage that the output of the resonator is automatically separated into its various frequency components ready for analysis. Ideally a Brewster prism should be used so that it introduces no further cavity losses. Finally, the use of a waveguide resonator of type 1 requires that quite complicated beam matching calculations must be performed for the pump beam. Because of the extra lens (or curved mirror) present, the input beam must have just the right curvature and spotsize such that the lens (or curved mirror) will transform it into a waist of size $W_o = 0.644$ a at the entrance to the capillary. Despite these requirements the correct beam can generally be provided using only a single lens of a convenient focal length.

Type 1

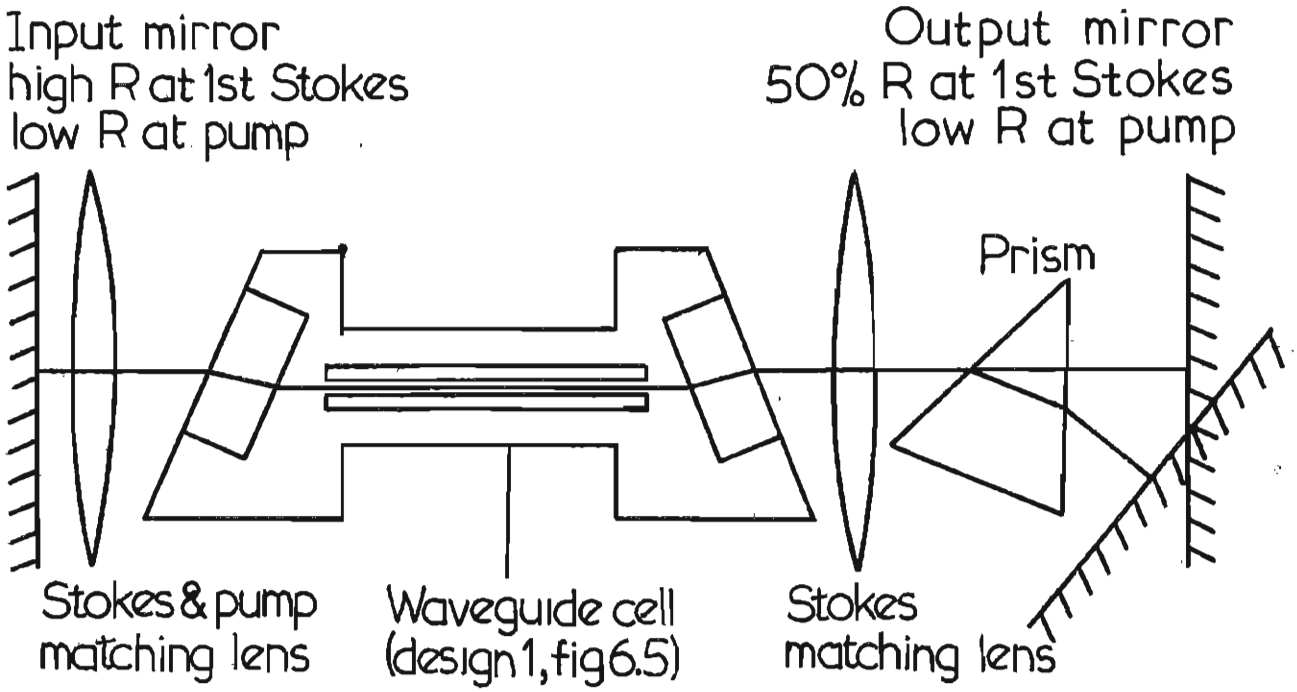

Type 2

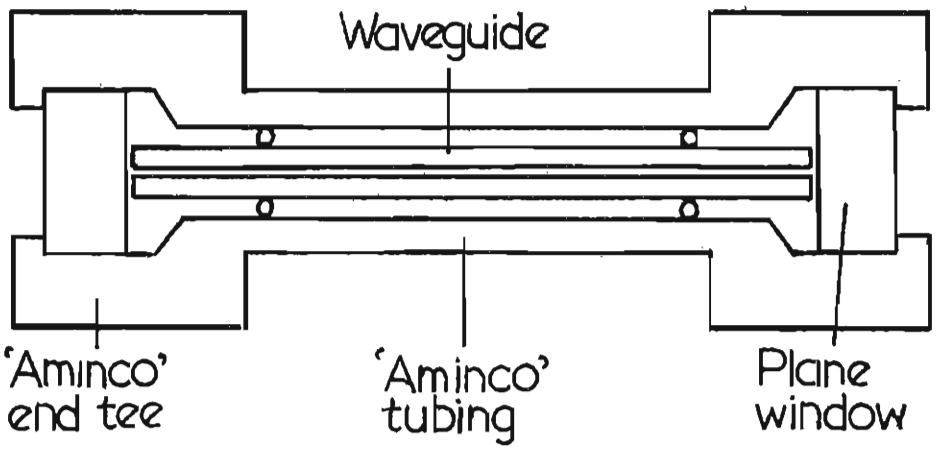

Figure 6.8: The two basic waveguide resonator designs.

The waveguide resonator of type 2, however, is much more convenient to use. As shown in fig. 6.8 it comprises two uncoated glass flats (if possible with an angle about the same size as the beam divergence to reduce etalon effects) where one face of each is held normally up against the two ends of the waveguide. This forms a resonator between two mirrors each of $\sim 4\%$ reflectivity. In practice the glass flats perform the additional function of high pressure gas cell windows and fit inside standard 'Aminco' bolts. The waveguide itself, generally short and supported on two O-rings, is made to be just the right length to fit between the glass flats when the whole cell is assembled. The body of the cell itself is again made from two 'Aminco' end tees and a piece of stainless steel tubing. Ideally, the input glass flat would be replaced by a 100% reflecting mirror at the Stokes wavelength. This is prevented in practice by the fact that the coatings on such a mirror would be damaged by the high pump intensities resulting from the small spotsizes required. We have seen, however, that the difference in final threshold between this case and a 4% mirror is not a very large one. The matching conditions for this oscillator are, of course, just the same as those for a single pass capillary. There are no mirror adjustments to be made and so the necessary adjustments are also just the same as those for the single-pass case. The only important criterion to satisfy is Abram's criterion for the plane mirror i.e.;

$$z/b \lesssim 0.1$$

where z is the distance between capillary and glass flat. Since $b = 1.35$cm for a 100μm bore capillary (held inside one of 165μm bore radius) we require that z does not get much bigger than 1mm.

6.3.2 Stimulated Raman Scattering in Hydrogen

The first experiment was performed in a waveguide resonator of type 1 without the prism. The waveguide used was a 32cm long piece of 100μm bore radius, thin-walled capillary held within a 165μm bore radius capillary. The lenses and spacings were the same as mentioned in the previous subsection giving an overall length of 65cm. The net reflectivities of the mirrors (taking into account uncoated lenses and 98% coupling) were $R_1 = 0.82$ and $R_2 = 0.21$. The pump wavelength was 1.064μm and its transmission through the capillary was 70% when properly matched. The pulse length was 46ns, the telescopic resonator having been turned down to low energy output. The pulse was still, however, a pre-lase Q-switched single longitudinal mode. Threshold was measured by monitoring the transmitted pump in the normal way. This time, however, we expect the tiny notch taken out of the Gaussian profile to be somewhere down the trailing edge. The lowest threshold power that could be obtained experimentally was 38kW at a hydrogen pressure of 350psi. This represents a 30-fold reduction in threshold from the tight focussing case and seems to suggest that waveguide resonators are working qualitatively as expected. This is brought out more clearly by comparing it with the single pass threshold result for a capillary with the same bore and similar length given in subsection 6.2.2. This was 265kW, showing that the resonating process has lowered the threshold by a factor of about 7. The theoretical threshold prediction obtained by evaluating equations 5.35 and 5.36 on a computer using the data above is 28kW. Threshold should also be reached at a time of $\sim$25ns after the peak of the pulse. This threshold prediction is in reasonable agreement with our experimental result given the possible errors and approximations involved.

It is felt however, that since this was the first experiment performed on the waveguide resonator, the experimental result could probably have been got lower. The time at which threshold was reached, however, was more accurately predicted. The notch was taken out of the temporal profile at around 22-23ns after the peak of the pulse.

A much more rigorous test of the theory was performed using waveguide resonators of type 2, fig. 6.8. Thresholds were measured using 1.064μm pumping for waveguides of two different bore radii filled to varying pressures with hydrogen gas. Also, the thresholds were measured in a 100μm bore radius waveguide resonator for pumping at 1.064μm, 532 and 355nm, the hydrogen pressure being around 400psi in each case.

The two bore radii used in the pressure dependent threshold measurements were 100μm and 165μm. (again the 100μm bore capillary was held inside a 165μm bore one). They had transmissions at 1.064μm of 62% and 80% respectively and both were 30cm long. The pump pulse length was 36ns (FWHM) in both cases. In the computer calculations performed using equations 5.35 and 5.36 both R_1 and R_2 were set to 4%, the reflectivity of a single face. The second face of the slightly wedged glass flats used as the mirrors was at a distance of 12mm from the capillary exit and could be responsible for some additional etalon effect which would alter the net reflectivity. We have already seen, however, that the threshold is quite insensitive to small reflectivity differences and so a value of 4% is sufficiently accurate.

Experimental thresholds were measured in the normal way, the notch again being taken out of the smooth Gaussian somewhere down the falling edge. They are plotted in fig. 6.9, the lines being the threshold predicted from the computer performed calculations. As can be seen, there is excellent agreement between theory and experiment. Again the 42kW threshold power at ~30Atm for the 100μm bore radius represents almost a 30-fold reduction below the tight focussing value.

At an input power equal to twice the threshold power the energy outputs and photon conversion efficiencies for the 100μm bore radius waveguide resonator operating at ~30Atm were measured. A pyroelectric energy meter and suitable filtering was used to measure forwards and backwards first Stokes energies. In the forwards direction there was also an appreciable amount of 1st anti-Stokes at 738nm along with a detectable amount of green 2nd anti-Stokes at 565nm. The energies and photon conversion efficiencies were as follows;

Input pump energy	4810μJ		
1st Stokes forward	245 μJ	; η_{ph} =	9%
1st Anti-Stokes forward	24.5μJ	; η_{ph} =	0.35%
2nd Anti-Stokes forward	0.7μJ	; η_{ph} =	0.008%
1st Stokes backwards	174 μJ	; η_{ph} =	5.5%

Thus, the overall conversion efficiency to the 1st Stokes at 1.907μm is 15%. Typical depleted pump and generated Stokes temporal profiles are similar to those of fig. 6.7. the latter being measured with a Judson J12 photodiode which only had a rise time of order 5ns.

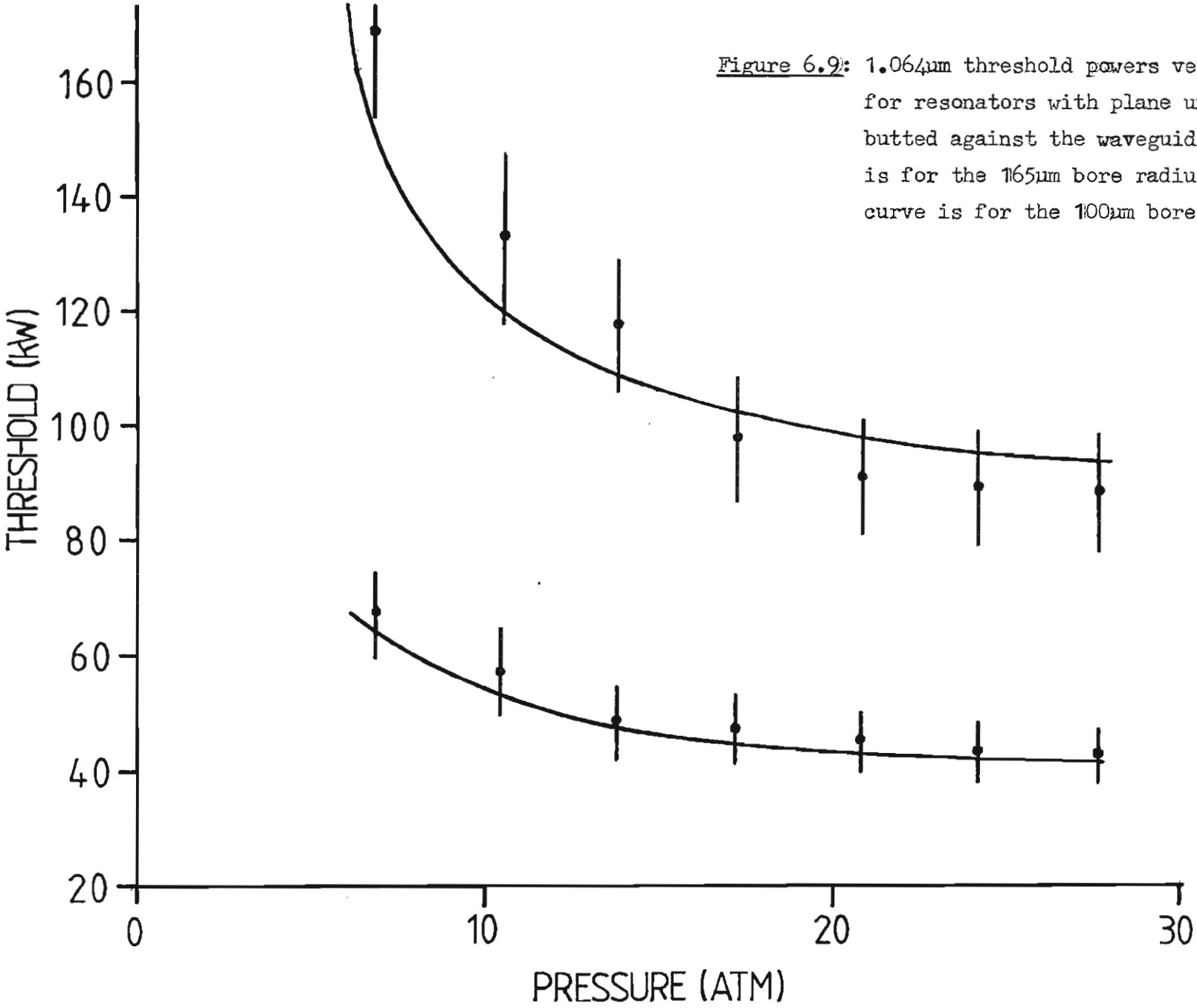

Figure 6.9: 1.064μm threshold powers versus H_2 pressure for resonators with plane uncoated glass flats butted against the waveguide ends. Upper curve is for the 165μm bore radius capillary, lower curve is for the 100μm bore radius capillary.

In general the depletion was more than a 15% conversion efficiency would suggest, a possible explanation being the generation of 2nd Stokes at 9.19μm which has a very high loss coefficient for a 100μm bore radius capillary, and in any case would be absorbed by the cell windows.

The pump wavelength dependence of the threshold power was investigated for a 31cm long, 100μm bore radius capillary between the 4% reflecting flats. The results and theoretical predictions are presented in Table 6.6 below;

Table 6.6: Experimental and theoretical SRS thresholds for the simple resonator

Pump Wavelength (nm)	Transmission (%)	Pulse Length (ns)	Expl. Thresh. (kW)	Theory Thresh. (kW)	1st Stokes (nm)
1064	62	30	42	43	1907
532	84	22	22.5	10.3	683
355	85	20	8.5	6.0	416

The agreement is not as good for the two harmonics as it was for the fundamental, the most likely reason being the degradation in pump beam quality caused by the passage through poor quality nonlinear crystals and the now quite numerous optical components. Another possible cause is destructive interference due to reflections from the second surface of each end mirror. As the Stokes wavelength gets shorter its confocal parameter increases and so z/b decreases. Consequently, etalon effects are more likely.

Despite this, however, the results still indicate the advantages of using a waveguide resonator. The thresholds are all substantially lower than the single-pass thresholds for the same capillary.

The same behaviour above threshold was also investigated for 532 and 355nm pumping, where in each case multiple Stokes components were generated in both forwards and backwards directions, and also anti-Stokes components in the forwards direction. These phenomena can only be accounted for by extending the theory presented in this report to account for pump depletion and additional four-wave mixing effects. This has been looked at many times in the literature (e.g. Von der Linde et al, 1969 and Newton and Schindler,1981) and will not be gone into here. A computational model of the situation is, however, being developed at Southampton University (M T Pacheco, 1983). In the present work just the results will be presented and some qualitative comments made.

Figure 6.10 shows the energy outputs per pulse in the 1st Stokes forwards (683nm), 1st Stokes backwards (683nm) and 2nd Stokes forwards (954nm), for various 532nm pump energies above threshold. As can be seen, the forwards 1st Stokes grows rapidly and then levels off as the 2nd Stokes forward starts to grow. We anticipate that if a higher pump energy could have been used at the time the 1st Stokes would have decreased as the 2nd Stokes power depleted it, in accordance with the predictions of Newton and Schindler. As it is, the overall energy conversion efficiency to all components reaches about 30% at the highest input energies.

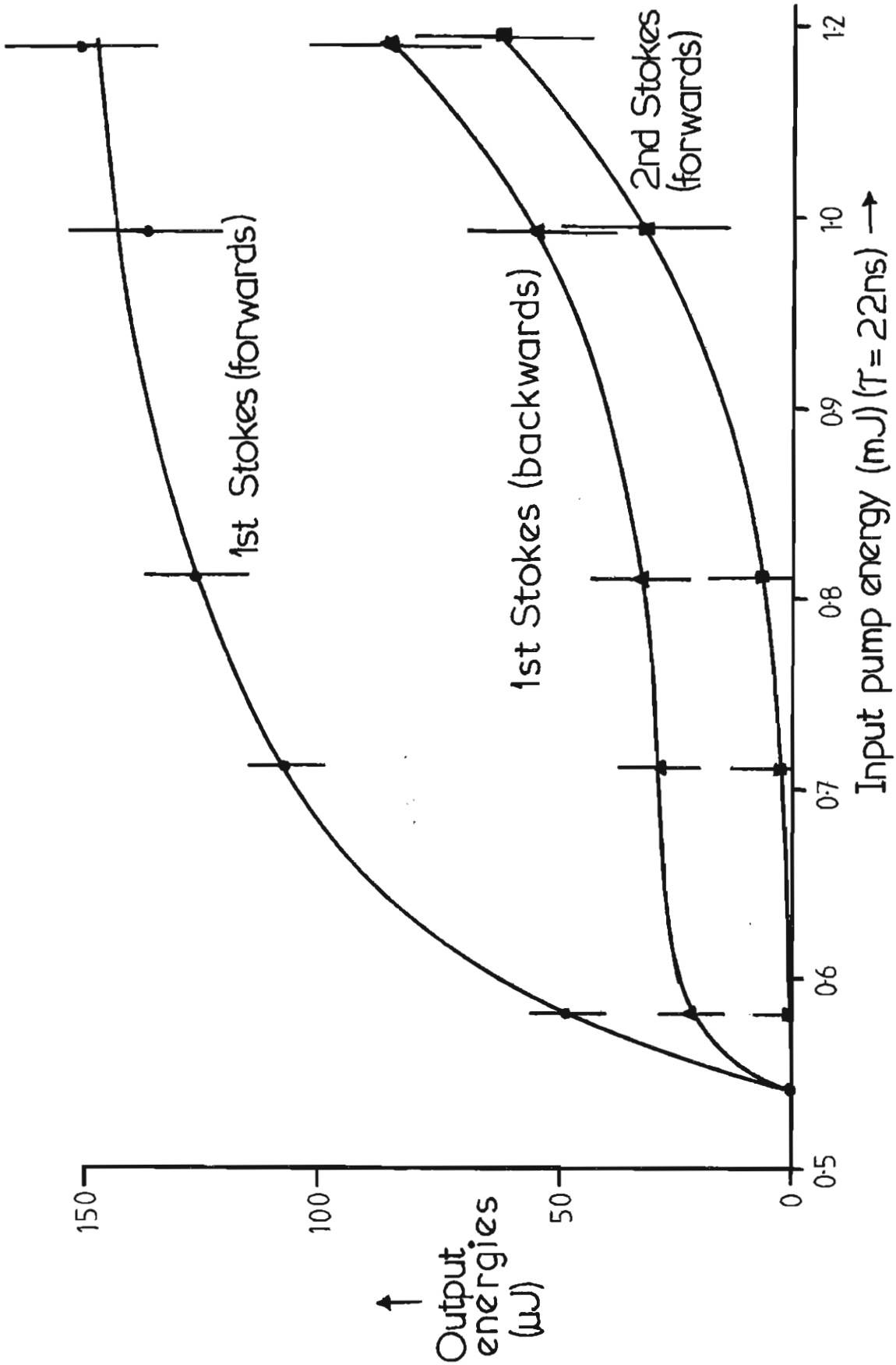

Figure 6.10: Graph of output Stokes component energies against input pump energy at 532nm for a H_2 filled waveguide resonator as described in the text. The curves are only a guide to the eye.

All this is shown much more clearly for 355nm pumping above threshold. At this wavelength it was possible to generate 1st, 2nd, 3rd and even 4th Stokes in the forwards and backwards directions, the wavelengths being 416, 503, 636 and 864nm respectively. Various antistokes components were also generated but with much lower output energies. As with the 532nm pumping, all energies were measured with a pyroelectric energy meter after a prism had been used to separate the frequencies. The results for the forwards components are shown in the graph of fig. 6.11. Here it is clear that each Stokes component reaches a maximum energy at which point a rapid increase in the next Stokes component occurs. Each Stokes component must reach an energy (more accurately a power) which is higher than the maximum of the component preceeding it before it can start to generate the next Stokes component. This is in agreement with the idea of a cascade process (Von der Linde et al, 1969) where the gain for each successive Stokes component is lower than that for the one before it. Of particular interest, however, is the occurrence of a low level output for each Stokes component which begins at the same point as the previous Stokes component starts its rapid increase. This output generally takes the form of a somewhat messy ring pattern. When the output starts to rise sharply with input power, however, the normal intense central spot appears. It is believed that the low energy ring pattern is the result of Stokes generation by four-wave mixing processes and that the sudden rapid increase in energy accompanied by the central intense spot in the output is the normal cascade Raman scattering process. It is hoped that the calculations of M C Pacheco (1983) will throw light on this hypothesis. Suffice it to say that pumping this simple waveguide resonator with between 0.2 and 1.0mJ of 355nm radiati can produce about 100μJ at any of three wavelengths across the visible region of the spectrum. This output should be in a beam which is diffraction limited to within about 10% (though this has not been checked). In addition to this output in the forwards direction there was, when operating at 350psi, a corresponding output in the backwards direction.

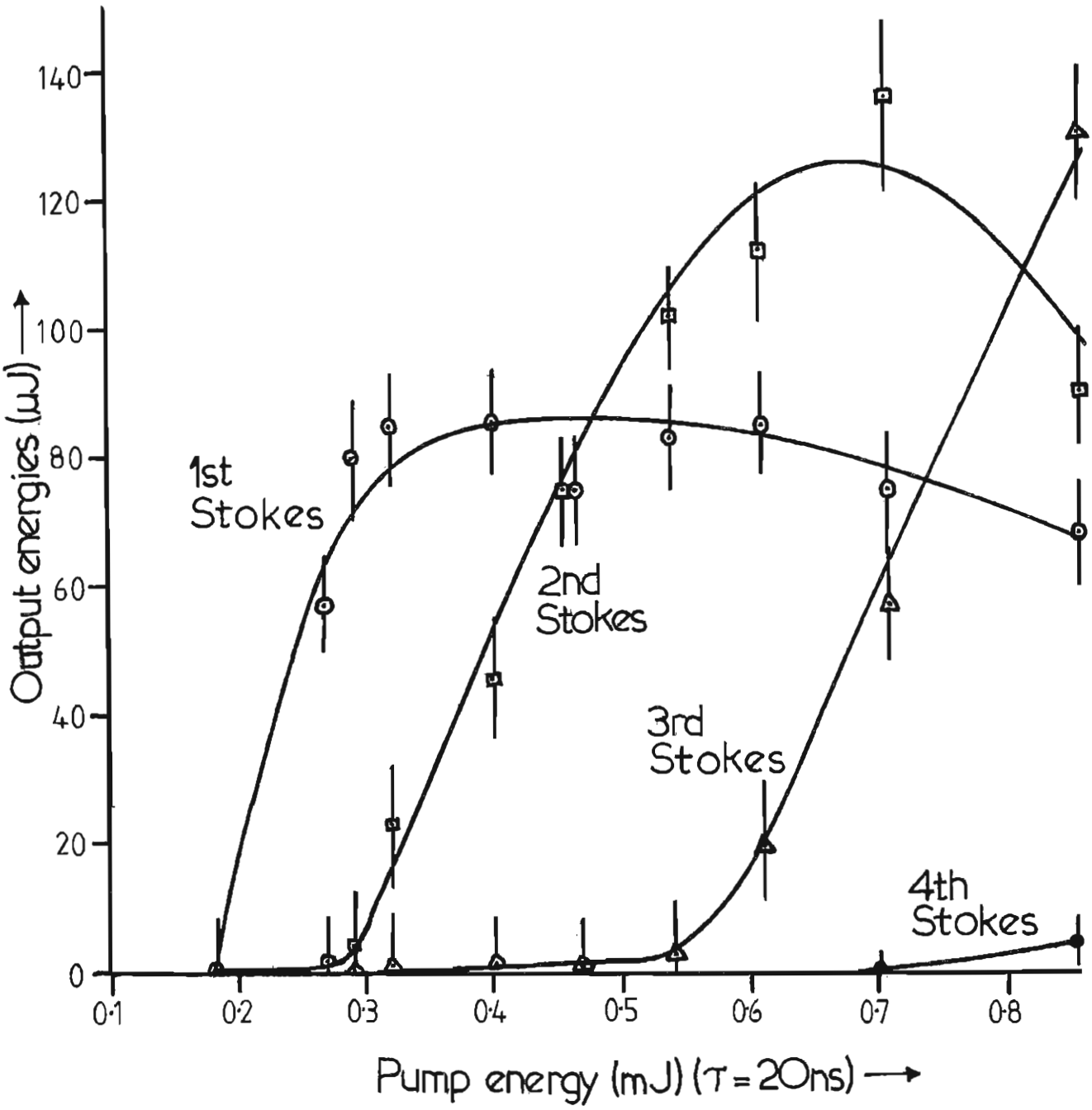

Figure 6.11; Stokes output energies in the forwards direction versus the input pump energy at 355nm.

The energies in the various backwards Stokes components tended to be between 10 and 20% of the energies in the corresponding forwards Stokes components. Overall, the total photon conversion efficiencies to all components, forwards and backwards (but not counting anti-Stokes) varied between 50% at the peak of the 1st Stokes forwards energy, to 65% at the highest energy input used.

6.3.3 Stimulated Raman Scattering in Methane

A waveguide resonator of type 2, fig. 6.8 cannot be used to generate 1.544μm 1st Stokes radiation by Raman shifting SLM 1.064μm pulses of 10's of nanoseconds duration in methane. The reason for this is that the resonator effect is present for the Brillouin Stokes wave as well as the Raman Stokes wave and so both thresholds are lowered by approximately the same factor below the single pass case. From subsections 5.3.3 and 5.3.4 it is expected that for the single pass case the Brillouin thresholds will be considerably lower than the Raman thresholds, and consequently the resonator case should be no different. It was pointed out towards the end of section 5.4, however, that in certain cases, particularly at low methane pressures, the difference between the Brillouin and Raman thresholds was not too great, and that if the Raman Stokes could be resonated and the Brillouin Stokes prevented from so doing, the Raman threshold power might be lowered below that of the Brillouin threshold. Such an effect can be obtained by using a waveguide resonator of type 1, fig. 6.8, where now the prism is included as the dispersive element. Such a resonator was built with more or less the same parameters as the one used for the first measurement on hydrogen, the differences being that now the capillary was 32cm long, the overall length of the resonator was 74.5cm (partly due to the inclusion of the prism between lens and output mirror) and the net reflectivities at 1.544μm were $R_1 = 0.81$ and $R_2 = 0.3$. A slight change in the lens to capillary end spacing was also required when searching for optimum alignment, in accordance with Abrams' coupling theory.

The behaviour of the cell was investigated at various methane pressures between about 5 and 10 Atm, but because of the inaccuracies of the gauge down at such low values, the actual pressures in the waveguide cells could be different to those read on this gauge by up to 2 or 3 Atm.

Raman threshold was looked for in the normal way by monitoring the transmitted pump radiation. In practice the mirrors were aligned to first produce oscillation at powers well above threshold, the power then being reduced to such a level where no amount of mirror adjustment could give more than a slight notch on the falling edge of the Gaussian temporal profile. It was indeed possible, therefore, to obtain Brillouin-free Raman scattering. Table 6.7 below lists the expected threshold powers from equations 5.35 and 5.36 for various methane pressures. The measured transmission of the waveguide was 65%, the pump pulse length was 32ns. Also shown are the experimental threshold powers and the powers at which Brillouin scattering had still not appeared.

Table 6.7 Experimental and Theoretical SRS Thresholds for the CH_4 filled dispersive resonator

Pressure (Atm)	Theory Thresh. (kW)	Expl. Thresh. (kw)	Highest Brillouin Free Power Tested (kW)
6.21	157	185	470
6.90	236	270	470
8.63	198		450
10.70	169	156	440

As can be seen, the experimental results are roughly in line with those expected theoretically. The thresholds have, of course, been substantially reduced below the values that would have been expected from single pass threshold experiments, had they been possible.

Of particular interest are the values to which the input powers can be raised above Raman scattering threshold and still not cause Brillouin scattering. As shown, powers of around 450kW can be used in all cases. These values are, in fact, higher than the single pass Brillouin scattering thresholds for a capillary of the present length and bore radius, as shown by the theoretical and experimental values in table 6.5. The reason for this can only be that the Raman scattering process, reaching threshold first, depletes the pump so much that Brillouin threshold cannot be reached. Confirmation of this explanation came from the observation that if the Raman resonator mirrors are completely misaligned at both ends, Brillouin scattering does occur at the powers expected.

Typical 1.544μm output energies at ~125 psi varied between 300 and 500uJ for pump input powers that were typically 2 to 2.5 times threshold (i.e. about 440kW). This corresponds to a 5% photon conversion efficiency. This is a lower conversion efficiency than had been hoped for, part of the explanation possibly being due to the fact that 2nd Stokes was not transmitted and a significant conversion to 2nd Stokes may have occurred. Despite this, however, the 1.544μm beam appeared to be a good TEM_{oo} mode as revealed by burn patterns taken and the fact that it could be injected into another waveguide and produce transmissions of an equivalent standard to those obtained using the output of the telescopic resonator.

As a summary to this section therefore, the use of waveguide resonators provides even further threshold reductions over the single-pass waveguide method and consequently even greater reductions below the single-pass, unguided cases. Furthermore, the experimental results are in line with a simple theory. Secondly, the use of dispersive waveguide resonators also allows for selective lowering of a particular nonlinear threshold, again in agreement with the simple theory.

6.4 Raman Scattering Experiments in Waveguides using Picosecond Pulses

It was pointed out in subsection 5.3.5 of the previous chapter that the use of shorter pump pulses allows for the discrimination between SRS and SBS by moving the undesirable SBS process into the transient regime. Here the gain decreases and the thresholds are correspondingly raised above those of the required SRS process. It was shown as an example that sufficiently short 1.064μm pulses ought to be able to reach Raman threshold in methane gas in a single-pass waveguide configuration, free from the Brillouin scattering that would occur with tens of nanoseconds pulses.

Preliminary experiments on single-pass and synchronously pumped waveguide configurations will be presented here, where only 1.064μm pumping of methane gas will be considered.

6.4.1 The Experimental Arrangement

The experimental arrangement used for both the single-pass and the synchronously pumped experiments is shown in fig. 6.12. The pump source at 1.064μm is provided by a pre-lase Q-switched and mode-locked Nd:YAG laser.

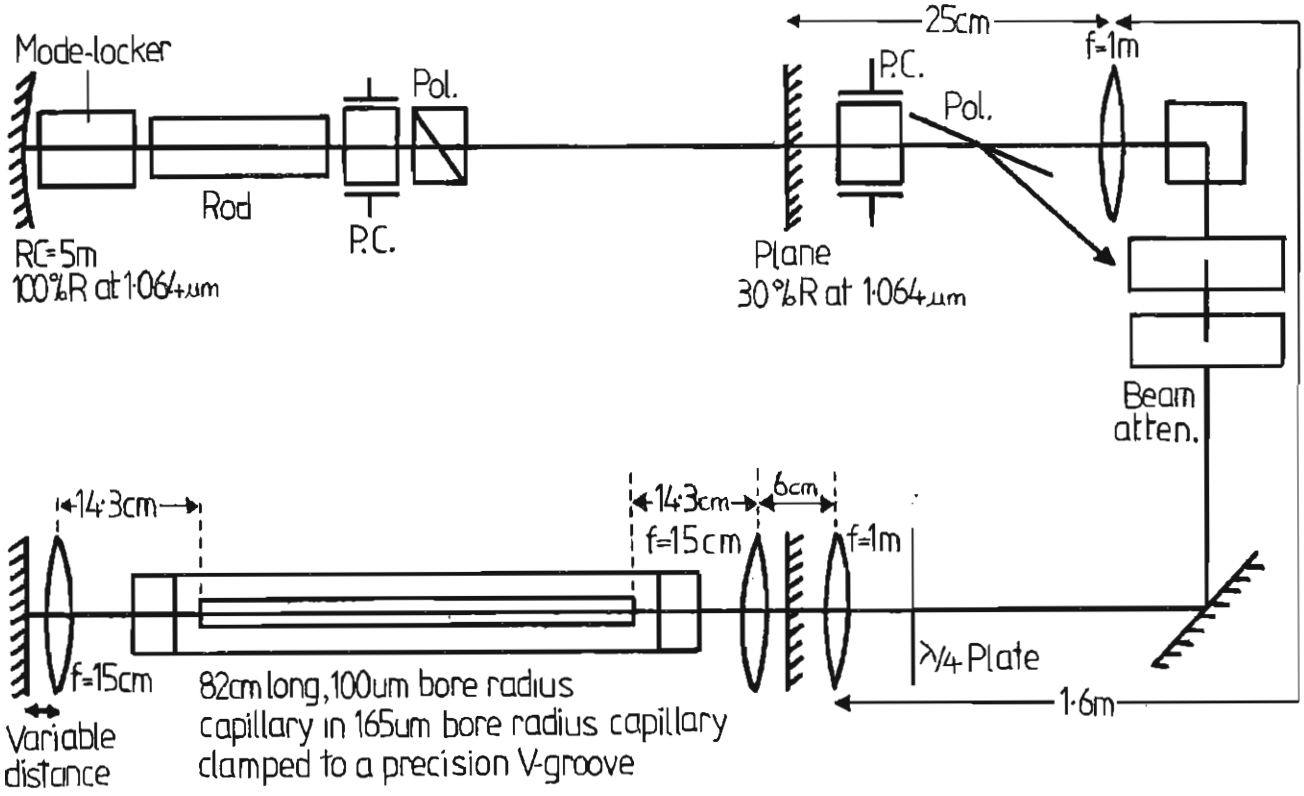

Figure 6.12: Actual experimental arrangement for the picosecond pulse Raman scattering experiments.

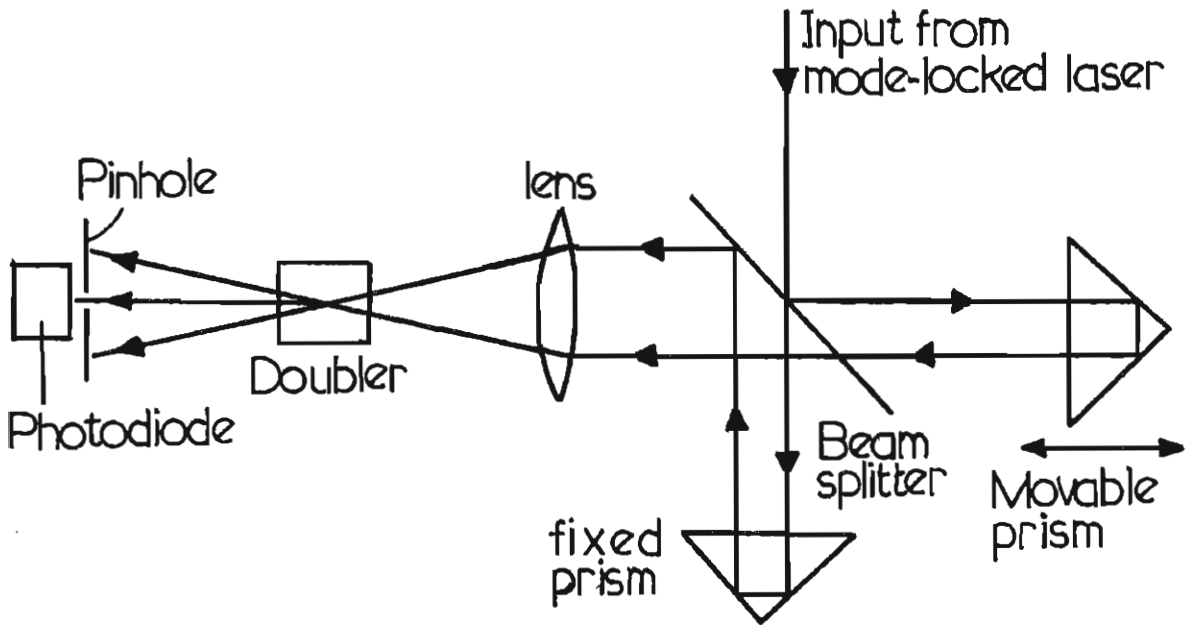

Figure 6.13: Schematic of the auto-correlation technique used to measure the pulse lengths.

(Kuizenga 1977, 1981). The construction of this laser was not part of the work of this thesis. Suffice it to say that it provided a train of 470ps long pulses with a total energy of around 3mJ. The spacing between the individual pulses, of which there were about 10, was equal to the cavity round trip time of 7.7ns. The peaks of these pulses marked out an approximately Gaussian envelope function. The pulse train, therefore, had the general appearance of fig. 5.7.

The waist size at the output of the laser was about 0.75mm. This was matched into a 100μm bore radius capillary using a 1.1m, a 1m and a 15cm lens spaced as shown in the diagram. The passage through so many optical elements is clearly not ideal and will result in a poor waveguide transmission. The waveguide itself was 82cm long and was held within a 165μm bore capillary. The waveguide cell was made in design 2 of fig. 6.8. For the single pass experiments the λ/4-plate, the input mirror for the waveguide cell and both the output components were not present. All these components are necessary for the synchronously pumped resonator experiments, these functions requiring a few comments.

The focal lengths of the lenses, and in fact the length of the waveguide itself, are chosen such that the normal coupling requirements can be satisfied (see section 5.2) whilst at the same time ensuring that the resonator is approximately the correct length to allow synchronous pumping i.e. the Stokes round trip time must be equal to the spacing between the mode-locked pump pulses. To this end, 15cm lenses were used in the resonator.

The output mirror was provided with a longitudinal adjustment so that the exact resonator length could be found by optimisation whilst running. Its reflectivity was 50% at 1.544μm and small for 1.064μm. The input mirror had a reflectivity of ~98% at 1.544, but,unfortunately, had ~10% reflectivity at 1.064. Thus, when optimally aligned it provided sufficient feedback to the laser to alter its performance and, in fact, lengthen the pulses. To prevent this a $\lambda/4$-plate and a polariser were added as shown. This sufficiently isolated the waveguide resonator from the laser, but does mean that the input to the waveguide is now circularly polarised when being synchronously pumped. We have mentioned that Rivoire et al (1983) predict a negligible difference between Raman thresholds for linearly and circularly polarised pump beams in single-pass experiments. This has been verified by K H Wong (private communication) for both unguided tightly-focussed and waveguided configurations when Raman scattering in hydrogen. We made the assumption, therefore, that the same thing should apply for the synchronous pumping of the Raman process in methane.

An additional feature of the experimental arrangement is the Pockels cell placed between the laser output and the polariser. When a half-wave voltage was applied to it the output of the laser was deflected off the polariser into an auto-correlator. In this way, the pulse lengths could be measured at will without constant realignment. The auto-correlation technique used is the well known 2nd harmonic generation method, the experimental arrangement used being shown in fig. 6.13.

If, therefore, d is the distance between the two prism positions at which the monitored 2nd harmonic power is half the maximum value it reaches, the pulse length of the individual mode-locked pulses is given by;

$$T = \frac{2d}{c\sqrt{2}}$$

In our case d was measured to be 10cm implying 470ps pulses.

6.4.2 Single-Pass Threshold Measurements

Single-pass threshold was detected by monitoring the output beam for 1.544μm radiation. This was done with a Judson J12 photodiode and suitable 1.064μm filtering. At threshold there should only be one very small 1.544μm pulse corresponding to threshold being reached by only the central maximum pulse in the pulse train. Thresholds were measured at various methane pressures, but all for the same capillary. The transmission of this capillary was measured to be ~36% at 1.064μm. The experimental results are given in table 6.8 along with the theoretical predictions for a steady-state, SLM pulse taken from subsection 5.34, table 5.4. The experimental results for the central pulse powers and energies were calculated from the fraction of the total pulse train energy that was in the central pulse as revealed by a photograph taken of the train using a vacuum photodiode and transient digitiser. This has an overall response time somewhere between 0.5 and 1ns, capable of providing a clear indication of the relative pulse heights. The experimental results are all lower than the theoretically predicted ones, typically by about 20-30% of the latter. As discussed in section 5.4 the reason for this is probably that the pulse is not bandwidth limited.

Pressure (ATM)	Experimental Threshold			Theoretical Threshold		
	Central Pulse Power (kW)	Central Pulse Energy (mJ)	Total Energy in train (mJ)	Central Pulse Power (kW)	Central Pulse Energy (mJ)	Total Energy in train (mJ)
10	440	0.22	1.33	697	0.33	1.630
20	360	0.18	0.83	443	0.208	1.043
25	308	0.154	0.71	392	0.185	0.923
30	260	0.13	0.60	360	0.168	0.844

Table 6.8: Experimental and Theoretical Threshold Energies for Short Pulse, 1.064 Pumping of CH_4

The energy conversion efficiency to 1.544μm was measured at 30Atm. for a pump input of total energy 1.48mJ. The output of 1.544μm consisted of about 5 pulses, corresponding to the five most powerful pulses in the mode-locked pump pulse train. The total energy in these was 106uJ (as measured with a pyroelectric energy meter) and corresponds to an energy conversion efficiency of 7.2% at 1.75 times threshold (~10% photon conversion efficiency). 1.48mJ was the maximum energy that could be supplied to the cell. This corresponds to a power of ~650kW in the central pulse, well below the power required to reach Brillouin scattering threshold for this pulse length (see section 5.3.4 table 5.4). Thus, using short pulses allows the generation of 1.544μm by Raman scattering in methane in single-pass waveguide experiments, no evidence being found of Brillouin scattering.

6.4.3 Synchronous Pumping Threshold Measurement

The same waveguide cell used for the single-pass experiments was used again here, this time with the lenses and mirrors described in subsection 6.4.2 included. The transmission of the circularly polarised light created by the λ/4-plate was the same 36% as for linearly polarised light. A quick single-pass threshold measurement also revealed the same value, as far as could be judged taking into account experimental errors, as that obtained for linearly polarised pump radiation at the same methane gas pressure. For synchronous pumping the thresholds were detected in the same way as for the single-pass case.

To maximise the Raman gain a high methane pressure of about 30Atm was used. The lowest value obtained for the threshold energy in the entire pulse train was 0.45mJ, a factor of 1.33 below the value at 30Atm for single-pass threshold. The theoretical value obtained using equations 5.44 and 5.46 was 0.33 mJ, showing quite good agreement. The relative pulse heights for the summation in 5.46 were 2, 7, 14, 22, 23, 19, 13, 7, 4, 3 and were obtained from a photograph of the mode-locked laser output. Since uncoated lenses were used in the resonator, the effective reflectivities were reduced by 16%.

Despite the reasonable agreement between the experimental and theoretical threshold values it must be noted that the experimental value is above the theoretical one whereas for the single-pass results it was the other way round. The theoretical improvement factor should have been 2.5 as opposed to 1.33 and so it looks as though the synchronously pumped waveguide resonator, although partially successful, needs further investigations. This should also be done using much shorter pulse-lengths, an Nd:YAG laser being capable of getting down to pulses around 50ps long.

6.5 Raman Scattering Experiments in Waveguide Oscillator-Amplifier Systems

The purpose of our experiments with waveguide oscillator-amplifier systems was to demonstrate that large amounts of energy at 1.544μm could be obtained from a long pulse length (10's of nanoseconds), SLM, TEM_{oo} beam of 1.064μm radiation by the process of SRS in methane gas. As discussed in section 5.6 of the previous chapter this is normally prevented by the onset of Brillouin scattering in everything but a dispersive waveguide resonator. We have just seen that the typical energy output from such a device is typically only about 500μJ. It is, however, in a high quality beam, and does not require very much 1.064μm energy to generate it.

The experiments described in this section show how this small energy at 1.544μm could be amplified up to a much larger output energy using some of the remaining 1.064μm energy from the telescopic resonator. In practice the amplifier cells consisted of long, large bore waveguide cells of design 2, fig. 6.8 into which both the 1.064μm pump and the 1.544μm radiation needed to be injected with the correct matching conditions being satisfied as usual. Both forwards and backwards pumping were tried, the relative merits of each having been discussed in section 5.6.

6.5.1 The Experimental Arrangement

The experimental arrangement for the backwards pumping of the Raman amplifier is shown in fig. 6.14. A 30% reflecting mirror is used to separate off part of the telescopic resonator output to pump the methane filled (~8.6Atm) dispersive waveguide resonator dealt with in the last section. It needs about 12-13mJ to produce 0.5mJ of 1.544μm radiation. The rest of the output at 1.064μm passes through a system of matching optics that injects it into the waveguide amplifier cell. This system of optics also acts as a delay line to ensure that the pump pulse arrives in the amplifier at the same time as the 1.544μm radiation from the oscillator. This too requires careful matching in, a task which fortunately can be performed with a single lens. The capillary chosen for the waveguide amplifier had a length of 80cm and a rather large bore radius of a = 315μm. The cell was built to design 2 of fig. 6.8 and consequently had plane windows. The details of the matching arrangements are as follows; Spotsize W_o = 0.41mm at the telescopic resonator; 117cm from telescopic resonator to 1m lens; 131cm from lens to its focus; 436cm from focus to 2m radius of curvature 100% mirror; 122cm from 2m mirror to input of amplifier capillary.

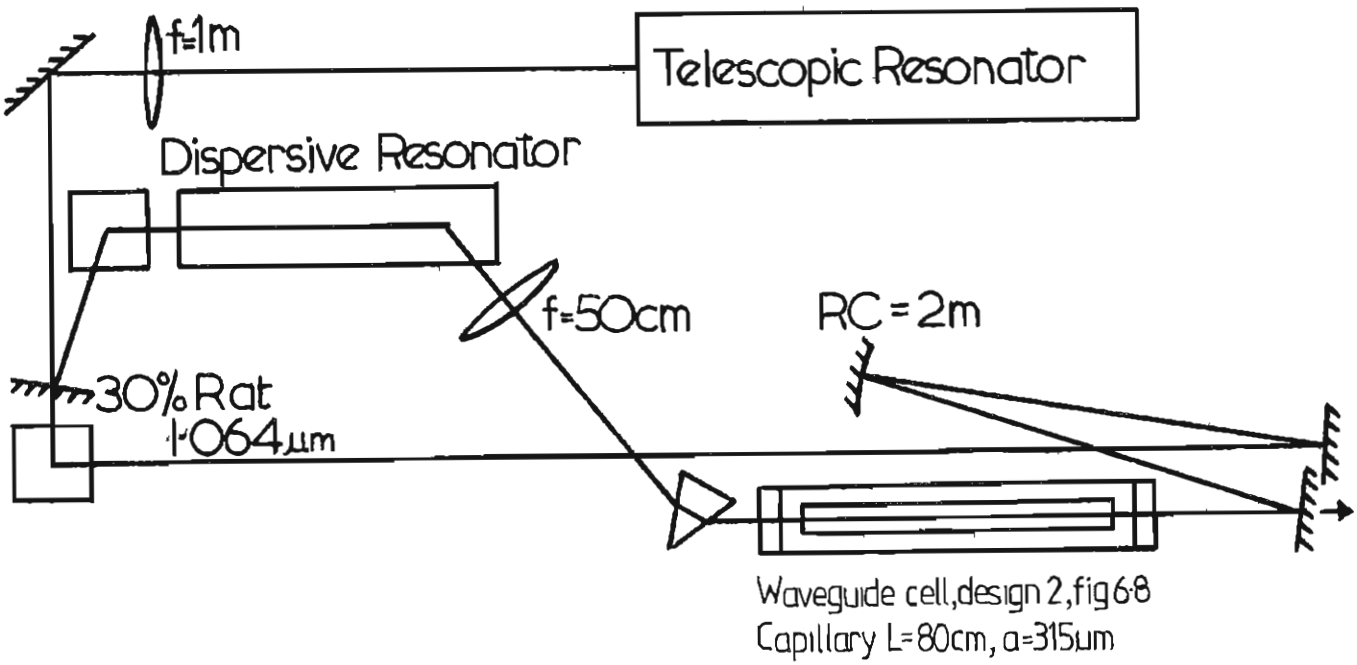

Figure 6.14: Experimental arrangement for the oscillator-amplifier experiment - backwards pumping of the amplifier.

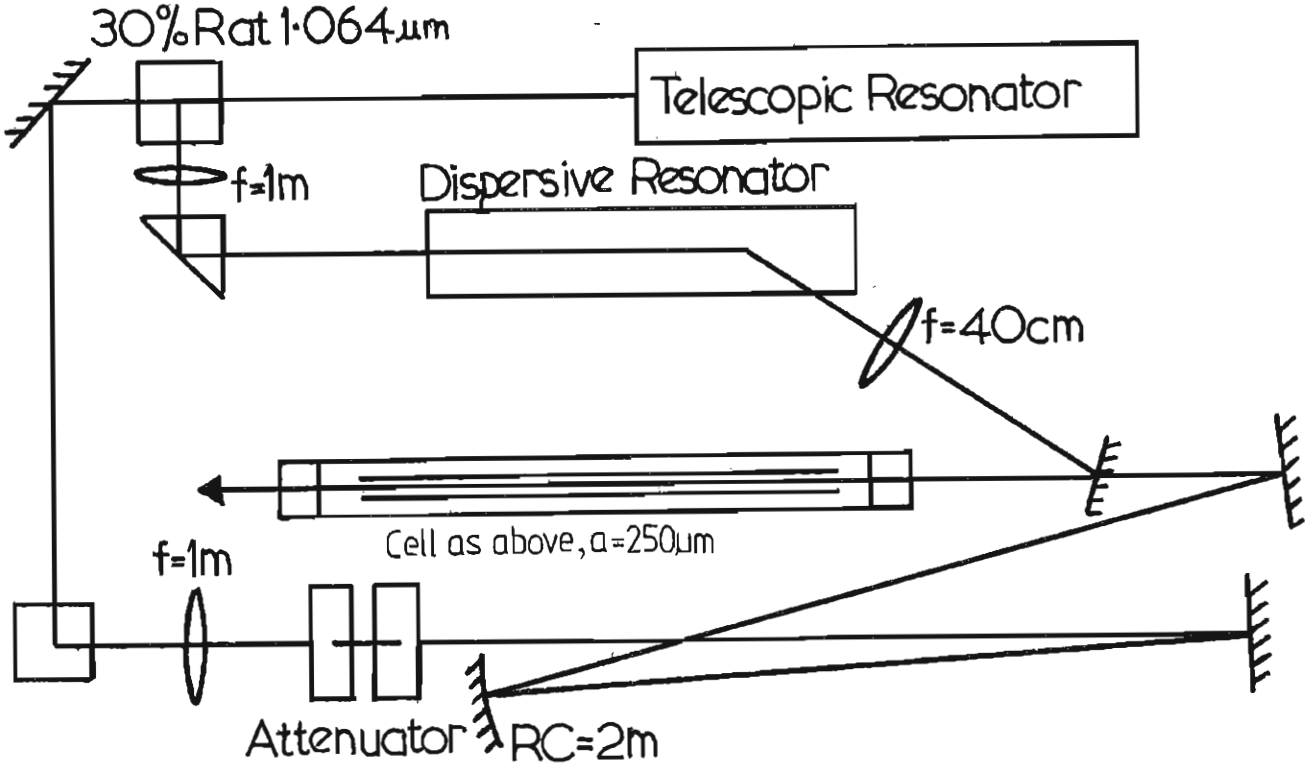

Figure 6.15: Experimental arrangement for the oscillator-amplifier experiment - forwards pumping of the amplifier.

For the 1.544μm radiation from the oscillator, $W_o \simeq 1.128$mm at the output, a 50cm lens produces the near optimum spotisze at its focus approximately 50cm away.

Care must be taken to ensure that the polarisation of the pump and Stokes is in the same plane, usually the horizontal since this eases the design of the dispersive Raman oscillator. The rest of the optical arrangement must be designed accordingly. A square block in the diagram represents a reflector consisting of a mirror and a prism, so as to change the beam height as well as the plane of polarisation.

The only other component of note is the final mirror used to input the pump pulse into the amplifier cell. It must have a high transmission at 1.544μm because this is where the final amplified output is obtained from. In practice the one used had a transmission of 90%.

The experimental arrangement for the forwards pumping of the amplifier is shown in fig. 6.15. Most of the diagram is self explanatory in view of what has been said about the backwards pumping case, the actual beam matching parameters being as follows; For the pump, $W_o = 0.41$mm at the telescopic resonator; 256cm from resonator to 1m lens; 407cm from lens to 2m radius of curvature 100% mirror; 166cm from 2m mirror to amplifier waveguide entrance. This should produce a pump waist size of 161μm, satisfying Abrams criterion. The 1.544μm radiation from the oscillator now requires only a 40cm focal length lens to optimally match it into a 250μm bore radius amplifier capillary.

6.5.2 Backwards Pumping of the Waveguide Amplifier

The dispersive Raman waveguide resonator filled with methane gas to ~8.6Atm was pumped with 13.5mJ of 1.064μm radiation and produced 0.5mJ at 1.544μm. This was injected into the waveguide amplifier of fig. 6.14 when that, too, was filled to~8.6Atm with methane. The transmission was measured with a pyroelectric energy meter when the waveguide had been optimally aligned and was found to be 85%. The theoretical value may be 95%, but this still indicates a high quality beam, particularly since the best transmission for the pump beam was also 85%. The pump needed to be correctly aligned for optimum injection into the amplifier waveguide by adjustments to its matching mirrors alone. The amplifier cell itself could not be moved once set up for optimum Stokes beam transmission. The timing of Stokes and pump arrival was checked by monitoring them both with the same detector at the Stokes output end of the amplifier waveguide. A Judson J12 was used, and the coincidence of the peaks of the pulses was checked from the oscilliscope traces produced.

The pump energy reaching the entrance to the amplifier waveguide was 27.5mJ in a 25ns pulse. When this was blocked off the Stokes energy leaving the amplifier cell was 360uJ (measured with a pyroelectric energy meter and corrected for the 90% transmitting mirror). When the pump was allowed to enter the cell the Stokes output at 1.544μm rose to 6.07mJ of which 5.46mJ was useable energy emerging through the mirror.

When the pressure in the amplifier waveguide cell was raised to 13 Atm, a pressure just below that which would cause Brillouin scattering to be also present for a 27.5mJ, 25ns pump input, the output energy at 1.544μm rose to 6.7mJ of which 6.0mJ was useable output. This amount of energy was sufficient to give a good burn pattern on photographic paper.

Again, the burns look just like those of fig. 2.7, chapter 2, good evidence for suggesting that they too are TEM_{oo}, although this was not checked experimentally.

Fig. 6.16 is an expanded picture of a photograph showing the temporal profile of the pump radiation transmitted by the amplifier cell with and without the injected Stokes radiation from the oscillator being present. When the Stokes is not injected the pump is undepleated; when it is present the pump is severely depleated. Thse profiles were obtained using a vacuum photodiode and transient digitiser. The photon conversion efficiency can be estimated from a comparison of the area of the depleted part of the pulse with the area of the whole undepleted part. Counting the squares gives $\eta_{ph} \approx 38\%$. Our Stokes energy output of 6.7mJ for a 27.5mJ input corresponds to a photon conversion efficiency of 35.4% and so on this occasion we seem to have quite good agreement.

A 250μm bore radius capillary of the same length as before was tried as the amplifier waveguide cell. It was necessary to change the matching optics for both pump and Stokes, and this time the transmissions obtained were only 80% and 65% respectively. When operating at 8.6Atm with a pump input energy of 25.4mJ and Stokes input of 500μJ, the best Stokes output achieved was 5.56mJ of which 5mJ was useable energy passing through the output mirror. This corresponds to a photon conversion efficiency of 32%. Increasing the pressure or the input energy to the amplifier cell would cause Brillouin scattering.

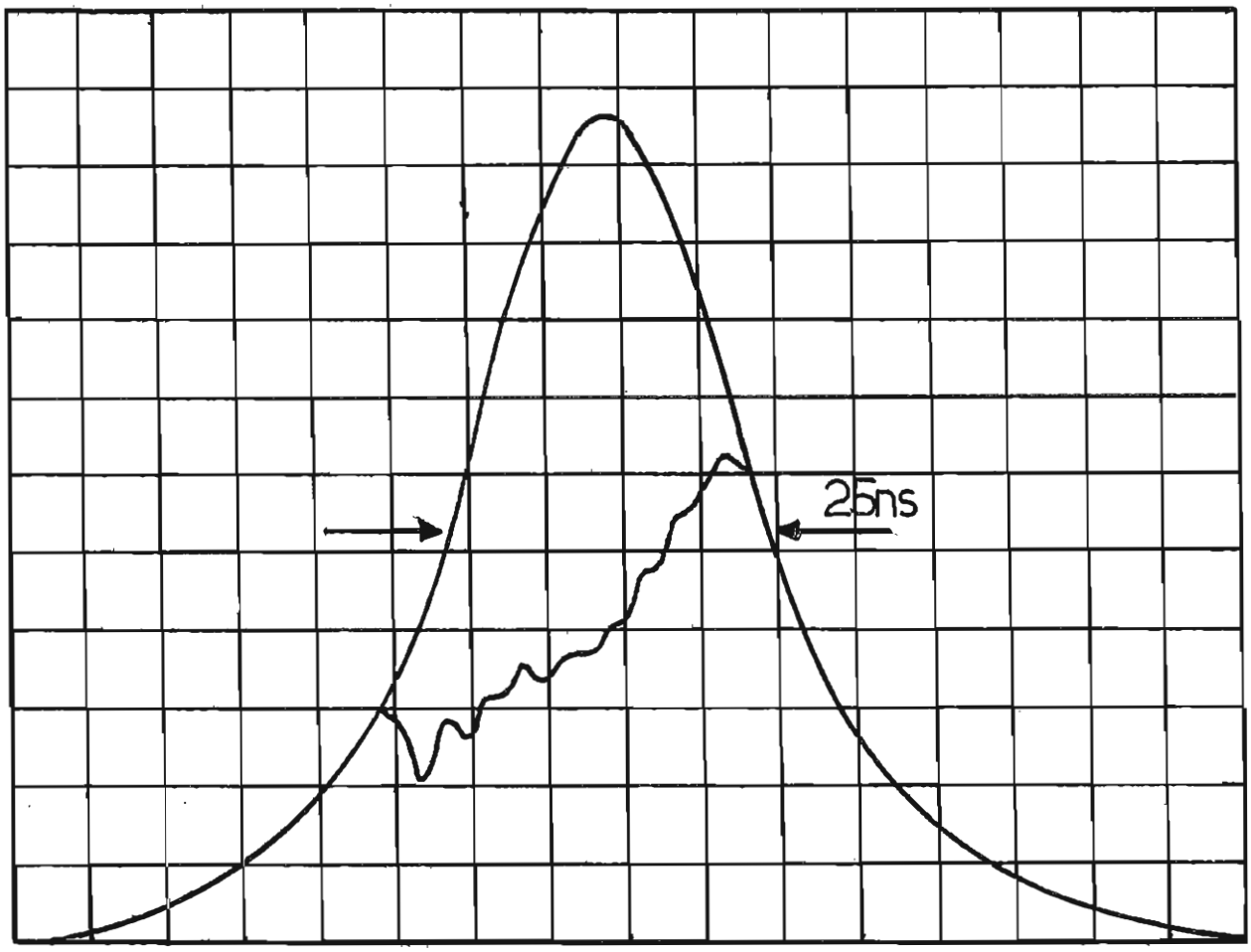

Figure 6.16; Temporal profiles of the pump beam transmitted by the waveguide amplifier cell with and without the injected Stokes beam being present. (see text)

6.5.3 Forwards Pumping of the Waveguide Amplifier

Forwards pumping was looked at briefly using the experimental arrangement shown in fig. 6.15. The amplifier waveguide was again 80cm long and had a bore radius of 250μm. Again, the alignment procedure was to adjust for optimum Stokes transmission (~80%) and then align the pump using only its input mirrors. 80% transmission was also obtained for the pump. When operating the cell at 8.6Atm the input pump energy could not be raised above 27.5mJ in a 25ns pulse because Brillouin threshold was reached. When operating at this level, however, and with 500μJ of 1.544μm radiation from the oscillator being injected, the amplified energy output at 1.544μm was 5.5mJ, of which 5.0mJ was useful output. Again this corresponds to a 30% photon conversion efficiency. The energy was measured with a pyro-electric energy meter after the output frequencies, which include the transmitted pump, had been separated off using a prism. Also present were 1st, 2nd and occasionally flashes of 3rd anti-Stokes radiation, none of which were present in the backwards pumping case. Again the 1.544μm output was a good beam that looked like a TEM_{oo} mode on burn paper.

In conclusion, therefore, it would seem that the oscillator-amplifier arrangement can be used to produce quite large amounts of energy at 1.544μm using the "clean" output from the telescopic resonator. In all the experiments only about 40mJ was actually used in Raman scattering processes themselves, the rest being lost in the optical matching system. This implies an overall energy efficiency of 12.5%. However, with care over the losses and all the various design parameters it is probable that this technique could provide much higher conversion efficiencies, certainly if instead of 1.064μm pumping we used shorter wavelengths.

CHAPTER 7 : CONCLUDING REMARKS

By far the most important conclusion to be derived from the work of this thesis is that the use of guided configurations substantially reduces the pump powers required to reach threshold for nonlinear processes such as SRS and SBS. For SRS in particular, since it is this process that produces the near and mid-infrared frequencies we are interested in (as mentioned in the Introduction), threshold reductions have been obtained that are more than a factor of 20 below the unguided, tight-focussing limit.(For example, when using high pressure hydrogen gas as the nonlinear medium and 1.064um radiation as the pump, a factor of 35 reduction has been obtained in a Raman resonator configuration.) Analysis of the nonlinear processes themselves and also of the waveguiding properties of hollow quattz capillaries have enabled a satisfactory theory to be developed to describe nonlinear optics in guided configurations, and in particular to provide expressions for the expected thresholds of the various nonlinear processes. When these predictions were tested experimentally excellent agreement was found with the theory, any discrepencies generally being within 10-15%. It is felt, therefore, that the theory presented can be confidently used to make predictions for the performance of guided SRS using any wavelengths and waveguide parameters that might be of interest. Thus, as mentioned in the Introduction, the pump wavelengths of interest might be provided by the tunable output of a "vibronic" or an F-centre laser operating somewhere in the 0.8-3.5um region. The threshold reductions obtainable may bring the SRS process within the capability of a laser producing only a modest power output, or alternatively will increase the achievable Raman scattered tuning range.

A further conclusion reached in this work is that the use of a dispersive waveguide resonator is a useful tool in the discrimination between competing nonlinear processes. Thus, we obtained Raman scattering in methane

using a steady state, SLM, 1.064um pump, which generated 1.544um untroubled by Brillouin Scattering. To our knowledge this is the first time this has been achieved with a SLM pump.

A further conclusion to be drawn is that for media with very short response times for a particular nonlinear process, the use of short (picosecond) pulses in conjunction with a waveguide allows very small energy thresholds to be obtained. Thus, for SRS in methane (where the short pulses have the additional advantage of placing the Brillouin Scattering process in the transient regime and hence eliminating it as a competing process) threshold was reached with 130uJ fpr a 470ps long 1.064um pulse. This hassince been lowered to around 40uJ using a 100ps pulse (D J Pratt, Private Communication). At shorter wavelengths the energies will be even smaller. Again in methane, a threshold of 12uJ has been obtained for a 66ps long, 532nm pulse (D J Pratt, Private Communication). We envisage, therefore, the use of tunable, mode-locked dye laser pulses (from a c.w. laser) after amplification in dyes pumped by a copper vapour laser being used as pump pulses for SRS in gases. Such a system would have a very high repetition rate and would, we feel, provide a very versatile source of widely tunable coherent picosecond radiation.

APPENDIX I

Volume 40, number 1 OPTICS COMMUNICATIONS 1 December 1981

HIGH POWER, SINGLE FREQUENCY OPERATION OF A Q-SWITCHED TEM_{00} MODE NdYAG LASER

A.J. BERRY, D.C. HANNA and C.G. SAWYERS
Department of Electronics, University of Southampton, Highfield, Southampton S09 5NH, UK

Received 15 July 1981

An actively Q-switched NdYAG laser, using a telescopic resonator configuration has produced single longitudinal mode. TEM_{00} outputs of 100 mJ with output pulses free from any observable mode-beating.

A telescopic resonator configuration has recently been described [1,2] in which reliable operation of a Q-switched NdYAG laser with TEM_{00} energies of ~100 mJ was achieved. We have now applied to this laser a technique of active Q-switching which allows selection of a single longitudinal mode. Single frequency TEM_{00} outputs of ~100 mJ are obtained and the ripple-free output pulses show excellent amplitude stability. These results demonstrate the advantage the stable telescopic resonator holds over unstable resonator configurations, since frequency selection is more difficult in unstable resonators (see [3]) and more complex techniques involving injection from a stable single mode master oscillator have had to be adopted [4]. In our laser no attempts were made at temperature stabilisation of the overall resonator length, but despite this it was found that single frequency operation can persist for several hundred shots at 10 Hz repetition rate. With simple stabilisation techniques it is expected that single frequency operation with ripple-free output pulses could be maintained indefinitely.

The layout of the laser resonator is shown in fig. 1. The details of the telescopic resonator design have been given in [1,2] and the active Q-switching technique which we briefly summarise here was first described in [5,6]. The technique consists of initially setting the Pockels cell voltage to such a level that the laser is just able to reach oscillation threshold. The laser oscillation is monitored by a detector (see fig. 1. the monitored output consisting of light reflected off the polariser after being slightly depolarised by passing through the laser rod). The laser pulse grows slowly, taking very many cavity transits to reach a preset level

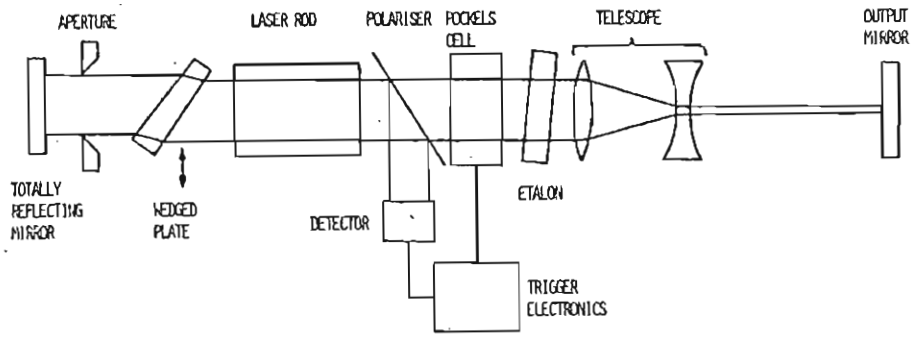

Fig. 1. Schematic layout of TEM_{00} mode telescopic resonator which single mode Q-switching.

0 030-4018/81/0000–0000/S 02.75

at which the output from the detector is used to trigger the Pockels cell open. As a result of these many transits a very large cumulative degree of mode-selection, enough for selection of a single mode, can be obtained from a selector such as a resonant reflector or tilted intracavity etalon even though these provide only a small selectivity per transit. When the Pockels cell is switched fully open this mode-selected radiation is amplified to the full Q-switched pulse energy.

Clearly it is the suppression of modes adjacent to the selected mode that presents the greatest problem and we adopt here as our criterion of "single-mode operation" the requirement that the displayed output pulse of the laser using a fast detector and oscilloscope (~1 ns response) must show no observable ripple due to beating between adjacent modes. This proves to be a very stringent requirement as the following example will show, but it does reflect the practical requirement for many experiments in which a high power pulse of very well defined intensity is needed. Consider the situation where a pulse contains just two oscillating modes with a ratio of their powers given by N (where $N > 1$), and let k be the difference in power between peak and trough of the modulation, normalised with respect to the mean power (see fig. 2). Then it can be shown that for $k \ll 1$, the relationship $k = 4N^{-1/2}$ applies. Typically one requires $k < 10^{-2}$ if beating is to be unobservable, hence the mode selection must ensure that one mode dominates its adjacent modes by a factor $N > 1.6 \times 10^5$. In [5], equations were derived for the power ratio P_m/P_n for two adjacent longitudinal modes after q round trips of a resonator containing either a resonant reflector (RR) or a transmission etalon (TE). In calculating the intensity ratio it was assumed in [5] that the selected mode is at a reflectivity maximum of the RR or a transmission maximum of the TE. The results are

$$\left(\frac{P_m}{P_n}\right)_{\mathrm{TE}} = \left[1 + \frac{8\pi^2\mu^2 l^2 R}{L^2(1-R)^2}\right]^q, \tag{1}$$

$$\left(\frac{P_m}{P_n}\right)_{\mathrm{RR}} = \left[1 + \frac{\pi^2\mu^2 l^2 (1-R)^2}{L^2(1+R)^2}\right]^q, \tag{2}$$

where, in each case the mode selector has surfaces of reflectivity R separated by a medium of thickness l and refractive index μ. L is the overall optical length of the laser resonator. It is clear from (1) and (2) that it is advantageous to make L small since this increases the expression in brackets i.e. enhances the mode selectivity. In addition a smaller L implies a larger number of transits q before the preset intensity is reached ‡. On the other hand, the telescopic resonator design favours a long resonator [1,2]. Despite these conflicting requirements, our results have shown that the conditions for single mode operation can in practice be met quite readily.

The value of L used for most of these experiments was 1.3 m, this being the length originally adopted in our telescopic resonator design [1,2] and the value of q was roughly estimated as 1000 [5]. If we consider the use of a tilted solid etalon of thickness l = 10 mm, refractive index 1.45, and reflectivity 60% it is found from (1) that $P_m/P_n = 5 \times 10^{15}$, which is clearly a large enough ratio to satisfy our criterion of single mode operation. Similarly, if we consider an uncoated resonant reflector of thickness 5 cm, and refractive index 1.45 (hence R = 0.0337), then (2) indicates that $P_m/P_n \approx 3 \times 10^{11}$. We have indeed found experimentally that single mode operation can be obtained with either a tilted etalon or a resonant reflector having the parameters indicated above and figs. 3a and 3b show multiple exposures of ~250 shots (at 12 Hz) and 50 mJ and 100 mJ output respectively, using the resonant reflector. After some tens of seconds, i.e. several hundred shots, the laser

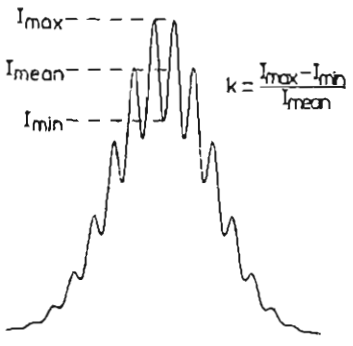

Fig. 2. Intensity I as a function of time showing beating between two modes having an intensity ration N. The normalised depth of modulation k is given by $k = 4N^{-1/2}$

‡ This fact is perhaps not obvious at first sight, but it must be remembered that the net round-trip gain is itself growing during the pulse growth.

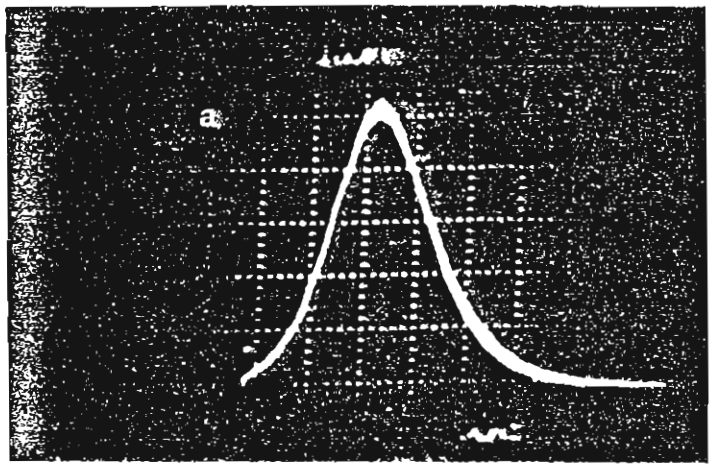

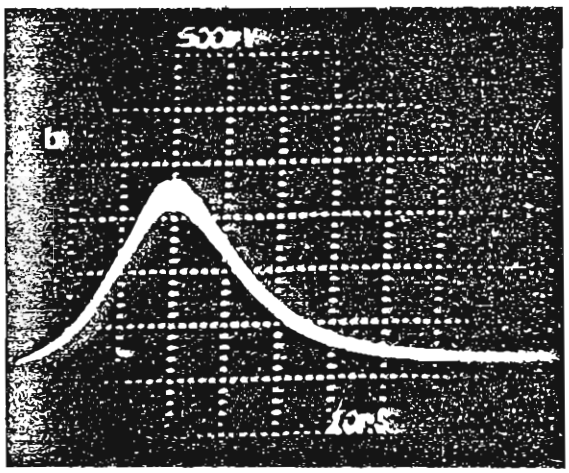

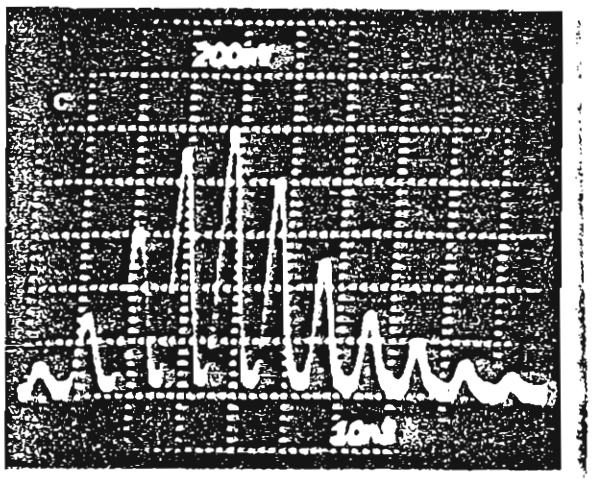

Fig. 3 (a). A multiple exposure of 250 output pulses (12Hz repetition rate) at 50mJ pulse energy in a TEM_{00} mode (20ns/division) (b). As (a) but at 100 mJ pulse energy (10ns/division). (c). A typical pulse showing beating between two modes after the resonator length has drifted. The beat-free pulse of (a) is restored by translating a wedged plate across the resonator axis.

drifts into two-mode operation (due to a drift of the overall optical length of the resonator) and fig. 3c shows a typical output pulse under those conditions. Single mode operation is restored very simply by translating an intracavity wedged plate across the beam, thus tuning the resonator length, until beat-free pulses are again observed. The simplicity of this operation, and the length of time before adjustments are required (~1 min) suggests that a simple feed-back scheme should permit essentially beat-free pulses to be maintained indefinitely.

The single mode Q switching technique described here relies for its success on the cumulatively large mode selection that results when a small degree of frequency discrimination is experienced for many round trips. The required frequency selection can then be provided by a single device and this offers the advantage that the degree of mode selection can both be calculated and controlled with ease. On the other hand it does mean that care must be taken to avoid any spurious, unwanted frequency selection, since even quite small effects can end up by modifying or even dominating the intended frequency selection. Examples of this are etalon effects from the laser rod faces and from the various surfaces in the Pockels cell. Our Pockels has wedged windows and a wedged crystal to avoid such effects. Similarly, a laser rod with wedged faces can be used. In our case the rod had parallel

faces, so these were misaligned by ~30 min from the beam axis. It has been noted [7] that alignment of the rod faces parallel to the resonator mirror can give a very large degree of mode selection, enough to achieve single mode using conventional Q-switching. We have also observed this behaviour, but the realibility was poor and the effect was therefore deliberately suppressed by tilting the laser rod. With these precautions taken the dominant cause of mode selection was then provided by the resonant reflector or tilted etalon.

When considering whether to use a transmission etalon or resonant reflector it appears at first sight that the tilted etalon has two advantages. Firstly (1) suggests that provided R is made large enough then l can be made quite small. Thus oscillation on adjacent resonances of the etalon would be suppressed since with one resonance arranged to coincide with the peak of the gain curve, the adjacent resonances would fall well outside the gain-narrowed line. One must however use (1) with caution, since it assumes the theoretical finesse corresponding to a situation with plane waves incident on the etalon. In practice the walk-off loss of a finite size beam within a tilted etalon leads to a degradation of its finesse [8,9] and hence a smaller selectivity than (1) suggests. The magnitude of this effect is not easy to quantify, although rough estimates have been derived [10,11]. The walk-off loss can be kept to a minimum by using the etalon as close to normal incidence as possible while avoiding laser oscillation due to the etalon reflection. Despite this precaution we found that the high reflectivity etalon (R ~ 60%, l = 10 mm) still showed a significant insertion loss and an increased pumping level was therefore required to restore the output to the 100 mJ level. To tune the etalon transmission into coincidence with the gain curve one can either adjust the angle of tilt or change its temperature. The resonant reflector does not suffer from problems of beam walk-off. It is however necessary to use a larger l to get sufficient selection between adjacent modes and this in turn means that some additional selection is required to suppress oscillation on adjacent resonances of the reflector. With the 5 cm RR used in our experiments it is found that an uncoated silica plate of 6 mm thickness, used as a tilted transmission etalon, is quite enough to achieve this suppression, as can be confirmed using (1) with L interpreted as the optical thickness of the resonant reflector. This transmission etalon was tilted to ensure that its transmission maximum coincided with the resonance of the reflector. Operated in this way we found that it was not necessary to temperature tune the resonant reflector to coincide with the gain maximum of the laser medium. An advantage of this RR mode selection scheme is that the tilted, low reflectivity etalon was found to exhibit only a small insertion loss. Eqs. (1) and (2) both assume that the mode to be selected is situated at the peak of the selector's frequency response. This can be achieved by fine-tuning the angle of the tilted etalon or tuning the temperature of the resonant reflector, or (and this has proved the most convenient) by tuning the resonator length by means of the wedged plate.

A number of further precautions have contributed to the realibility of single mode operation. Mechanical stability is clearly important and all components have therefore been firmly bolted down to a good quality optical table (NRC). The laser rod has been positioned as close as possible to the resonator mirror, thus exploiting the spatial hole-burning behaviour to discourage growth of adjacent modes when the dominant mode has saturated the gain [12]. Before taking this precaution the laser rod has been situated close to the centre of the resonator and the main laser pulse was seen to be followed by a weaker secondary pulse (up to ~15% of the main pulse energy). With the rod placed near the mirror this secondary pulse was no longer observed. Finally, we found that the krytron switching circuit which opened the Pockels cell produced a considerable amplitude of voltage spiking, which in turn led to amplitude modulation of the output pulse. This could easily be misinterpreted as mode beating. By cleaning up the voltage step to the Pockels cell this effect was removed and completely smooth pulses were then obtained as shown in fig. 3.

In conclusion, we have shown that the telescopic resonator, whose capability of producing large TEM_{00} mode volume has already been demonstrated, can also be operated so as to give reliable single longitudinal mode output.

This work has been supported in part by the Science Research Council and J.K. Lasers. One of us (A.J.B.) holds a Case studentship sponsored by J.K. Lasers. We also wish to acknowledge the loan of the 5 cm etalon by Dr. Malcolm White, with whom we also had valuable discussion.

Note added

Park and Byer [13] have recently reported the application of a Q-switching technique, which they refer to as electronic linewidth narrowing ("ELN"), to an unstable resonator Nd : YAG laser. Apart from the fact that their Q-switch is triggered open during the second rather than the first prepulse, their ELN technique is identical to that reported in the present paper and first reported by Hanna et al. in 1972 [5,6]. The two-step-Q-switching technique referred to by Park and Byer is incorrectly referenced. It was first reported by Hanna et al. in 1971 [14], but was quickly abandoned in favour of the simpler technique of our ref. [5]. It should also be noted that the application of "ELN" to an unstable resonator NdYAG laser, with a discussion of the special problems posed by unstable resonators was previously reported by Hanna and Laycock in 1979 [3].

References

[1] D.C. Hanna, C.G. Sawyers and M.A. Yuratich, Optics Comm. 37 (1981) 359.
[2] D.C. Hanna, C.G. Sawyers and M.A. Yuratich, to be published (Opt. Quant. Electron.).
[3] D.C. Hanna and L. Laycock, Opt. Quant. Electron. 11 (1979) 153.
[4] Y.K. Park, G. Giuliani and R.L. Byer, Optics Lett. 5 (1980) 96.
[5] D.C. Hanna, B. Luther-Davies and R.C. Smith, Opto-Electron. 4 (1972) 249.
[6] D.C. Hanna, B. Luther-Davies and R.C. Smith, Electron. Lett. 8 (1972) 369.
[7] D. Bua, D. Fradin and M. Bass, IEEE J. Quant. Electron QE-8 (1972) 916.
[8] D.G. Peterson and A. Yariv, Appl. Optics 5 (1966) 985.
[9] W. Culshaw, J. Kannelaud and J.E. Peterson, IEEE J. Quant. Electron. QE-10 (1974) 253.
[10] H.G. Danielmeyer, IEEE J. Quant. Electron. QE-6 (1970) 101.
[11] M. Hercher, Appl. Optics 8 (1969) 1103.
[12] B. Luther-Davies and V. Del Pizzo, Optics Comm. 30 (1979) 403.
[13] Y.K. Park and R.L. Byer, Optics Comm. 37 (1981) 411.
[14] D.C. Hanna, B. Luther-Davies, H.N. Rutt and R.C. Smith, Opto-Electron. 3 (1971) 163.

APPENDIX II

Optical and Quantum Electronics **15** *(1983)* · *Short Communication*

Short Communication

Dependence of stimulated Raman threshold on the pump bandwidth

The question of Raman gain (or threshold) dependence on pump laser bandwidth, $\Delta\nu_L$, has received considerable attention, both theoretical and experimental ([1, 2] and references therein). One aspect of this question has been particularly emphasized, namely the comparison between Raman gain for a single-mode pump pulse and for a multi-mode pump pulse. To be specific, let us consider the case of a single-mode pump pulse having a bandwidth much less than the Raman medium linewidth, $\Delta\nu_L \ll \Delta\nu_R$, and a multi-mode pump pulse for which the inequality is reversed, i.e. $\Delta\nu_L \gg \Delta\nu_R$. Let us also consider these two pulses (temporally smooth in the single-mode case and deeply modulated in the multi-mode case) to have envelopes of the same overall duration. Then the conclusion reached by theoretical analysis and confirmed by experiments [1, 2] is that for forward Raman scattering in a dispersionless medium the threshold pump energy is the same in each of these two cases.

This is a useful result since it indicates that in some circumstances the requirements on frequency selection of the pump laser can be greatly relaxed. It is important to note however that the Raman gain is not entirely independent of the pumping laser bandwidth [3], a fact that is in danger of being overlooked. We refer to a situation, which is quite likely to be encountered experimentally, where the laser output is in more than one mode but still with a bandwidth $\Delta\nu_L$ less than $\Delta\nu_R$. We shall refer to this as a multi-mode narrowband pump. In this case the threshold will be less than for the single-mode and multi-mode broadband ($\Delta\nu_L \gg \Delta\nu_R$) cases. A simple explanation of this can be given by considering the behaviour in the time domain. Temporal structure in the pump pulse cannot be shorter than $\sim 1/\Delta\nu_L$ and provided this structure is long in duration compared to the characteristic response time ($\sim 1/\Delta\nu_R$) of the Raman medium, i.e. $\Delta\nu_L \ll \Delta\nu_R$, then the medium will show a steady state response to the intensity variations within the pulse. (Strictly, one should also take account of the highly nonlinear dependence of Stokes wave growth on the pump intensity, so the above inequality becomes $\Delta\nu_L \ll \Delta\nu_R/G$ where G is the gain exponent [4]). Since a multi-mode pulse contains peaks of greater intensity than a single-mode pulse of the same energy, the multi-mode narrowband pulse will yield a lower energy threshold for forward stimulated Raman scattering. This situation was not explicitly considered in the various experimental investigations into threshold dependence on pump bandwidth [1, 2, 5]. To clarify this point we have therefore measured the stimulated vibrational Raman scattering threshold in hydrogen gas for 1.06 μm pump pulses with the following characteristics: 1. single mode, $\Delta\nu_L \ll \Delta\nu_R$, 2. two-modes, $\Delta\nu_L \ll \Delta\nu_R$, 3. multi-mode broadband, $\Delta\nu_L \gg \Delta\nu_R$. As expected we have found the threshold to be the same for cases 1 and 3. For case 2 the threshold was found to be lower by a factor of ~ 1.5, in principle a factor of 2 would be expected if steady state conditions had been achieved since the peaks are twice as intense as in a single-mode pulse.

The laser used in these measurements has been described in [6–8]. It provided a TEM_{00} output and when Q-switched in a conventional way its output linewidth was $\sim 0.3\ cm^{-1}$, thus satisfying the requirement for multi-mode broadband pumping. When operated with prelase-triggered Q-switching [8], single-longitudinal mode (SLM) operation was obtained, with pulses free from intensity modulation. The periods of SLM operation, which lasted for typically 1–2 min, were separated by periods of 10–20 s during which the pulses showed a sinusoidal intensity modulation. The modulation frequency corresponded to adjacent mode beating, i.e. at a frequency $C/2L$ = 115 MHz, and the depth of modulation varied from shot to shot, occasionally reaching the base line when the two modes were of equal intensity. The lowest Raman threshold was observed, as expected, with these deeply modulated pulses.

The Raman scattering medium was hydrogen gas, contained in a cell of 58 cm length. The cell was equipped with Brewster-angle windows to suppress any Stokes or pump feedback. This is an important precaution to take since the backward

0306–8919/83 $03.00 + .12.

Raman gain is very different for narrowband and broadband pumping (see e.g. [9]), and the presence of any feedback between forward and backward waves could lead to a spurious dependence of threshold on pump linewidth. The laser beam was tightly focussed into the cell, with the beam waist at the cell centre having a confocal parameter of 2.5 cm. The laser was operated at the same flashlamp input for all measurements and the laser energy input to the cell was varied by means of an attenuator consisting of a pair of tilted glass plates. This arrangement ensured that the beam profile and pulse duration were unchanged as the intensity was adjusted. The stimulated Raman scattering (SRS) threshold was detected by visual observation of the appearance of a green beam (564 nm) resulting from the second anti-Stokes scattering and the threshold pump energy was measured by a calorimeter at the input to the cell.

Fig. 1 shows the results of these threshold measurements for a range of hydrogen pressures. The threshold power is defined as (threshold energy) x 0.94/pulse envelope duration (full width at half maximum, FWHM), the factor 0.94 being appropriate to a Gaussian time dependence. The pulse duration was found to have the following values: (a) 32 ns for SLM operation and two-mode operation and; (b) 29 ns for broadband operation. The abscissa in Fig. 1 includes some calculated values (using data from [5]) for the Raman linewidth $\Delta\nu_R$ (FWHM). The upper solid curve in the figure shows the calculated threshold for SLM pumping assuming a steady state response. It can be seen that the experimental results for both SLM and broadband pumping agree well with the calculation. Fig. 1 also clearly indicates a significantly lower threshold for the two-mode pumping. What is also apparent is that the threshold reduction for two-mode pumping is less significant at lower pressures. The explanation for this probably lies in the fact that for narrower Raman linewidths (e.g. ~ 450 MHz at 10 atm pressure) the requirement for steady state response to the variations of intensity of the two-mode pump is clearly not satisfied. In fact it is likely that steady state conditions were not fully reached even at the highest pressure used and this could account for the fact that the two-mode threshold reduction was less than the expected factor of two.

In conclusion, we have given a direct experimental confirmation of the fact that although the Raman threshold is the same for single-mode and broadband pumping ($\Delta\nu_L > \Delta\nu_R$) it is reduced when the pump laser is narrowband ($\Delta\nu_L < \Delta\nu_R$) but not single-mode.

It is important to note, therefore, that in measurements of Raman threshold where a narrowband pump laser is used ($\Delta\nu_L < \Delta\nu_R$), the laser must be single-mode if the results are to be unambiguous. On the other hand, it is also clear that if the aim is to achieve SRS for a minimum pump energy then it is advantageous to use a narrowband ($\Delta\nu_L < \Delta\nu_R$) but multi-mode pump.

Acknowledgements

This work has been supported by the Science and Engineering Research Council and one of us (AJB)

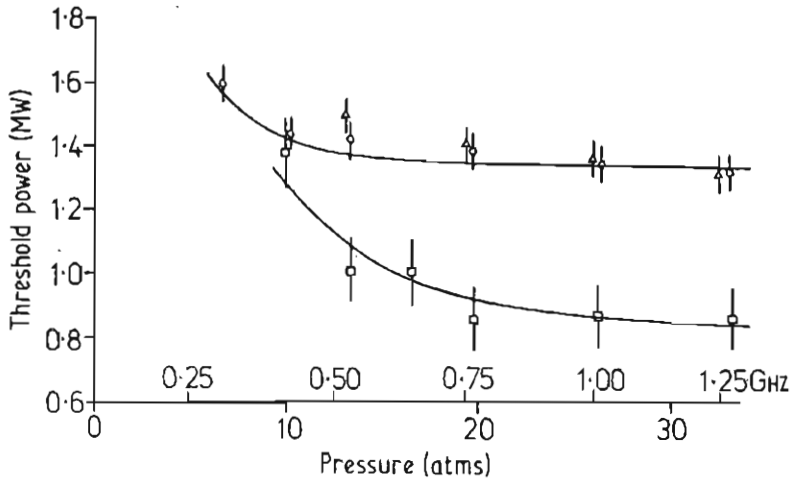

Figure 1 Stimulated vibrational Raman threshold power for a 1.06 μm pump in hydrogen gas, as a function of gas pressure. Linewidths (FWHM) of the Raman transition in GHz are also indicated. Threshold power is defined here as (threshold energy) X 0.94/pulse duration (FWHM). The upper solid curve is a theoretical calculation assuming steady state response. Experimental points correspond to; ○ – SLM pump, □ – two-mode pump, △ – broadband pump.

Short Communication

holds a CASE studentship sponsored by J. K. Lasers Ltd. We acknowledge valuable discussions with M. C. Ibison.

References

1. S. A. AKHMANOV, Yu. E. D'YAKOV and L. I. PAVLOV, *Sov. Phys. JETP.* 39 (1974) 249–56.
2. W. R. TRUTNA, Y. K. PARK and R. L. BYER, *IEEE J. Quant. Elect.* QE-15 (1979) 648–55.
3. N. BLOEMBERGEN and Y. R. SHEN, *Phys. Rev. Lett.* 13 (1964) 720–4.
4. S. A. AKHMANOV, K. N. DRABOVICH, A. P. SUKHORUKOV and A. S. CHIRKIN, *Sov. Phys. JETP* 32 (1971) 266–73.
5. W. R. TRUTNA and R. L. BYER, *Appl. Opt.* 19 (1980) 301–12.
6. D. C. HANNA, C. G. SAWYERS and M. A. YURATICH, *Opt. Commun.* 37 (1981) 359–62.
7. *Idem, J. Opt. Quant. Elect.* 13 (1981) 493–507.
8. A. J. BERRY, D. C. HANNA and C. G. SAWYERS, *Opt. Commun.* 40 (1981) 54–8.
9. J. R. MURRAY, J. GOLDHAR, D. EIMERL and A. SZÖKE, *IEEE J. Quant. Elect.* QE-15 (1979) 342–59.

Received 24 November 1982

A. J. BERRY
D. C. HANNA
Department of Physics
University of Southampton
Highfield
Southampton
UK

APPENDIX III: REALISTIC PUMP TEMPORAL PROFILES IN RAMAN OR BRILLOUIN RESONATOR THEORY

We treat here the general case of a resonator of length L bounded by mirrors with Stokes reflectivities R_1 and R_2. These mirrors are assumed to be transparent at the pump wavelength implying that the pump pulse experiences only a single transit of the resonator. Because of the pump pulse duration, however, the Stokes wave is capable of making many transits of the resonator whilst some pump power is within it. In this way the effective interaction length is increased.

In the two configurations we will look at in this thesis the Stokes power $P_s(L)$ after an interaction length L is given by;

$$P_S(L) = P_s(L=0)\ \exp\{gCP_p - 2\gamma_s L\} \qquad A1$$

Where the constant C includes terms which account for the transverse profile of the pump and also any linear pump losses. The term $-2\gamma_s L$ is a linear Stokes loss. Clearly equation 3.65 is an example of this, where $C = 4A\tan^{-1}(LB/2)$ and $\gamma_s = 0$. We now allow P_p to vary with time.

$$P_p(t) = P_{P0}.f(t)$$

After one transit of the resonator (i.e. one pass in one direction) the Stokes power emerging from mirror 2 can be written as;

$$P_{s,out_1} = P_{S,N}\ \exp\{g_F C P_{P0} f(t=0) - 2\gamma_s L\}\ (1-R_2) \qquad A2$$

after three transits the power emerging from mirror 2 can be written as;

$$P_{s,out_3} = P_{S,N} \exp\left\{ g_F C P_{P0} f(t=0) - 2\gamma_s L \right\} R_2 \exp\left\{ g_{Ba} C P_{P0} f(t=t_T) - 2\gamma_s L \right\}$$

$$\times R_1 \exp\left\{ g_F C P_{P0} f(t=2t_T) - 2\gamma_s L \right\} (1-R_2)$$

and after n transits (n odd); A3

$$P_{s,out,n} = P_{S,N} (R_1 R_2)^{\left(\frac{n-1}{2}\right)} (1-R_2) \exp\left\{ -2n\gamma_s L \right\} \quad A4$$

$$\times \exp\left\{ g_F C P_{P0} \left[f(t=0) + b f(t=t_T) + f(t=2t_T) + \ldots. \right.\right.$$

$$\left.\left. \ldots. f(t=(n-1)t_T) \right] \right\}$$

where g_F and g_{Ba} are the gain coefficients for forwards and backwards Stokes respectively, $b = g_{Ba}/g_F$ and t_T is the cavity transit time. Note that except for a possible pump loss across the resonator of the form $P_p(L) = P_p(0) \cdot \exp(-2\gamma_p L)$ it has been assumed that the pump seen in the backwards Stokes direction is a constant with time for the duration of the transit. This is an acceptable approximation as long as $dP(t)/dt \ll P(t)/t_T$. If we now take the case of a pump pulse with a Gaussian temporal profile as given by equation 3.63, and shift the origin of time to the peak of the Gaussian, equation A4 can be rewritten;

$$P_{s,out,n} = P_{S,N} (R_1 R_2)^{\left(\frac{n-1}{2}\right)} (1-R_2) \exp\left\{ -2n\gamma_s L \right\} \exp\left\{ g_F C P_{P0} \, S \right\} \quad A5$$

Where $S = 1 + 2b \exp\left\{ \frac{-a t_T^2}{T^2} \right\} + 2 \exp\left\{ \frac{-a(2t_T)^2}{T^2} \right\} + \ldots.$

$$\ldots. + 2 \exp\left\{ \frac{-a\left[\left(\frac{n-1}{2}\right) t_T \right]^2}{T^2} \right\} \quad A6$$

If we now require that $\ln(P_{s,outn}/P_{S,N}) = 30$, as usual, for threshold, equation A5 can be rearranged to give;

$$P_{P0} = \frac{30 - (\frac{n-1}{2}) \ln (R_1 R_2) - \ln(1-R_2) + 2n\gamma_s L}{g_F CS} \qquad A7$$

This equation is our final expression for the threshold pump power in an arbitrary Stokes resonator using pump pulses with Gaussian temporal profiles.

APPENDIX IV

Volume 43, number 3 OPTICS COMMUNICATIONS 1 October 1982

LOW THRESHOLD OPERATION OF A WAVEGUIDE H_2 RAMAN LASER

A.J. BERRY, D.C. HANNA and D.B. HEARN
Department of Electronics, University of Southampton, Highfield, Southampton SO9 5NH, UK

Received 13 July 1982

The use of a fused silica capillary for reduction of stimulated Raman scattering threshold in H_2 gas has been investigated. A threshold pump power at 1.06 μm of 70 kW has been obtained, a twentyfold reduction over free space propagation. Further threshold reduction should be possible by taking care over capillary straightness.

Stimulated Raman Scattering (SRS) provides a convenient and efficient means of shifting the frequency of high power lasers [1]. This is particularly interesting in the case of tunable lasers since their tunability can then be extended to other regions of the spectrum. In this context high pressure H_2 gas has been widely used as a Raman medium since it offers a number of attractive features such as a large Raman shift, a narrow transition linewidth, a good transparency and freedom from problems caused by stimulated Brillouin scattering and self-focussing. Its drawback is that to reach SRS threshold, pump power levels of around 1 MW are typically required. A reduction of these threshold powers by one or two orders of magnitude could offer much more scope for the application of SRS, in particular to frequency down-conversion of various tunable near-infrared lasers operating at more modest power levels, e.g. vibronic lasers, colour centre lasers or optical parametric oscillators. A further advantage of achieving a low threshold is that one can divide the available pump power to drive a Raman oscillator and amplifier. This configuration can result in a more efficient channeling of the pump power into the intended Stokes radiation [2].

Techniques which have been applied to reduce the SRS threshold include the use of multiple pass configurations [3,4], the use of resonators to provide feedback of the Stokes radiation [5] and the use of hollow dielectric waveguides to guide the pump and Stokes radiation [6,7]. In fact a combination of waveguiding and feedback could be used, as in waveguide lasers [8] and this should in principle give a reduction of SRS threshold by something like two orders of magnitude. To investigate this possibility we chose first to address the question of how great a threshold reduction can be achieved in practice simply by using a capillary waveguide. The experiments described by Rabinowitz et al. [6] and Hartig and Schmidt [7] emphasized a comparison of conversion efficiency with and without guiding but they do not give an explicit comparison of threshold powers. In this letter we report results for the generation of 1.9 μm Stokes radiation from a 1.06 μm pump in H_2 gas contained in a capillary waveguide. A threshold pump power of 70 kW has been achieved, representing a factor of twenty reduction compared with unguided propagation. With better quality capillaries and with feedback of the Stokes wave a further significant reduction appears feasible.

The pump source used in our experiments was a Q-switched NdYAG laser providing a high output power in a clean TEM_{00} beam and in a single longitudinal mode [9,10]. This well-defined laser output is helpful for a careful comparison of measured and predicted thresholds. The use of a TEM_{00} beam also conferred other advantages. It allowed well-defined launching conditions into the capillary and this has enabled us to avoid optical damage even when operating with an on-axis beam intensity up to an order

0 030-4018/82/0000–0000/$ 02.75

of magnitude higher than the damage threshold of the capillary material (fused silica). The TEM_{00} mode couples very efficiently into the lowest loss mode (EH_{11}) of the capillary [8]. The TEM_{00} beam was also helpful in the procedure for adjusting the capillary for optimum transmission, since this was based on the visual observation (via burn paper and phosphor card) of a clean beam of circular symmetry leaving the output end of the capillary. A photodiode array was used to confirm that the emerging beam was diffraction-limited.

Initial measurements of SRS threshold were made in H_2 gas in a high pressure cell of large bore (i.e. no guiding was involved). Brewster angle end windows were used to suppress pump and Stokes feedback. The cell length was 58 cm and the pump beam was focussed to a beamwaist at the centre of the cell, with a spot size ($W_0 = 0.10$ mm) chosen to make the confocal parameter ($b = 2\pi W_0^2/\lambda$) much less than the cell length. Using the value of plane wave Raman gain coefficient as calculated by Trutna and Byer [4], and the analysis of Cotter et al. [11] to account for the actual gaussian beam profile of pump and Stokes waves we have calculated the threshold pump power as a function of gas pressure. Above ~4 atmospheres the threshold is essentially independent of pressure and the predicted threshold (1.4 MW) and measured threshold (1.3 ± 0.15 MW; 35 mJ in a 25 ns FWHM pulse) are in good agreement. In the calculation of threshold it was assumed that a net single pass Stokes gain of exp(30) was required and this coincided with the experimentally defined criterion that a Stokes energy of ~10 μJ corresponded to threshold being exceeded. This criterion was found to correspond to the experimentally more convenient observation of a visually detectable green beam of 2nd antiStokes radiation (564 nm).

For the capillary waveguide measurements we have used a variety of capillary lengths and internal diameters, all made of fused silica. We confine ourselves mainly to a discussion of the results obtained from a 1 m length of capillary of 330 μm bore diameter and outside diameter of 5 mm. The high pressure cell made use of the capillary itself as the walls of the pressure vessel. This was an important feature of the design since it allowed the capillary to be clamped into a V-groove and thus some control could be exercised over the tube straightness. The end windows were held in high pressure metal fittings which were O-ring sealed to the outside of the capillary and also clamped to ensure they could not slide off the end. Unfortunately with the metal fittings available the distance from the window to the capillary end was only ~5 cm and the small pump spotsize on the window ($W = 190$ μm, corresponding to $W_0 = 110$ μm at the capillary) meant that the input energy was limited to <15 mJ to avoid window damage. In a separate measurement we have transmitted 50 mJ, 25 ns pulses through a 25 cm length of 300 μm bore capillary with no sign of damage, even though dust particles in the capillary cause air breakdown.

The pump spot size W_0 at the capillary entrance was matched to the capillary diameter, $2a$, by arranging that $3W_0 = 2a$, for which condition the input gaussian beam should couple with 98% efficiency to the EH_{11} mode of the guide [12]. The entire assembly of V-groove and guide was then positioned by horizontal and vertical adjustments applied at the input and output ends (the former being the more critical), until the output beam was seen to have good circular symmetry. A maximum measured guide transmission of 60% was obtained in this way, and it was confirmed using a photodiode array that the exit beam was diffraction-limited. In fact a calculation of the guide transmission following the analysis of Marcatili and Schmeltzer [13] yields a transmission, T, of 86.5% for a straight guide ($T = \exp(-2\alpha_{11}l)$, $\alpha_{11} = 0.216\,\lambda^2/a^3$ for fused silica with $n = 1.455$). It is thought that most of the loss in this capillary arises from bends. Marcatili and Schmeltzer show that a bend of radius R gives rise to an additional loss (to be added to α_{11}) which, in the case of fused silica, is given by $19.4\,a^3/\lambda^2R^2$. To give some idea of the sensitivity to bends we note that a bend radius of 25 m (caused for example by the core oscillating transversely with an amplitude of 200 μm over a period of 0.2 m) would account for ~22% loss in this guide. These numbers underline the importance of holding the capillary straight. However it is also apparent that even a small, and difficult to detect, wander of the core relative to the outer capillary wall could introduce large losses.

Despite the imperfect transmission properties of this capillary (i.e. a measured loss α which is 3.5 times greater than predicted for a straight guide) the SRS threshold was found to be only 130 kW (3.5 mJ in 25 ns), an order of magnitude less than for the un-

guided situation. For a pump energy input of 12 mJ, a 1 st Stokes output of 1 mJ was measured in the forward direction (15% photon conversion efficiency). A rough estimate of the expected threshold reduction can be made by comparing the input powers, P, required to give the same product of medium length and on-axis intensity. For unguided propagation this product is given by

$$\int_{-l/2}^{+l/2} \frac{2P}{\pi W^2(z)}\,\mathrm{d}z = \frac{4P}{\lambda}\tan^{-1}(l/b)\,, \qquad (1)$$

where $b \equiv 2\pi W_0^2/\lambda$ and $W_0 = W(0)$. When $l \gg b$ the integral has the value $2\pi P/\lambda$. For the case of guided propagation, we assume the power decays according to $P\exp(-2\alpha z)$ and the product is given by

$$\int_0^l \frac{2P\exp(-2\alpha z)}{\pi W_0^2}\,\mathrm{d}z = \frac{2Pl}{\pi(2a/3)^2}\,\frac{[1-\exp(-2\alpha l)]}{2\alpha l}, \qquad (2)$$

where we have put $3W_0 = 2a$. Comparing this with $2\pi P/\lambda$, and putting in the values $l = 1$ m, $a = 165$ μm, $\exp(-2\alpha l) = 0.6$ yields a predicted threshold reduction of ~7, in reasonable agreement with the observed reduction. The discrepancy is probably due to the additional reduction which arises from Stokes guidance. More detailed calculations taking account of the radially varying gain distribution, and also Stokes diffraction and guiding will form the subject of a further publication [14].

Thus we have demonstrated experimentally that a reduction of SRS threshold by an order of magnitude can be achieved even with a capillary tube having significantly greater losses than predicted for a straight tube. If one considers the possibility of a perfectly straight capillary one can show [13] that a 60% transmission of a 1.06 μm beam over a 1 m length of guide would imply $a = 100$ μm, and hence from (1) (i.e. neglecting the effect of Stokes losses) a further reduction in threshold of $(165/100)^2 \sim 3$ is implied. We have carried out some further measurements which confirm the importance of capillary straightness and which also show that a reduction of bore diameter offers a further threshold reduction. The results discussed above were obtained when the capillary was held in a piece of extruded aluminium angle. The same tube held in a precision V-groove (tolerance of <50 μm) gave a transmission of 75% instead of 60%, implying that the loss coefficient α had been further reduced by a factor of 1.8. Good results have also been obtained with thin wall fused silica capillaries of 300 μm diameter (outside diameter 400 μm). A He-Ne laser beam, at 633 nm, gave a measured transmission of 92% over a 1 m length of capillary held in the precision V-groove; theoretical transmission [13] is 95%, and this theoretical value does not include the ~2% loss due to launching [8]. Clearly a more systematic set of loss measurements is called for (as e.g. in [15]) to check how closely the observed losses approach the predictions of Marcatili and Schmeltzer [13]. We have observed SRS in H_2 contained in a thin walled capillary (150 μm bore, 270 μm outside diameter) by inserting the thin capillary into a thick walled capillary of 300 μm bore which was held in the precision V-groove and equipped with end windows as described above. The best transmission for the 1.06 μm pump was only 15%, nevertheless a threshold energy as low as 1.9 mJ (i.e. 70 kW power) was observed, corresponding to a twentyfold reduction compared with unguided propagation. These results confirm that with proper attention to capillary quality and straightness a very substantial threshold reduction is possible. It should be noted that the threshold power we have reached is already comparable to the power output available from some vibronic laser systems [15].

This work has been supported by a grant from the Science and Engineering Research Council and one of us (AJB) wishes to acknowledge support from the SERC and from J.K. Lasers Ltd. in the form of a CASE studentship. We also wish to acknowledge M. Ibison for helpful discussion, I. Carr for measurements on the thin walled capillary and Dr. D.N. Payne and Colleagues in the Optical Fibre group for producing the thin walled capillary.

References

[1] M. Maier, Appl. Phys. 11 (1976) 209.
[2] H. Komine, E.A. Stappaerts, S.J. Brosnan and J.B. West, Appl. Phys. Lett. 40 (1982) 551.
[3] N.V. Kravtsov and N.I. Naumkin, Sov. J. Quantum. Electron. 6 (1976) 1438.
[4] W.R. Trutna and R.L. Byer, Appl. Optics 19 (1980) 301.
[5] A.Z. Grasiuk and I.G. Zubarev, Appl. Phys. 17 (1978) 211.
[6] P. Rabinowitz, A. Kaldor, R. Brickman and W. Schmidt, Appl. Optics 15 (1976) 2006.

[7] W. Hartig and W. Schmidt, Appl. Phys. 18 (1979) 235.
[8] R.L. Abrams, in: Laser handbook, Vol. 3, ed. M.L. Stitch (North Holland, Amsterdam, New York, Oxford, 1979) Ch. A2.
[9] D.C. Hanna, C.G. Sawyers and M.A. Yuratich, Optics Comm. 37 (1981) 359.
[10] A.J. Berry, D.C. Hanna and C.G. Sawyers, Optics Comm 40 (1981) 54.
[11] D. Cotter, D.C. Hanna and R. Wyattt, Appl. Phys. 8 (1975) 330.
[12] R.L. Abrams, IEEE J. Quant. Electron. QE-8 (1972) 838.
[13] E.A.J. Marcatili and R.A. Schmeltzer, Bell Syst. Tech. J. 43 (1964) 1783.
[14] D.C. Hanna and M. Ibison (in preparation).
[15] D.R. Hall, E.K. Gorton and R.M. Jenkins, J. Appl. Phys. 48 (1977) 1212.
[16] P.F. Moulton, XII Intern. Quantum Electronics Conf., Munich, June 1982.

APPENDIX V

Volume 45, number 5 OPTICS COMMUNICATIONS 1 May 1983

STIMULATED RAMAN OSCILLATION IN CAPILLARY WAVEGUIDE RESONATORS

A.J. BERRY and D.C. HANNA
Department of Physics, University of Southampton, Highfield, Southampton, SO9 5NH, UK

Received 26 January 1983

The threshold for stimulated Raman scattering in H_2 gas using a 1.06 μm pump has been reduced by a factor of 30 (to ~40 kW in a 35 ns pulse) by the combined use of a capillary waveguide and a resonator providing Stokes feedback. Similar enhancement has been observed in CH_4 where, in addition, the use of a dispersive resonator has allowed suppression of stimulated Brillouin scattering even with single mode pumping.

The application of capillary waveguide techniques [1] to stimulated Raman scattering (SRS) was first reported by Rabinowitz et al. [2] and Hartig and Schmidt [3]. In a recent paper [4] we gave results of an investigation into the threshold reduction that can be achieved by the use of such waveguides. In this paper we report results obtained with the combined use of waveguiding and feedback of the Stokes wave. With this waveguide resonator the threshold for SRS in H_2 gas was reduced to ~40 kW for a 1.06 μm pump (Stokes wavelength 1.9 μm) corresponding to a reduction of threshold by a factor of 30 compared with the case of an unguided gaussian beam pump without Stokes feedback. A simple analytical model of the Raman oscillator gives good agreement with the experimental results and thus suggests that the analysis should provide a useful guide in extrapolating to different experimental conditions (e.g. different pump wavelength, guide dimension, resonator length, pump pulse duration etc.) The low threshold is attractive since it brings the technique of SRS within reach of lasers of modest power. An interesting example would be the use of a Cu vapour pumped dye laser as the pump for a waveguide Raman laser, offering a pulsed source of high repetition rate and wide infrared tunability via multiple Stokes shifts [3]. Besides leading to a reduction of threshold the use of an oscillator configuration can provide further advantages. For example, we have used a dispersive Raman resonator, containing a prism, to suppress Brillouin feedback when using CH_4 as the Raman medium. With this technique, CH_4 now looks a more attractive Raman medium since it has suffered from the twin disadvantages of a high threshold for Raman scattering and a relatively low threshold for Brillouin scattering.

The pump laser used in these experiments was a TEM_{00} mode Q-switched NdYAG laser operating in a single longitudinal mode, as described in [5], giving an output energy up to 100 mJ in a pulse of duration τ, between 30 and 40 ns. Various capillary dimensions have been tried but typically had a length $l \sim 30$ cm, and an inside diameter ($2a$) of ~200 μm. Usually the capillary was in the form of a thin-walled tube (~300 μm outside diameter) inserted into a supporting capillary of inside diameter ~300 μm and outside diameter ~5 mm [4]. This was then placed inside a pressure vessel consisting of a steel tube equipped with end fittings holding Brewster angled fused silica windows to suppress window feedback. The Brewster windows were spaced by 44 cm, thus leaving a gap of ~7 cm between capillary and window at each end. In all our measurements the pump was focussed into the capillary to satisfy the condition $3w'_0 = 2a$ [6]. A representative measurement of Raman threshold in H_2 for a single pass through the capillary (i.e. without feedback) was as follows: $l = 27.5$ cm, $2a = 200$ μm, pump transmission $T = 60\%$, gas pressure 25 atm, threshold energy 9.1 mJ, hence peak power 260 kW ($\tau = 33$ ns). With some simplifying assumptions a

0 030-4018/83/0000–0000/S 03.00

theoretical prediction of threshold can be made which agrees well with the experimental results. We assume that the Stokes loss and gain within the capillary can be separated so that the net Stokes gain is

$$\exp(-2\gamma_s l)\exp\left\{\int_0^l \frac{2P_p(z)}{\pi W_0^2}\, fg\,dz\right\}. \quad (1)$$

The Stokes field attenuation constant γ_s is assumed to be given by the theoretical value from Marcatili and Schmeltzer [1] whereas the pump field attenuation constant γ_p, where

$$P_p(z) = P_p(0)\exp(-2\gamma_p z) \quad (2)$$

is derived from the measured pump transmission. (This experimentally derived value of γ_p is usually significantly greater than the theoretical Marcatili and Schmeltzer value, most probably due to imperfect capillary straightness). The factor g is the usual plane wave Raman gain coefficient (see e.g. Trutna and Byer [7]). The quantity $2P_p(z)/\pi W_0^2$ is the on-axis pump intensity and the numerical factor f accounts for the transverse variation of pump and Stokes fields via an overlap integral as discussed by Boyd et al. [8]. Taking the pump and Stokes waves to be both pure EH_{11} modes of the guide gives $f = 0.56$ [9], (if they are both assumed to be gaussian beams of the same spotsize one obtains $f = 0.5$ [8]), and by equating the net Stokes gain at threshold to exp(30), it is found from (1) and (2) that the threshold pump power $P_{p,th}$ is

$$P_{p,th} = \pi W_0^2(30 + 2\gamma_s l)/1.12 g l_{eff}, \quad (3)$$

where

$$l_{eff} = [1 - \exp(-2\gamma_p l)]/2\gamma_p. \quad (4)$$

Using (3) and (4) for the experimental conditions referred to above, a predicted threshold power of 230 kW is obtained.

In the case of a resonator configuration we have again used this same analysis to calculate the net gain for each transit through the capillary.

Various resonator configurations have been used and fig. 1 shows one arrangement. The pump beam passes through a plane resonator mirror having a transmission of ~90% at 1.06 μm and total reflection at the Stokes wavelength (1.907 μm). The second resonator mirror also transmitted most of the pump and

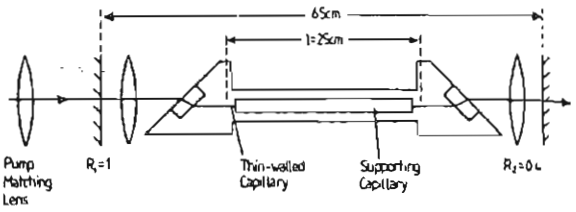

Fig. 1. Capillary waveguide resonator.

had a reflectivity of 40% at the Stokes wavelength. Intra cavity lenses of focal length 15 cm were placed close to the mirrors to match the resonator to the assumed Stokes spotsize leaving the capillary (i.e. $3W_0 = 2a$, as for the pump). With this arrangement and a pump pulse of 36 ns FWHM, threshold was reached at 40 kW pump power into the capillary. This represents a factor of ~6 reduction in threshold as a result of the Stokes feedback and a factor of 30 reduction compared with the case for an unguided pump without Stokes feedback. We have also tested a much simpler resonator configuration in which the feedback was provided by two uncoated plane reflectors very close (i.e. within a few mm) to the ends of the capillary. This was achieved by using plane glass flats as the windows of the high pressure cell, and ensuring that the capillary filled the space between them.

This arrangement gave a threshold of ~90 kW for a capillary of internal diameter 330 μm, and 42 kW for a capillary of 200 μm diameter. When pumped at twice the threshold level, the 200 μm capillary gave a measured photon conversion efficiency to first Stokes of 15% (9% in the forward direction, 6% in the backward direction). On the other hand, observation of the transmitted pump intensity showed almost total depletion of the pump over most of the pulse and it is not yet clear why the measured conversion efficiency was not greater. The calculated threshold powers for the oscillator were in good agreement with a simple model. It was assumed in this model that Stokes feedback was determined solely by the mirror reflections R_1, R_2, that the maximum Stokes gain from multiple resonator transits would be experienced by those Stokes photons travelling forward at the peak of the pump pulse, and that the pump pulse power has a gaussian time dependence $P(t) = \exp[-(t/\tau')^2]$ where $\tau' = \tau_{FWHM}/2\sqrt{\ln 2}$. With these assumptions, the condition that threshold is reached with n resonator transits, with a pulse peak

power P_{th}, becomes

$$P_{th} = \{\pi W_0^2 [30 + 2n\gamma_s l - [(n-1)/2] \ln(R_1 R_2)]\}$$
$$\times \{1.12 l_{eff} [g_f + g_B \exp[-(T/\tau')^2] + g_B \exp[-(T/\tau')^2]$$
$$+ g_F \exp[-(2T/\tau')^2] + g_F \exp[-(2T/\tau')^2] + \ldots]\}^{-1}, \quad (5)$$

where g_F, g_B are respectively the forward and backward Raman gain coefficients, $2T$ is the time for a resonator round trip, and the sum in the denominator continues to n terms. One can now vary n to obtain the minimum P_{th} from (5) and this then represents the predicted oscillator threshold. For the resonator of fig. 1, the predicted threshold is ~30 kW whereas the observed threshold was ~40 kW. For the plane/plane resonator it was not obvious what values of reflectivity to use for the windows, as one of these had parallel faces and the other had a 5 mrad wedge. Also, they were only approximately normal to the capillary axis. Fig. 2 shows the observed threshold as a function of gas pressure and the predicted thresholds for assumed reflectivities of 4% and 4% at the two end windows. Again the agreement is good, with the model coping adequately with changes in capillary bore diameter. It should be noted, however, that the predicted threshold is fairly insensitive to the assumed values of Stokes feedback.

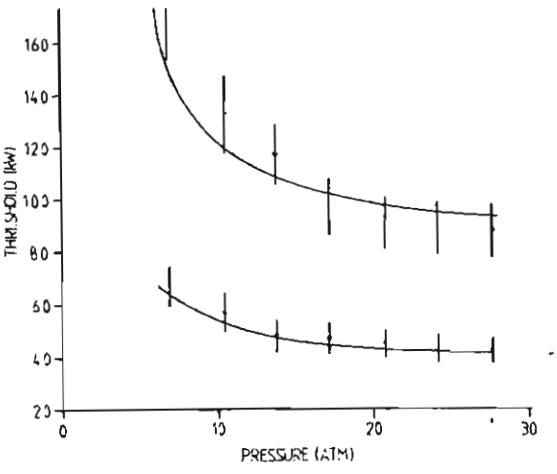

Fig. 2. 1.06 μm pump threshold power (kW) versus H_2 gas pressure (atmospheres) for resonator with plane uncoated reflectors butted against the waveguide ends. Upper curve is for 330 μm bore capillary, lower curve is for 200 μm bore. Solid lines are calculated using eq. (5).

As a further test of the waveguide/resonator we investigated stimulated Raman scattering in CH_4 gas. The case of CH_4 as a Raman medium presents some problems for pump wavelengths in the near infrared since the threshold is higher than for H_2 (the peak Raman cross-section is about a factor of 4 less than for H_2 at ~12 atm [10] and a factor of ~2 less at ~30 atm). In addition the stimulated Brillouin scattering threshold is rather low, leading to competition between SRS and SBS [11]. Murray et al. [12] show that, assuming the Raman linewidth to be independent of pressure, the ratio of Brillouin gain to Raman gain for a Raman Stokes frequency ν_s is given by $g_{SBS}/g_R = C\rho/\nu_s$ where ρ is the density in amagats and C is a factor depending on the particular gas molecule involved. This factor C can be determined from the results of Minck et al. [11] for the case of a ruby laser pump and CH_4. One can then predict that for a 1.06 μm pump the ratio is $g_{SBS}/g_{R,F} = \rho/8.5$, ρ again in amagats. Thus, a low enough pressure, say a few atmospheres, would discriminate against stimulated Brillouins scattering but would also imply a very high Raman threshold. Another way to discriminate against Brillouin scattering is to use a short pump pulse or a multimode pump pulse which contains temporal structure of short duration. The forward Raman Stokes wave can take advantage of the high intensity in one of the pump pulse spikes whereas the backward travelling Brillouin Stokes wave only experiences the average pump intensity. Thus, by using high pressures (30–60 atm) and a multimode Nd : YAG pump, Bruns et al. [13] have achieved efficient conversion to the first Stokes wave at 1.544 μm. The waveguide/resonator scheme allows another approach. Since a low Raman threshold can be achieved it is possible to work with a low pressure and also add extra discrimination against the Brillouin Stokes wave by means of frequency selection in the resonator. The resonator configuration we have used is the same as in fig. 1 but with a 60° prism placed between the lens and the output mirror (R = 0.5 at 1.544 μm). The output mirror was aligned to provide feedback of the Raman Stokes wave thus suppressing Brillouin Stokes feedback. With a CH_4 pressure ~6 atm the measured Raman threshold power (and this is using a single longitudinal mode pump pulse) was 180 kW (6.2 mJ in 32 ns FWHM), whereas the calculated threshold using the previous analysis was 200

kW. No Brillouin scattering was observed until pump powers in excess of 500 kW were reached. At a pump intensity of 2.5 X threshold the 1st Stokes output was measured to be ~330 μJ. No sign of thermal blooming was observed even at pulse repetition rates of 20 Hz, whereas in the scheme reported by Bruns et al. this was evident and necessitated gas circulation. A further advantage of the waveguide/resonator approach is that it provides a diffraction limited output whereas the output from the Raman laser of Bruns et al. was multimode. The threshold requirement for our CH_4 Raman laser is small enough to leave a very substantial amount of pump energy for pumping a Raman amplifier cell. This arrangement offers advantages for efficient Raman conversion [14] and in particular it means that the amplifier can be pumped at a level below that required for SBS. We anticipate that efficient conversion from 1.06 μm to 1.544 μm could then be achieved with a diffraction limited Stokes output.

In conclusion, we have demonstrated low threshold operation of a Raman laser by the combined use of a capillary waveguide and a resonator to provide Stokes feedback. An obvious benefit of the reduced threshold is that efficient stimulated Raman scattering is now within reach of pump lasers of much lower power. One can also consider further exploration of the waveguide resonator concept, for example using a ring resonator in which the Raman medium is synchronously pumped by a mode locked pulse train [15]. CH_4 gas should be well suited to this scheme as it has a short T_2 and a large integrated Raman cross section. We plan to perform experiments to evaluate this scheme. In fact it would seem to us that there is now a case for re-examining a number of nonlinear processes in gases to see whether they may find wider application as a result of the enhancement that waveguide/resonator techniques can offer.

This work has been supported by the Science and Engineering Research Council and one of us (A.J.B.) holds a CASE studentship sponsored by J.K. Lasers Ltd. We acknowledge valuable discussions with M.C. Ibison.

References

[1] E.A.J. Marcatili and R.A. Schmeltzer, Bell Syst. Tech.J. 43 (1964) 1783.
[2] P. Rabinowitz, A. Kaldar, R. Brickman and W. Schmidt, Appl. Optics 15 (1976) 2006.
[3] W. Hartig and W. Schmidt, Appl. Phys. 18 (1979) 235.
[4] A.J. Berry, D.C. Hanna and D.B. Hearn, Optics Comm. 43 (1982) 229.
[5] A.J. Berry, D.C. Hanna and C.G. Sawyers, Optics Comm. 40 (1981) 54.
[6] R.L. Abrams, IEEE J. Quant. Electron. QE-8 (1982) 838.
[7] W.R. Trutma and R.L. Byer, Appl. Optics 19 (1980) 301.
[8] G.D. Boyd, W.D. Johnson and I.P. Kaminow, IEEE J. Quantum Electron QE-5 (1969) 203.
[9] M.C. Ibison (private communication).
[10] W.R. Fenner, H.A. Hyatt, K.M. Kellam and S.P.S. Porto, J. Opt. Soc. Am. 63 (1973) 73.
[11] R.W. Minck, E.E. Hagenlocker and W.G. Rado, J. Appl. Phys. 38 (1967) 2254.
[12] J.R. Murray, J. Goldhar, D. Eimerl and A. Szöke, IEEE J. Quantum Electron QE-15 (1979) 342.
[13] D.G. Bruns, H.W. Bruesselbach, H.D. Stoval and D.A. Rockwell, IEEE J. Quantum Electron QE-18 (1982) 1246.
[14] H. Komine, E.A. Stappaerts, S.J. Brosnan and J.B. West, Appl. Phys. Lett. 40 (1982) 551.
[15] M.J. Colles, Appl. Phys. Lett. 19 (1971) 23.

REFERENCES

R.L.ABRAMS. IEEE J.Quant.Electron. QE-8,(11),(1982),838-843.

M.J.ADAMS. "An Introduction to Optical Waveguides", Wiley, Chichester (1981).

S.A.AKHMANOV,Yu.E.D'YAKOV,A.S.CHIRKIN. JETP Lett. 16,(1972),166-169.

S.A.AKHMANOV,Yu.E.D'YAKOV,L.I.PAVLOV. Sov.Phys.JETP 39(3),(1974),249-256.

J.A.ARMSTRONG,N.BLOEMBERGEN,J.DUCUING,P.S.PERSHAN. Phys.Rev. 127(6),(1972),1918-39.

P.V.AVIZONIS,R.M.HEIMLICH. Jnl.Appl.Phys. 40(9),(1969),3650-3656.

P.BAUES. Opto-Electron. 1,(1969),37-44.

A.J.BERRY. Mini-Thesis, University of Southampton, 1982.

A.J.BERRY,D.C.HANNA,C.G.SAWYERS. Opt.Commun. 40(1),(1981),54-58.

A.J.BERRY,D.C.HANNA,D.B.HEARN. Optics.Commun. 43( ),(1982),229-232.

A.J.BERRY,D.C.HANNA. Jnl.Opt.Quant.Elect. 15,(1983),367-369.

A.J.BERRY,D.C.HANNA. Optics.Commun. 45(5),(1983),357-360.

N.BLOEMBERGEN. "Nonlinear Optics", Benjamin, New York, 1965.

G.D.BOYD,W.D.JOHNSON,I.P.KAMINOV. IEEE Jnl.Quant.Elect.QE-5(4),(1969),203-206.

G.D.BOYD,D.A.KLEINMANN. Jnl.Appl.Phys. 39,(1968),3597-3634.

D.G.BRUNS,H.W.BRUESSELBACH,H.D.STOVAL,D.A.ROCKWELL. IEEE Jnl.Quant.Elect. QE-18(8) (1982),1246-52.

P.N.BUTCHER. "Nonlinear Optical Phenomena", Bulletin 200,Exg.Exp.Station. Ohio State University, 1965.

I.D.CARR,D,C,HANNA. Opt.Quant.Electron. 15(5),(1983),447-450.

M.J.COLLES. Appl.Phys.Lett. 19(2),(1971),23-25.

D.COTTER,D.C.HANNA,R.WYATT. Appl.Phys. 8,(1975),333-340.

J.J.DEGNAN. Appl.Opt. 12(5),(1973),1026-1030.

R.H.DICKE. Phys.Rev. 89(2),(1953),472-473.

V.EVTUHOV,A.E.SIEGMAN. Appl.Opt. 4(1),(1965),142-143.

W.R.FENNER,H.A.HYATT,J.M.KELLAM,S.P.S.PORTO. Jnl.Opt.Soc.Am. 63(1),(1973),73-77.

L.GALATRY. Phys.Rev. 122(4),(1961),1218-1223.

A.J.GLASS.IEEE Jnl.Quant.Elect. QE-3(11),(1967),516-520.

D.R.HALL,E.K.GORTON,R.M.JENKINS. Jnl.Appl.Phys. 48(3),(1977),1212-1216.

D.C.HANNA,Y.W.KOO. Optics.Commun. 43(6),(1982),414-418.

D.C.HANNA,Y.W.KOO,D.J.PRATT. Optics.Commun. 44(3),(1983),188-191.

D.C.HANNA,B.LUTHER-DAVIES,R.C.SMITH. Electron.Letts. 8(15),(1972),269-370.

D.C.HANNA,B.LUTHER-DAVIES,R.C.SMITH. Opto-Electronics. 4,(1972),249-256.

D.C.HANNA,C.G.SAWYERS,M.A.YURATICH. Optics.Commun. 37(5),(1981),359-362.

D.C.HANNA,M.A.YURATICH,D.COTTER. "Nonlinear Optics of Free Atoms and Molecules", Springer series on Optical Sciences, Vol 17, Springer-Verlag, 1979.

W.HARTIG,W.SCHMIDT. Appl.Phys. 18,(1979),235-241.

D.HERRIOT,H.KOGELNIK,R.KOMPFNER. Appl.Opt. 3(4),(1964),523-526.

M.C.IBISON. Mini-Thesis, University of Southampton,1982.

M.C.IBISON. Ph.D. Thesis, University of Southampton. (In preparation)

W.KAISER,M.MAIER. In "Laser Handbook", F.T.Arrechi,E.O.Schultz-Dubois, Eds. North Holland, Amsterdam,(1972),1077-1150.

W.KOECHNER. "Solid-state Laser Engineering", Springer series in Optical Sciences, Vol.1, Springer-Verlag,1976.

H.KOGELNIK. Appl.Opt. 4(12),(1965),1562-1569.

H.KOGELNIK,T.LI. Appl.Opt. 5(10),(1966),1550-1567.

H.KOMINE,E.A.STAPPAERTS,S.J.BROSNAN,J.B.WEST. Appl.Phys.Lett. 40(7),(1982),551-3.

D.J.KUIZENGA. Optics Commun. 22(2),(1977),156-160.

D.J.KUIZENGA. IEEE Jnl.Quant.Elect. QE-17(9),(1981),1694-1708.

T.LI. Bell Sys.Tech.Jnl. 44,(1965),917-932.

D.von der LINDE,M.MAIER,W.KAISER. Phys.Rev. 178(1),(1969),11-17.

E.A.J.MARCATILI,R.A.SCHMELTZER. Bell Syst.Tech.Jnl.43,(1964),1783-1809.

A.D.MAY,M.A.HENESIAN,R.L.BYER. Can.Jnl.Phys. 56,(1978),248-250.

F.J.McCLUNG,D.H.CLOSE. Jnl.Appl.Phys. 40(10),(1969),3978-3981.

R.W.MINCK,E.E.HAGENLOCKER,W.G.RADO. Jnl.Appl.Phys. 38(5),(1967),2254-2260.

J.R.MURRAY,J.GOLDHAR,D.EIMERL,A.SZOKE. IEEE Jnl.Quant.Elect. QE-15(5),(1979),342-67.

J.R.MURRAY,A.JAVAN. Jnl.Mol.Spect. 42,(1972),1-26.

J.H.NEWTON,G.M.SCHINDLER. Optics Letts. 6(3),(1981),125-127.

M.T.PACHECO. 1st Year Report, Dept.Physics, University of Southampton, 1983.

P.RABINOWITZ,A.KALDOR,R.BRICKMAN,W.SCHMIDT. Appl.Opt. 15(9),(1976),2005-2006.

G.RIVOIRE,C.DESLANCS,J.L.FERRIER,J.GAZENGEL,N.PHU.XUAN. Opt.Quant.Elect. 15(3), (1983),209-216.

P.H.SARKIES. Optics Commun. 31(2),(1979),189-191.

C.G.SAWYERS. Ph.D. Thesis, University of Southampton, 1981.

H.W.SCHOTTER,H.W.KLOCKNER. In "Raman Spectroscopy of Gases and Liquids", A.Weber, Ed, Springer, Berlin, 1979, 123-164.

J.STEFFEN,J.P.LORTSCHER,G.HERTZIGER. IEEE Jnl.Quant.Elect. QE-8(2),(1972),239-45.

Y.TAIRA,K.IDE,H.TAKUMA. Chem.Phys.Lett. 91(4),(1982),299-302.

W.R.TRUTNA,R.L.BYER. Appl.Opt. 19(2),(1980),301-312.

W.R.TRUTNA,Y.K.PARK,R.L.BYER. IEEE Jnl.Quant.Elect. QE-15(7),(1979),648-655.

ACKNOWLEDGEMENTS

I would like, in particular, to thank my supervisor Dr.D.C.Hanna for his advice and guidance during the course of this work. Also, I would like to acknowledge the financial support of the SERC and J.K.Lasers who collaborated in the form of a CASE award. I would also like to thank the other members of the laser group at Southampton University, in particular Dave Hearn, Graham Smith, Dave Pratt, Ian Carr, Marcos Pacheco and even Ruth Forbes - none of whom were the least bit sympathetic when things were going badly. Thanks must also go to Dr.Clive Ireland at J.K.Lasers for useful discussions and supervision during a four weeks stay at the company. Finally, thanks to Diane Beresford-Walker for typing this thesis very quickly and at very short notice.